CANADIAN THESES

THÈSES CANADIENNES

NOTICE

The quality of this microfiche is heavily dependent upon the quality of the original thesis submitted for microfilming. Every effort has been made to ensure the highest quality of reproduction possible.

If pages are missing, contact the university which granted the degree.

Some pages may have indistinct print especially if the original pages were typed with a poor typewriter ribbon or if the university sent us an inferior photocopy.

Previously copyrighted materials (journal articles, published tests, etc.) are not filmed.

Reproduction in full or in part of this film is governed by the Canadian Copyright Act, R.S.C. 1970, c. C-30. Please read the authorization forms which accompany this thesis.

AVIS

La qualité de cette microfiche dépend grandement de la qualité de la thèse soumise au microfilmage. Nous avons tout fait pour assurer une qualité supérieure de reproduction.

S'il manque des pages, veuillez communiquer avec l'université qui a conféré le grade.

La qualité d'impression de certaines pages peut laisser à désirer, surtout si les pages originales ont été dactylographiées à l'aide d'un ruban usé ou si l'université nous a fait parvenir une photocopie de qualité inférieure.

Les documents qui font déjà l'objet d'un droit d'auteur (articles de revue, examens publiés, etc.) ne sont pas microfilmés.

La reproduction, même partielle, de ce microfilm est soumise à la Loi canadienne sur le droit d'auteur, SRC 1970, c. C-30. Veuillez prendre connaissance des formules d'autorisation qui accompagnent cette thèse.

THIS DISSERTATION HAS BEEN MICROFILMED EXACTLY AS RECEIVED

LA THÈSE A ÉTÉ MICROFILMÉE TELLE QUE NOUS L'AVONS REÇUE

Canadä

58

National Library
of Canada

Bibliothèque nationale
du Canada

Ottawa, Canada
K1A 0N4

TC – C

0-315-23256-0

PERMISION TO MICROFILM – AUTORISATION DE MICROFILMER

• Please print or type – Écrire en lettres moulées ou dactylographier

AUTHOR – AUTEUR

Full Name of Author – Nom complet de l'auteur

SUTENDRA Sivaperagasam

Date of Birth – Date de naissance

5-2-1946

Canadian Citizen – Citoyen canadien

☑ Yes / Oui   ☐ No Non

Country of Birth – Lieu de naissance

Sri Lanka

Permanent Address – Résidence fixe

#207, 3828 105 street,
Edmonton, Alberta T6J 2N1

THESIS – THÈSE

Title of Thesis – Titre de la thèse

An Experimental Study of Clear Water Scour
at Constriction

Degree for which thesis was presented
Grade pour lequel cette thèse fut présentée

M. Sc

Year this degree conferred
Année d'obtention de ce grade

1985

University – Université

University of Alberta

Name of Supervisor – Nom du directeur de thèse

Dr N. Rajaratnam

AUTHORIZATION – AUTORISATION

Permission is hereby granted to the NATIONAL LIBRARY OF CANADA to **microfilm** this thesis and to **lend** or **sell copies of the film.**

The author reserves other publication rights, and neither the thesis nor extensive extracts from it may be printed or otherwise reproduced without the author's written permission.

L'autorisation est, par la présente, accordée à la BIBLIOTHÈQUE NATIONALE DU CANADA de **microfilmer** cette thèse et de **prêter** ou de **vendre des exemplaires du film.**

L'auteur se réserve les autres droits de publication; ni la thèse ni de longs extraits de celle-ci ne doivent être imprimés ou autrement reproduits sans l'autorisation écrite de l'auteur.

► ATTACH FORM TO THESIS – VEUILLEZ JOINDRE CE FORMULAIRE À LA THÈSE ◄

Signature

Date

11/12/85

NL-91 (r. 84/03)

Canada

THE UNIVERSITY OF ALBERTA

AN EXPERIMENTAL STUDY OF CLEAR WATER SCOUR AT CONSTRICTIONS

by

SIVAPERAGASAM SUTENDRA

A THESIS

SUBMITTED TO THE FACULTY OF GRADUATE STUDIES AND RESEARCH

IN PARTIAL FULFILMENT OF THE REQUIREMENTS FOR THE DEGREE

OF MASTER OF SCIENCE

DEPARTMENT OF CIVIL ENGINEERING

EDMONTON, ALBERTA

FALL 1985

THE UNIVERSITY OF ALBERTA

RELEASE FORM

NAME OF AUTHOR   SIVAPERAGASAM SUTENDRA

TITLE OF THESIS   AN EXPERIMENTAL STUDY OF CLEAR WATER

SCOUR AT CONSTRICTIONS.

DEGREE FOR WHICH THESIS WAS PRESENTED MASTER OF SCIENCE

YEAR THIS DEGREE GRANTED   FALL 1985

Permission is hereby granted to THE UNIVERSITY OF

ALBERTA LIBRARY to reproduce single copies of this

thesis and to lend or sell such copies for private,

scholarly or scientific research purposes only.

The author reserves other publication rights, and

neither the thesis nor extensive extracts from it may

be printed or otherwise reproduced without the author's

written permission.

(SIGNED) ....

PERMANENT ADDRESS:

#207, 3828 - 105 Street

Edmonton, Alberta

T6J 2N9

DATED .27th September, ...1985

THE UNIVERSITY OF ALBERTA

FACULTY OF GRADUATE STUDIES AND RESEARCH

The undersigned certify that they have read, and
recommend to the Faculty of Graduate Studies and Research,
for acceptance, a thesis entitled AN EXPERIMENTAL STUDY OF
CLEAR WATER SCOUR AT CONSTRICTIONS submitted by
SIVAPERAGASAM SUTENDRA in partial fulfilment of the
requirements for the degree of MASTER OF SCIENCE.

....

Supervisor

....

....

Date.... 2 Oct. 85 ....

Author dedicates the thesis to **Bagavan Sri Sathya Sai Baba.**

" The purpose of Spiritual Education is to enable man
to have a Vision of the Divine in Society. When man
combines this Vision with Tapas, he merges with God.
The Vision of Divinity and merging with Divinity,
are like the two poles; one positive the other
negative. The positive and negative will join
together and take you to a position where you will
become Divine".

                                              - **BABA**

ABSTRACT

Observation and analysis of clear water scour at spur and interference spur type constrictions are presented in this thesis. Analysis is based on observations and dimensional considerations and a design chart for maximum clear water scour at spur, interference spur and jet is prepared from data collected from present work and the studies of Rajaratnam and Humphries, Nwachukwu, Gill, Garde et al. and Liu et al.

Location of maximum scour and scour profiles could be established from the relevant figures and length scales.

A brief study was carried out on backwater and a chart was prepared to estimate the maximum backwater.

A parallel analysis based on regime considerations is also included.

ACKNOWLEDGEMENTS

Table of Contents

List of Tables

List of Figures

List of Plates

LIST OF SYMBOLS

A_0 approach flow area

A_1 flow area at constriction

B   channel width

b   constriction opening

C   coefficient of discharge through constriction on

       mobile bed

D   median size of sand grain

F_* non-dimensional velocity scale $= V_*/\sqrt{g(\Delta\rho/\rho)D^3}$

F_0 Froude number at approach

F_t Froude number at tail end

FR   Q - factor at approach flow $= q/\sqrt{(\gamma_{sub}/\rho)D^3}$

h   approach flow depth + maximum scour depth

K   sand grain roughness(D)

K_s Nikuradse's equivalent sand grain roughness

m   constriction ratio = (B-b)/B

Q   discharge in l/s

q   discharge intensity

q_0 discharge intensity at approach section

q_1 discharge intensity at constriction

SG   specific gravity of material

T   water temperature in ^{o}C

t   duration of an experiment

u   approach velocity at y cm above channel bed

u_* shear velocity at approach flow

V_* velocity scale $= Q/by_0$

V_0 mean approach velocity

V_1 mean velocity at constriction

V_t mean tail end velocity

x co-ordinate in longitudinal direction

X_1 distance from constriction to upstream lip of scour
hole along channel centre

X_2 distance from constriction to upstream lip of scour
hole along the nose of constriction

X' distance from constriction to a point where $\epsilon_\alpha = 1/2 \; \epsilon_{mc\alpha}$

X'' distance from constriction to a point where $\epsilon_\alpha = 1/2 \; \epsilon_{mc}$

$\overline{X}$ distance along channel centre from spur constriction
to the maximum scour at channel centre

y co-ordinate in vertical direction

y_o approach depth flow

y_t depth of water at tail end

Δy backwater $(y - y_t)$

$\overline{y}$ depth of water above channel bed level

y' depth of water at constriction above final bed level

z co-ordinate in transverse direction

z_1 scour hole width along transverse at constriction

z' $z-(b/2 - z_1)$ considering positive values only

ϵ_∞ scour depth at equilibrium state measured from
original bed level

$\epsilon_{m\infty}$ Maximum scour depth at equilibrium state

$\epsilon_{mc\infty}$ Maximum scour depth along channel centre at
equilibrium state

$\Delta\epsilon_\alpha$ height of ridge at equilibrium state

ρ mass density of water

ρ_s mass density of sand particles

$\Delta\rho$ $\rho_s - \rho$

ν kinematic viscosity of water

τ_c critical shear stress

τ_0 approach bed shear stress

γ_{sub} submerged unit weight of sediment particles

1. INTRODUCTION

Constrictions, either man-made or occurring naturally in a river or channel, will change the original flow pattern in the vicinity of constrictions. Liu et al. (1961) confirmed this from observations on their laboratory experiments, which indicated that the stream lines at some distance away from the abutment was not affected by its presence in the flow. Some man-made constrictions are end-dump closures, bridge piers and abutments and spurs. The change in flow pattern in the vicinity of constrictions will affect the equilibrium and the river or channel will readjust to it after a period of time. The process of new equilibrium may involve scour near the constriction. Thus this scour is local in nature.

The problem of scour around constrictions is most important to engineers because many bridge failures recorded in the past were the result of inadequate knowledge of the scour and thus not providing adequate foundation depth or bad practice in maintenance. Many investigators have developed formulae to estimate the maximum scour depth for clear water scour and live bed scour. Their suggestions were based on experience (Regime theory) or dimensional analysis with the support of laboratory experiments.

Figure 1 shows the definition sketch of flow through a constriction which indicates the maximum clear water scour
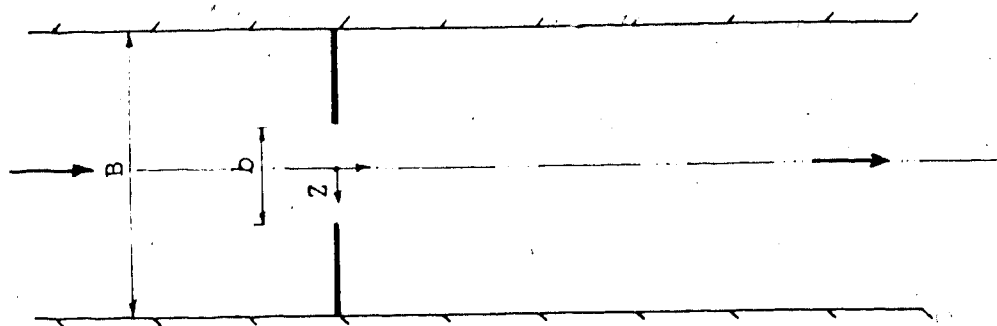
PLAN VIEW
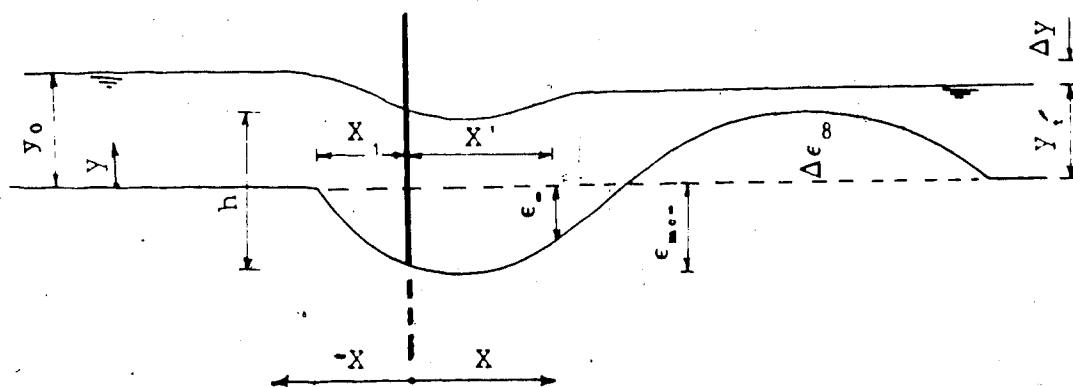
SECTIONAL VIEW

FIGURE 1 — DIMENSION SKETCH OF FLOW
THROUGH A CONSTRICTION

at channel centre $\epsilon_{mc\infty}$, distance of upstream lip of scour hole X_1, distance to a point where the scour depth equals to half the maximum scour depth at channel centre X', approach depth of water y_0, tail end water depth y_1, maximum backwater Δy and the height of ridge $\Delta\epsilon_\infty$.

It is reasonable to accept Neill's (1964) definition for depth of scour as depth of material removed during the scouring process measured below the original bed. The total scour depth is defined as the depth of scour measured from water surface. Clear water scour is defined as the scour which occurs when the bed material upstream of the constriction is not in transport. The bed shear stress in this area is less than critical shear stress. Live bed scour is the scour which occurs when there is general bed load transport in the river or channel. The bed shear stress in the approach flow is greater than the critical shear stress.

The aim of the present work is to carry out experiments to study the maximum clear water scour depth, pattern of the scour and finally to formulate a design chart to estimate the maximum scour at constrictions and also to compare the results with the predictions from a simple regime theory method.

Experiments were carried out in a flume 10.70 m long, 2.29 m wide and 0.305 m deep in the Civil Engineering Hydraulic laboratory at the University of Alberta. Twenty eight experiments were performed and in all these

experiments, the scour pattern was symmetrical.

From the results of the present experiments and the previous studies of Rajaratnam and Humphries, Nwachukwu, Gill, Garde et al. and Liu et al., a design chart was developed to estimate the maximum clear water scour at contrictions.

A brief study was also done on backwater produced by the constriction and a non dimensional chart relating the ratio of backwater to the tail end water depth and tail end Froude number with constriction ratio as a third parameter was developed.

Using sediment transport analysis, a plot was prepared for Q-Factor versus h/D. Quazi and Peterson (1973) prepared a plot for Q-Factor versus h/D for rip rap for piers and also included a compendium of sediment transport data for flumes by Peterson and Howells (1973) and for end-dump closure by Das (1972). This was included in the present plot. From this, an average clean water scour at constrictions can be calculated.

2. LITERATURE REVIEW

This chapter deals with the previous studies on maximum scour at the constrictions. It also includes the discussion on the disagreement of the factors causing the scour amongst different investigators. This chapter also presents studies carried out on backwater due to constrictions in alluvial channels.

2.1 MAXIMUM SCOUR DEPTH

Several studies have been carried out by engineers to predict the maximum scour depth at constrictions, which is important for the stability of the engineering structure.

The methods developed for predicting the maximum local scour can be grouped into three categories:

2.1.1 Equations based on Regime Considerations.

2.1.2 Method based on Dimensional Analysis.

2.1.3 Analogy with Long Constriction.

2.1.1 Equations Based on Regime Considerations.

Regime equations have been derived empirically from experience gained from Indian rivers and irrigation channels. It is believed that the discharge intensity and the normal flow depth are important factors and all the formulae are based on them.

Khosla (1936) modified Lacey's formula as,

$$\left[\epsilon_{m\alpha} + y_0 \right] = 0.9 \ C \left[\frac{q^2}{f_1} \right]^{1/3} \qquad \qquad 2.1$$

where f_1, is Lacey's silt factor $= 1.59 \ \sqrt{D}$, D is median size of sand in mm, q is the discharge intensity in approach section, $\epsilon_{m\infty}$ is the maximum scour depth below the original bed level, y_0 is the approach flow depth, C is a coefficient which ranges from 1.0 to 3.5 depending on the angle of attack.

Inglis (1949) analysed field data on maximum scour depth at spur dikes and suggested a formula for design purposes as,

$$\left[\epsilon_{m\infty} + y_0 \right] = 0.95 \left[\frac{Q}{f} \right]^{1/3} \qquad \qquad 2.2$$

where f is silt factor $= 1.76 \ \sqrt{D}$ and Q is the discharge.

Ahmad (1953) developed a formula from experimental tests for estimating maximum scour at spur nose as,

$$\left[\epsilon_{max} + y_o \right] = K\ q_1^{2/3}$$

2.3

where q_1 is the discharge intensity at the constriction and K is a constant depending on flow concentration, angle of inclination of spur and different angles of attack.

This formula is identical in form and power of q to the relation derived from Lacey by Khosla.

Blench (1957) prepared an empirical correlation between total scour and discharge intensity in the form,

$$\left[\epsilon_{max} + y_o \right] = 1.35\ q^{0.75}\ F_b^{-1/3}$$

2.4

where F_b is the Blench bed factor.

2.1.2 Method based on Dimensional Analysis

Based on dimensional analysis and their experimental data, Garde et al. (1961) concluded,

$$\frac{\epsilon_{m\infty} + y_0}{y_0} = \frac{k}{m} F^n \qquad 2.5$$

where k and n are functions of average drag coefficient of sediment and F is the Froude number of the normal flow and m is the constriction ratio defined as m = (B-b)/B.

Liu et al. (1961) conducted laboratory experiments on vertical wall spur and abutments and suggested formulae for clear water scour and live bed scour.

a) clear water scour,

$$\frac{\epsilon_{m\infty}}{y_0} = 12.5 \frac{F}{m} \qquad 2.6$$

b) live bed scour,

$$\frac{\epsilon_{m\infty} + y_0}{y_0} = 0.3 + 2.15 \left[\frac{a}{y_0}\right]^{0.4} F^{1/3} \qquad 2.7$$

where a is the length of the obstruction perpendicular to the flow.

2.1.3 Analogy with Long Constriction

Laursen (1963) extended his analysis for a long constriction to a local scour around abutments by taking the width of the zone influenced by the abutment as 2.75 , excluding the length of abutment itself. The resulting expression for clear water scour at abutment is,

$$\frac{1}{y_0} = 2.75 \frac{\epsilon_{m\infty}}{y_0} \left[\left[\frac{1}{r}\left[\frac{\epsilon_{m\infty}}{y_0} + 1\right]^{7/6} \left[\frac{\tau_0}{\tau_c}\right]^{-1/2}\right] - 1 \right] \qquad 2.8$$

$$\frac{\tau_0}{\tau_c} = \frac{V_0^2}{120\, D^{2/3}\, y_0^{1/2}}$$

where l is length of embankment, r is ratio of depth of scour at pier or abutment to depth of scour in equivalent long contraction.

Gill (1972) modified Straub's (1934) equation for scour in a long rectangular constriction to,

$$\frac{\epsilon_{m\infty} + y_0}{y_0} = \alpha \left[\frac{B}{b}\right]^{6/7} \left[\left[\frac{B}{b}\right]^{1/n}\left[1 - \frac{\tau_c}{\tau_0}\right] + \frac{\tau_c}{\tau_0}\right]^{-3/7} \qquad 2.9$$

In this equation

$$1 - \frac{\tau_c}{\tau_0} = 0 \qquad \text{when} \qquad \frac{\tau_c}{\tau_0} \geq 1$$

where α is a coefficient which depends on flow depth and size of bed material and equal to $8.375(D/y_0)$.

Equation 2.9 was modified for local scour around a spur to,

a) clear water scour $\left[\tau_0 < \tau_c\right]$

$$\frac{\epsilon_{m\infty} + y_0}{y_0} = 8.375 \left[\frac{D}{y_0}\right]^{0.25} \left[\frac{B}{b}\right]^{6/7} \left[\frac{\tau_0}{\tau_c}\right]^{3/7} \qquad 2.10$$

b) live bed scour $\quad \left[\tau_0 > \tau_c \right]$

$$\frac{\epsilon_{m\alpha} + y_0}{y_0} = 8.375 \left[\frac{D}{y_0} \right]^{0.25} \left[\frac{B}{b} \right]^{6/7} \left[\frac{B}{b} \right]^{6/7 - 3n/7} \qquad 2.11$$

where n varies from 3 to 1.5.

Gill suggested that the maximum scour occurs when critical shear stress of the bed material equals the bed shear stress.

Das (1972), from laboratory experiments for end dump closure of alluvial channels, developed non-dimensional design charts relating constriction ratio m, approach flow depth y_0 , maximum scour depth $\epsilon_{m\alpha}$, medium size of sand grain D, covering Froude number from 0.05 to 0.6.

Peterson (1975) used dimensional analysis and regression techniques to prepare a series of universal flow diagrams showing the relationship for discharge intensity, approach flow depth, median size of sand grain, sediment-concentration C and channel slope for mobile boundary channels. The depth of maximum scour at constriction can be estimated from these diagrams.

2.2 DISAGREEMENT ON FACTORS AFFECTING MAXIMUM LOCAL SCOUR

2.2.1 Effect of Sediment Size

Gill (1972) agreed with Ahmad (1953) that the rate of scour development of fine sand was higher than that of coarse sand, but disagreed that the maximum scour was unaffected by the size of bed material.

Garde et al. (1961) conclusion contradicted Laursen's (1953) statement that the bed material size does not affect the sco depth.

2.2.2 Effect of Approach Velocity

Laursen (1953) concluded that the velocity had no effect on the depth of scour, but Garde et al. (1961) found out from their experiments that the velocity of flow was an important factor in determining the maximum scour depth.

The ASCE Task Committee on Sedimentation (1966) stated that mean velocity alone cannot express the scouring action of the water at the bed and that to completely specify conditions the depth must also be given.

2.2.3 Effect of Approach Depth of Flow

Garde et al. (1961) suggested from their findings that there was no correlation of maximum scour depth with the approach depth of flow for spur dykes. According to Laursen (1953) and Gill (1972), scour was a function of flow depth.

2.3 MAXIMUM BACKWATER

Although many studies have been made to assess the maximum backwater caused by constrictions in rigid bed channels, only a few investigators have worked on the corresponding problem in an alluvial channel. These are Liu. et al. (1961), Sandover (1969) and Das (1972).

Liu et al. have done extensive studies on backwater on rigid channels. They found that the effect of scour made it quite difficult to measure the backwater satisfactorily, but the difference of water surface elevation across the embankment was fairly consistent. They concluded that the water surface drop across the embankment was approximately 60 percent of that in rigid channel.

Sandover (1969) studied the backwater effects of end-dumped dams. Using dimensional considerations and experimental observations, Sandover developed the following relationship between backwater Δy, Froude number and constriction ratio

$$\frac{\Delta y}{y_0} = f \left[F, \frac{b}{B} \right] \qquad 2.12$$

and presented curves, $\Delta y/y_0$ versus constriction ratio m with Froude number as the variable.

Das (1972) developed a plot of coefficient of discharge versus Froude number with constriction ratio as third

parameter. He considered the difference in water surface
elevation across the embankment in his calculations. On his
plot, the corresponding plot for flow on rigid bed due to
Vallentine was also included for comparison.

3. EXPERIMENTAL ARRANGEMENT, EXPERIMENTS AND EXPERIMENTAL RESULTS

This chapter describes the apparatus used for the experiments and discusses the various measurement methods. This section also presents procedure and the experimental results. The limitation due to the apparatus and experimental procedures are also pointed out.

3.1 EXPERIMENTAL ARRANGEMENT

The apparatus used in the experimental arrangements may be described under five headings:

3.1.1 Flume

3.1.2 Flow system

3.1.3 Models

3.1.4 Measuring devices

3.1.5 Material

3.1.1 Flume

a. The tilting flume, made out of metal sheets is 10.70 m long, 2.29 m wide and 0.305 m deep. This flume rests on I beams. The upstream I-beam was supported by pairs of electrically operated screw jacks. Inverted T-beams were used as guide rails for the instrument carriage and were mounted on top of the flume walls by means of bolts. The downstream end

of the flume was connected to the sump by means of a
25 mm pipe and a 125 mm pipe. The opening of 25 mm
pipe was controlled by a valve connected to it and
the 125mm pipe was adjusted by covering the top of
the opening by means of a metal plate. Figure 2
shows the plan and sectional views of the flume.

b. For the last three experiments the width of the
flume was reduced symmetrically to 1.20 m by means
of 250 mm x 12 mm plywood sheets placed parallel to
full length of the side walls.

3.1.2 Flow system

The water was pumped from an underlying sump by a 50 mm
centrifugal pump of maximum capacity of 14 L s^{-1}. A valve
and magnetic flow meter were fixed to the 50 mm delivery
pipe.

3.1.3 Models

The model used to provide constrictions was made out of
3 mm thick aluminum plate. The constriction opening was
varied by adding extensions to the aluminum plate.

3.1.4 Measuring Devices

3.1.4.1 Magnetic flow meter

The water was delivered through a magnetic flow
meter which sends signals to the digital multimeter to
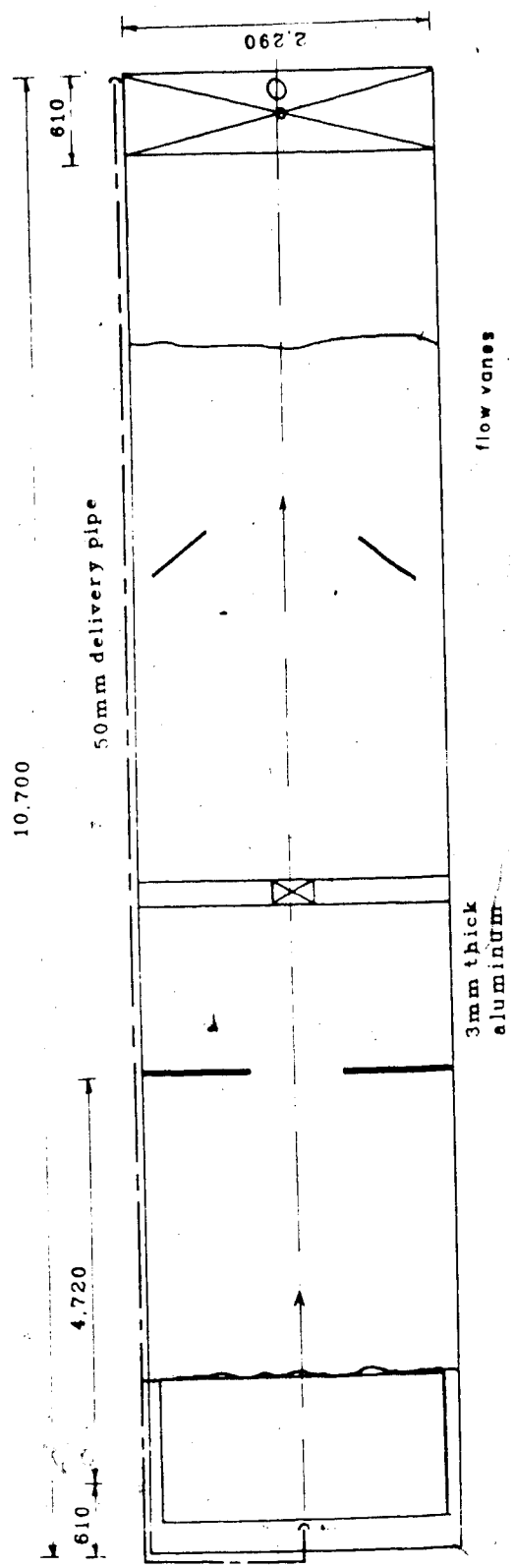
PLAN VIEW
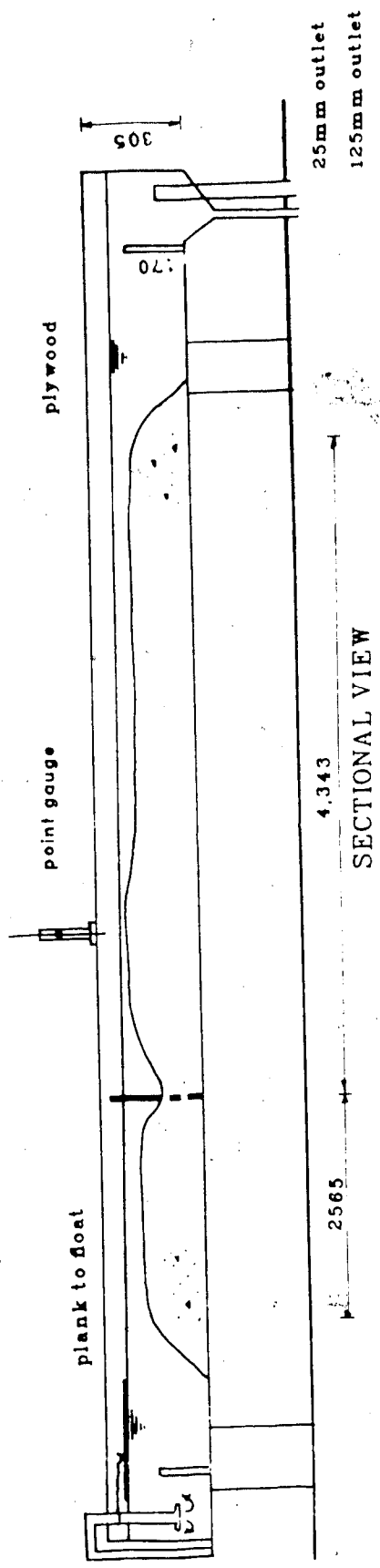
SECTIONAL VIEW

FIGURE 2 — TYPICAL PLAN AND SECTIONAL VIEW OF THE FLUME

read the discharge in L s^{-1}. The valve in delivery line was used to obtain the required discharge.

3.1.4.2 Point gauge

Water surface and bed surface elevations at any point in the flume were measured by a point gauge equipped with a vernier to measure to 0.01 in (0.25 mm). The point gauge was mounted on a carriage which travelled along the flume on guide rails. The point gauge was also fitted to slide transversely across the flume on rails mounted on the carriage. Steel tapes fixed on the wall of the flume and on the carriage were used for longitudinal and transverse location of the point gauge respectively.

3.1.4.3 Pitot tube

A 3 mm (external diameter) pitot tube was mounted to the point gauge carriage when velocity measurements were taken. The pitot tube was connected to a tilting manometer.

3.1.5 Material

One size of 1.32 mm median diameter sand was used as the bed material. The specific gravity of the sand was 2.64. The results of the sieve analysis on this sand are shown in Figure 3. The angle of repose of the sand, determined under submerged condition was 32 degrees. The Shield diagram with White data from Sedimentation
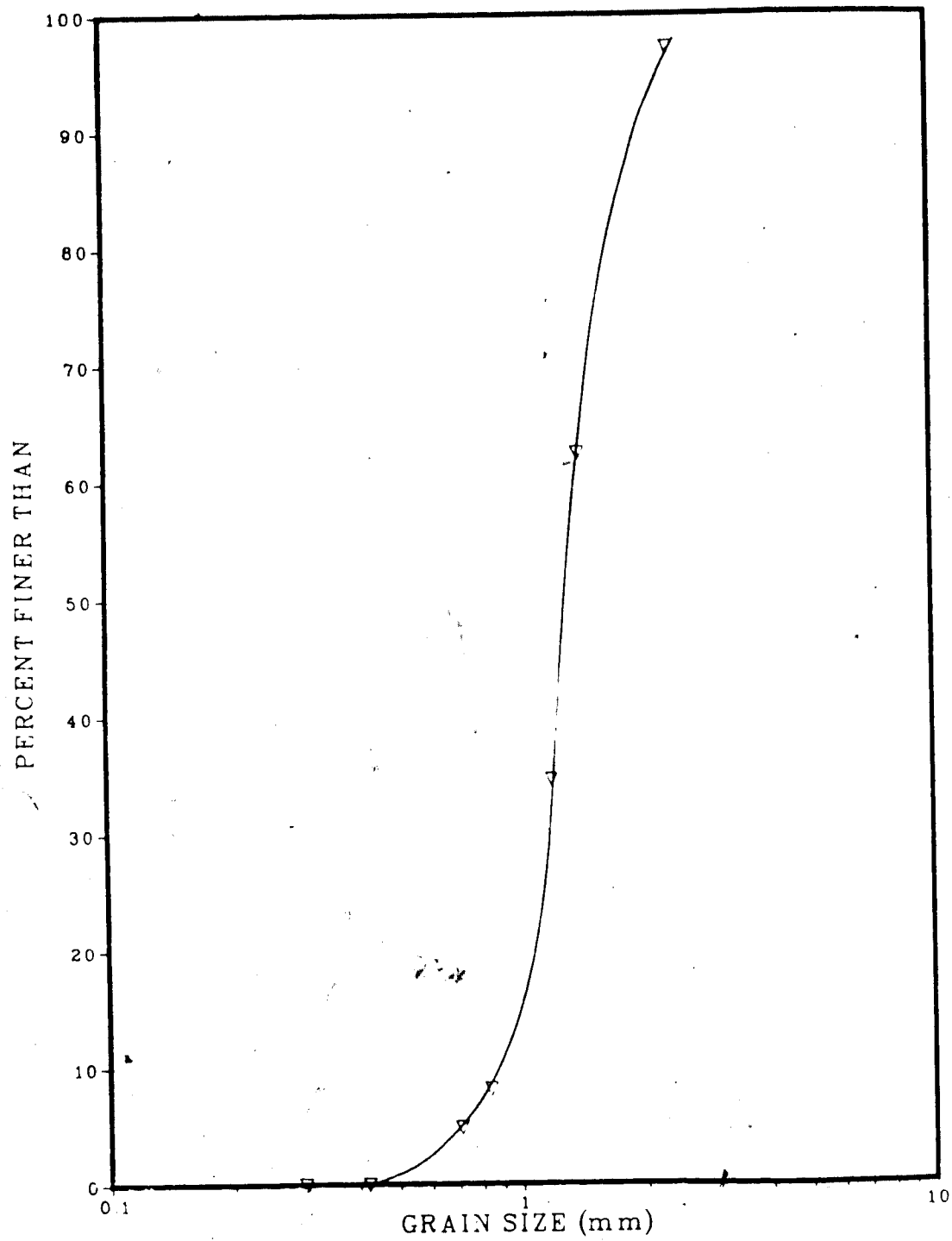
FIGURE 3 — SIEVE ANALYSIS

Engineering by Vanoni (1975) was modified to obtain the shear velocity on y axis only and is shown in Figure 4. Based on this Figure, the critical shear velocity for water temperature of 20° C is 2.80 cm/s. Using the following equation,

$$\tau_C = u_{*c}^2 \rho \qquad\qquad 3.1$$

where τ_C is the critical shear stress, u_{*c} is the critical velocity and ρ is mass density of water.

the critical shear stress is 0.78 N/m² and the critical particle Reynolds number $u_{*c}D/\nu$ is 36. The Nikuradse's equivalent sand grain roughness is 0.218 cm.

3.2 EXPERIMENTS

Experiments were carried out to measure the scour and ridge profiles for given velocity at approach, flow depths at approach and tail end.

3.2.1 Scour Profiles

The tilting flume was adjusted to be horizontal by the electrically adjusted screw jacks and checked by an engineering level. The aluminum plate was fixed symmetrically perpendicular to the long walls of flume by

$\gamma_{sub} D^3 / \rho \nu^2$

$u^2 \rho / \gamma_{sub} D$
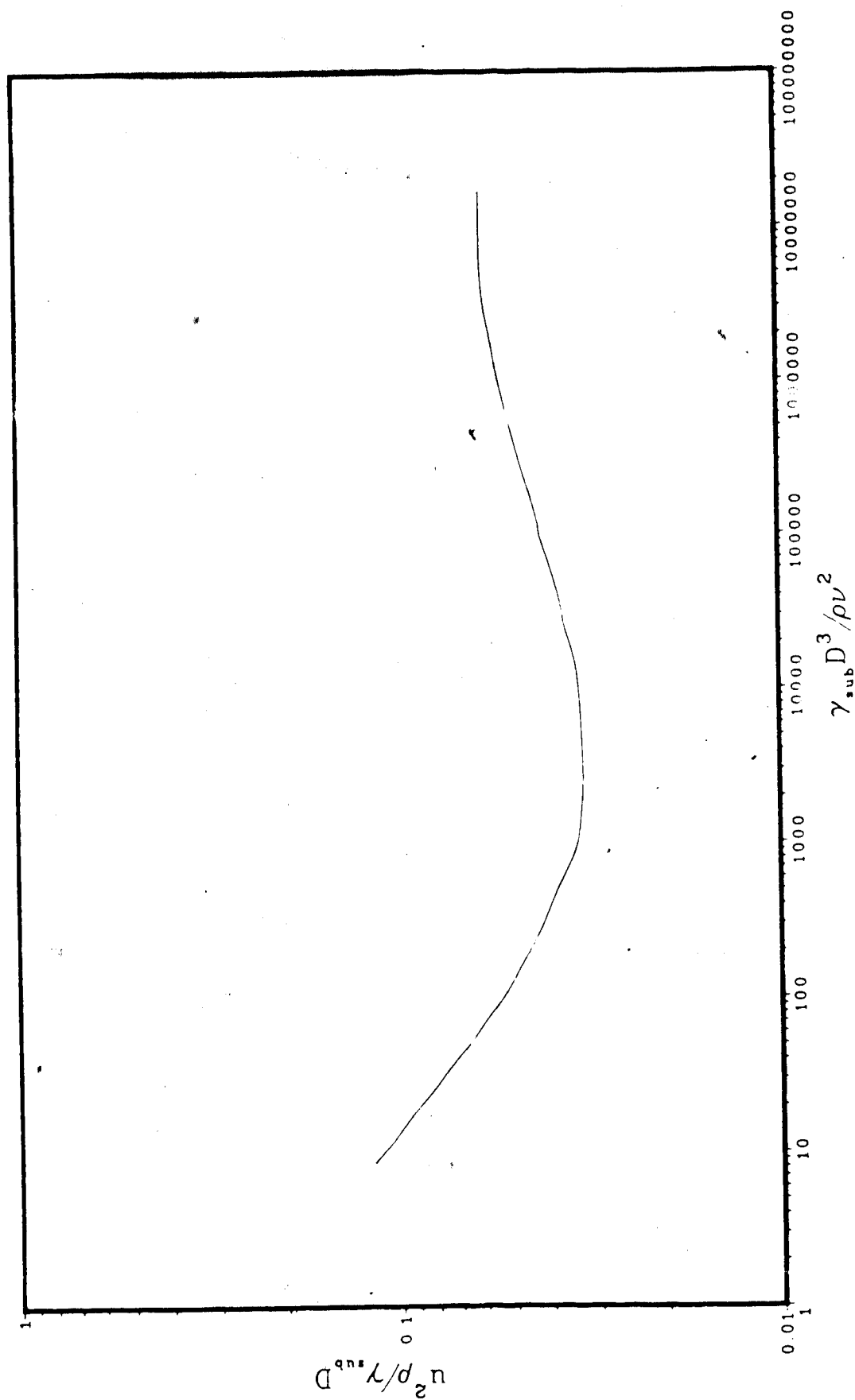
FIGURE 4 – MODIFIED SHIELD DIAGRAM WITH WHITE DATA ADDED

angles, bolted to the plate and to the flume tray. Sealant
was applied between the plate and the flume tray and walls
to stop water leakage. A floating plank of size 2 m x 1 m
x 12 mm was used as a damper to stop wave action. The plank
was tied to the delivery pipe at the upstream end of the
flume and allowed to float.

The flume tray was filled with sand to a length of 6.9
m, width of 2.29 m, and depth of 170 mm. The sand bed was
screeded to horizontal and bed measurements were taken by
point gauge. The outlets were closed and the water was
allowed, on the downstream of the flume by a 12 mm hose pipe,
till the sand bed was submerged. Then the water was sent
through the delivery pipe by opening the valve slowly until
the required discharge was obtained. The depth of the water
was maintained by adjusting the outlet openings. When the
outlet openings were slightly opened, the depth of water in
the flume was raised and when they were fully opened the
depth of water was lowered. Experiments which produced
non-symmetrical scour pattern were discarded. The duration
of experiments varied from 5 to 24 hours. It was observed
visually that there was no movement of sand particles at the
constriction after 4 to 6 hours. This time depends on
constriction ratio, velocity and would appear to depend on
the sand particle size.

When equilibrium was obtained, water surface
measurements were taken by point gauge and water temperature
was noted. The valve in delivery pipe was slowly closed and

outlet was controlled so that no disturbance was created to the scour or ridge. After the water was drained, detailed measurements of scour and ridge along longitudinal and transverse directions were taken by the point gauge. Before the next experiment, the sand was mixed thoroughly and screeded.

The constriction ratio was varied by changing opening width of the constriction by adding extensions to 3 mm thick aluminum plate. These extensions were placed on upstream face of the constriction and secured firmly by providing enough length towards the walls of the flume. Sealant was applied between the extension plate, fixed plate and flume tray to stop any leaks.

The last three experiments were conducted with a main channel width of 1.20 m. The reduction of the width gave more variation in the constriction ratio.

Twenty eight experiments were performed which gave symmetrical scour pattern along centre of the channel. In these experiments, the constriction ratio m was varied from 0.493 to 0.989, the approach depth of water varied from 1.86 to 7.62 cm and the Froude number varied from 0.011 to 0.313. The experimental data in tabulated in Table 1 (Appendix A).

3.2.2 Comments of Symmetry of Scour

When the outlet openings were adjusted the jet of water from the constriction deflected towards the walls of the flume. This may have been caused by a slight pressure

difference between either side of the jet water. Due to this deflection, a symmetrical scour pattern could not be obtained. The deflection of water was minimized by placing galvanized metal plates of about 300 mm x 200 mm downstream of the flume. The direction and location of these plates varied with each experiment. The scour and ridges due to constriction were not affected by these plates because they were placed away from constriction.

In experiments with free fall, i.e. outlet pipes opened fully, a symmetrical scour pattern was always obtained without any adjustment of the flow downstream of the constriction.

3.2.3 Approach Velocity

In all experiments the mean velocity V_o was small. Thus a pitot tube or current meter could not be used to obtain the velocity profiles for the approach flow. The use of Hydrogen bubble technique also failed because of the reflection of the light on sand grains. Fiber optic probe light reduced the reflection of the light, but still the pulse created by the bubbles were not seen through the camera.

To obtain a velocity profile, an extra experiment was carried out with increased mean velocity. Even though scour depth at the constriction reached the tray of the flume, care was taken to see that the was no bed material movement in the approach section. Pitot tube was used to

measure the velocity profile because of the increased mean velocity. In this experiment the constriction ratio was 0.493, the approach depth of water was 3.66cm and the mean approach velocity was 22.73 cm/s.

3.3 EXPERIMENTAL RESULTS

3.3.1 Mean Velocity at Approach and at Constriction

Approach mean velocity V_0 was calculated from the equation,

$$V_0 = \frac{Q}{By_0} \qquad\qquad 3.2$$

where Q is the discharge, B is the channel bed width, and y_0 is the approach flow depth.

The mean velocity at the constriction V_1 was calculated from

$$V_1 = \frac{Q}{A_1} \qquad\qquad 3.3$$

where A_1 is the flow area at the constriction in the equilibrium state.

3.3.2 Bed Shear Stress

Using "law of the wall" equation

$$\frac{u}{u_*} = 5.75 \ \log\frac{y}{K} + C \hspace{3cm} 3.4$$

a plot u versus log y was prepared (Figure 5) and from the slope of this plot the shear velocity was computed and found to be equal to 1.88 cm/s. Using the following equation

$$\tau_o = u_*^2 \rho \hspace{3cm} 3.5$$

where τ_o is the bed shear, u_* is the shear velocity and ρ is the mass density of water,

the bed shear stress was calculated and found to be equal to 0.353 N/m².

3.3.3 Scour Ridge and Water Surface Profiles

Data of the experiments for scour, ridge and water surface were presented in graphical form. Profiles of scour and ridge along the channel centre for experiments 1111 to 1119, 1121 to 1126, 1131 to 1134, 1141 and 1221 were presented in the plots. Scour profiles along the line
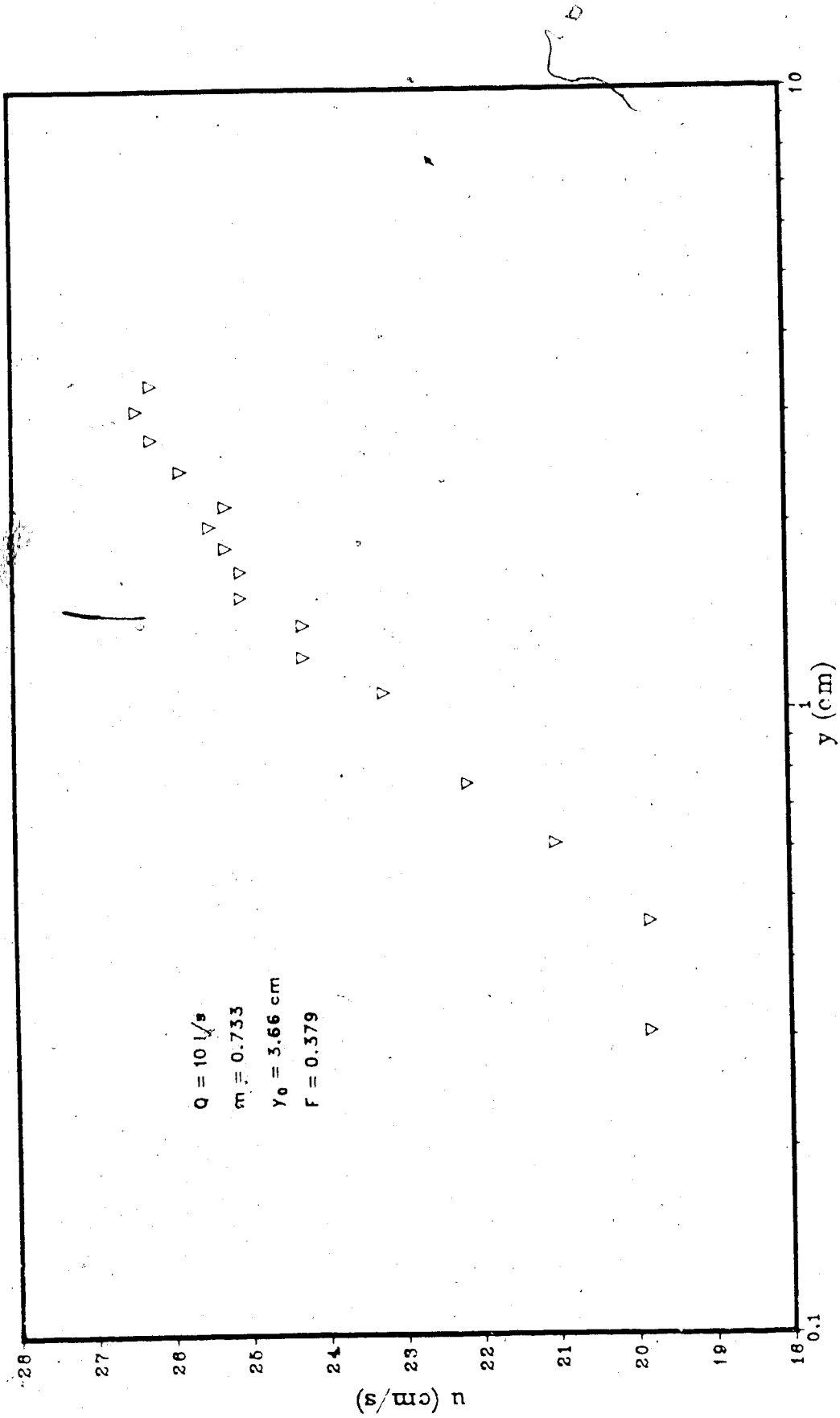
FIGURE 5 – APPROACH VELOCITY PROFILE

passing through the nose of the constriction for experiments 1111, 1114, 1118 to 11112, 1151 to 1153 and 1211 to 1212 were also presented in the plots. Typical plots are shown in Figures 6 and 7. In these Figures the location of the constriction is at x axis equals to zero. The negative and positive x values indicate the upstream and downstream of the experiments respectively. Similarly, the negative and positive y values indicate scour and ridge respectively. Figure 1 shows the direction of x,y,z axis.

Scour profiles across the constrictions and water surface profiles along the channel centre are also shown in respective plots. Typical plots are shown in Figure 8 and 9 respectively.

Additional plots for scour and ridge profiles along channel centre, scour profiles along the line passing through the nose of the constriction, scour profiles across constriction and water surface profiles at channel centre are presented in Appendix B.

3.3.4 Classification of Experiments

From the results, experiments were classified into three categories; namely,

    a) spur type constriction

    b) interference spur type constriction

    c) jet type constriction
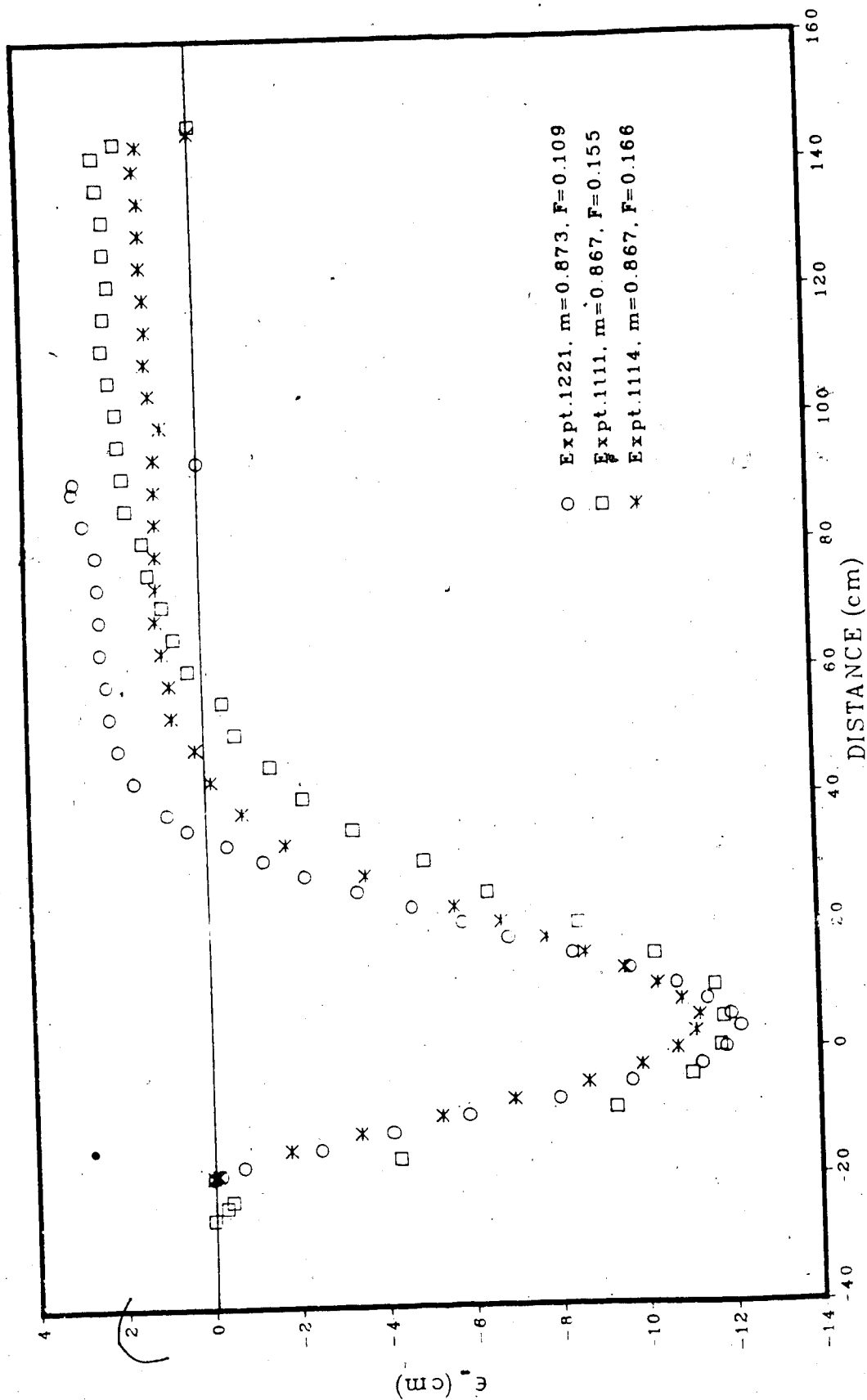
FIGURE 6 – SCOUR AND RIDGE PROFILES ALONG CHANNEL CENTRE

○ Expt.1221. m=0.873. F=0.109
□ Expt.1111. m=0.867. F=0.155
✳ Expt.1114. m=0.867. F=0.166

DISTANCE (cm)

ε (cm)
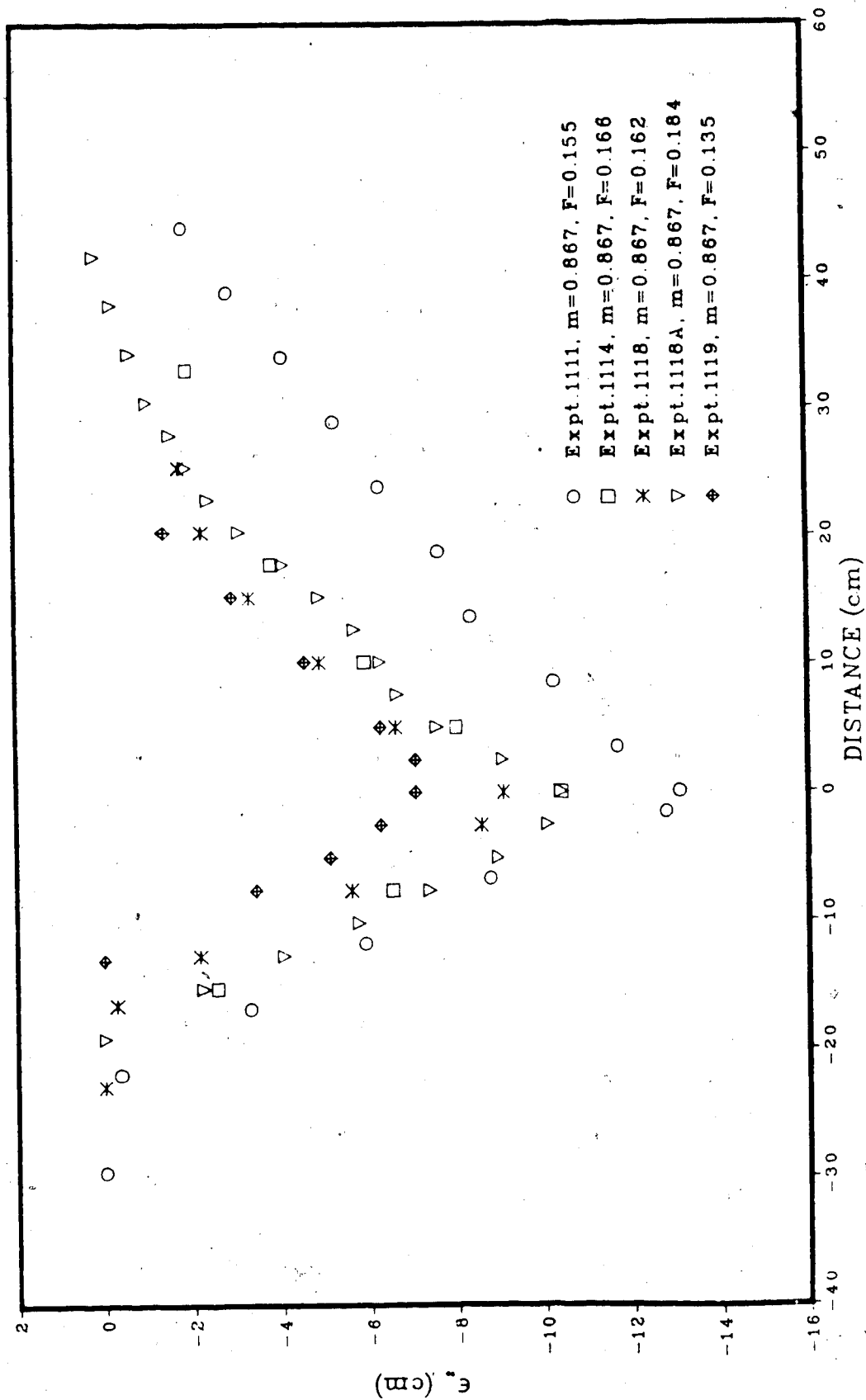
FIGURE 7 – SCOUR PROFILES ALONG THE LINE PASSING THROUGH THE NOSE OF CONSTRICTION
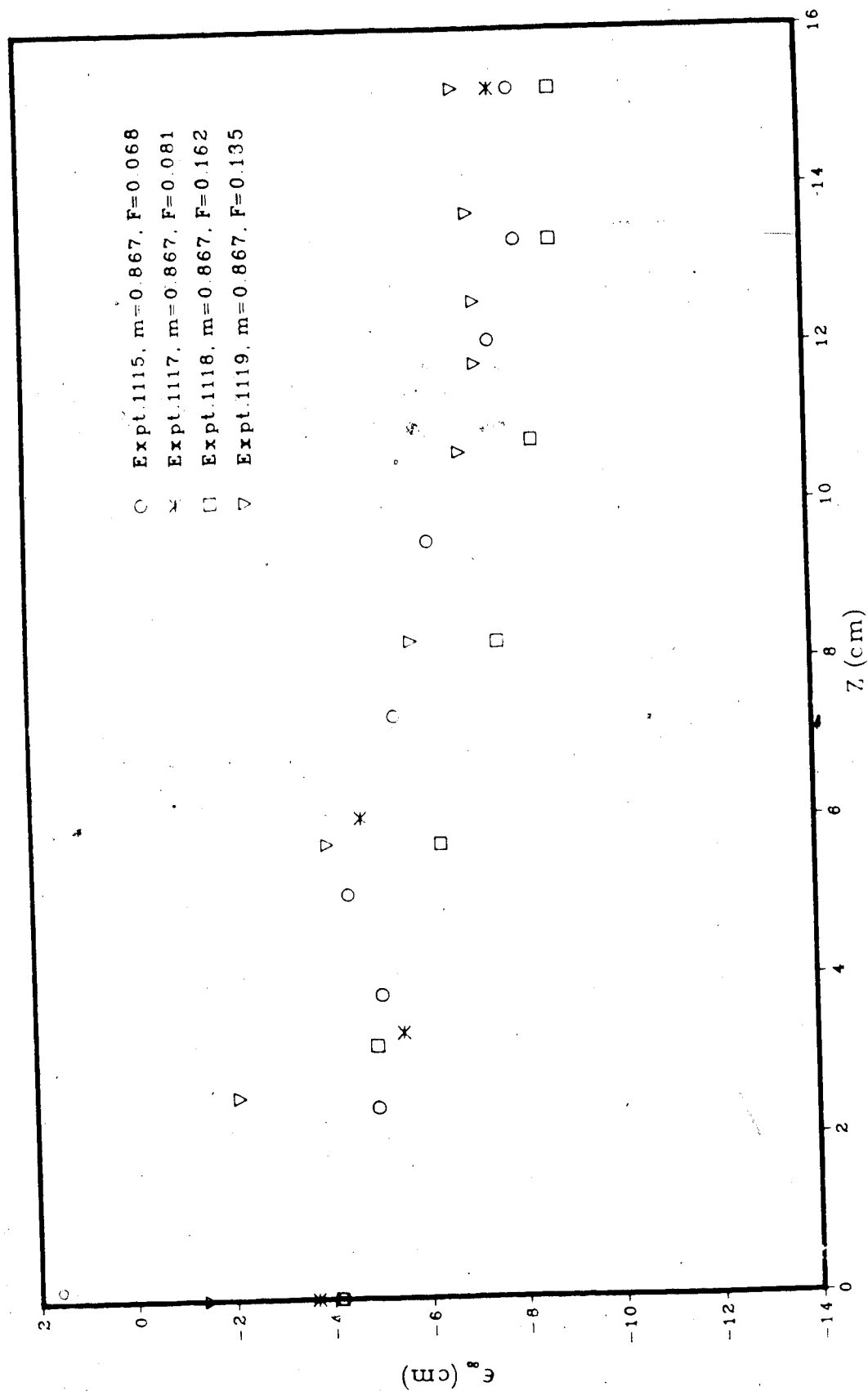
FIGURE 8 – SCOUR PROFILES ACROSS THE CONSTRICTION; X = 0
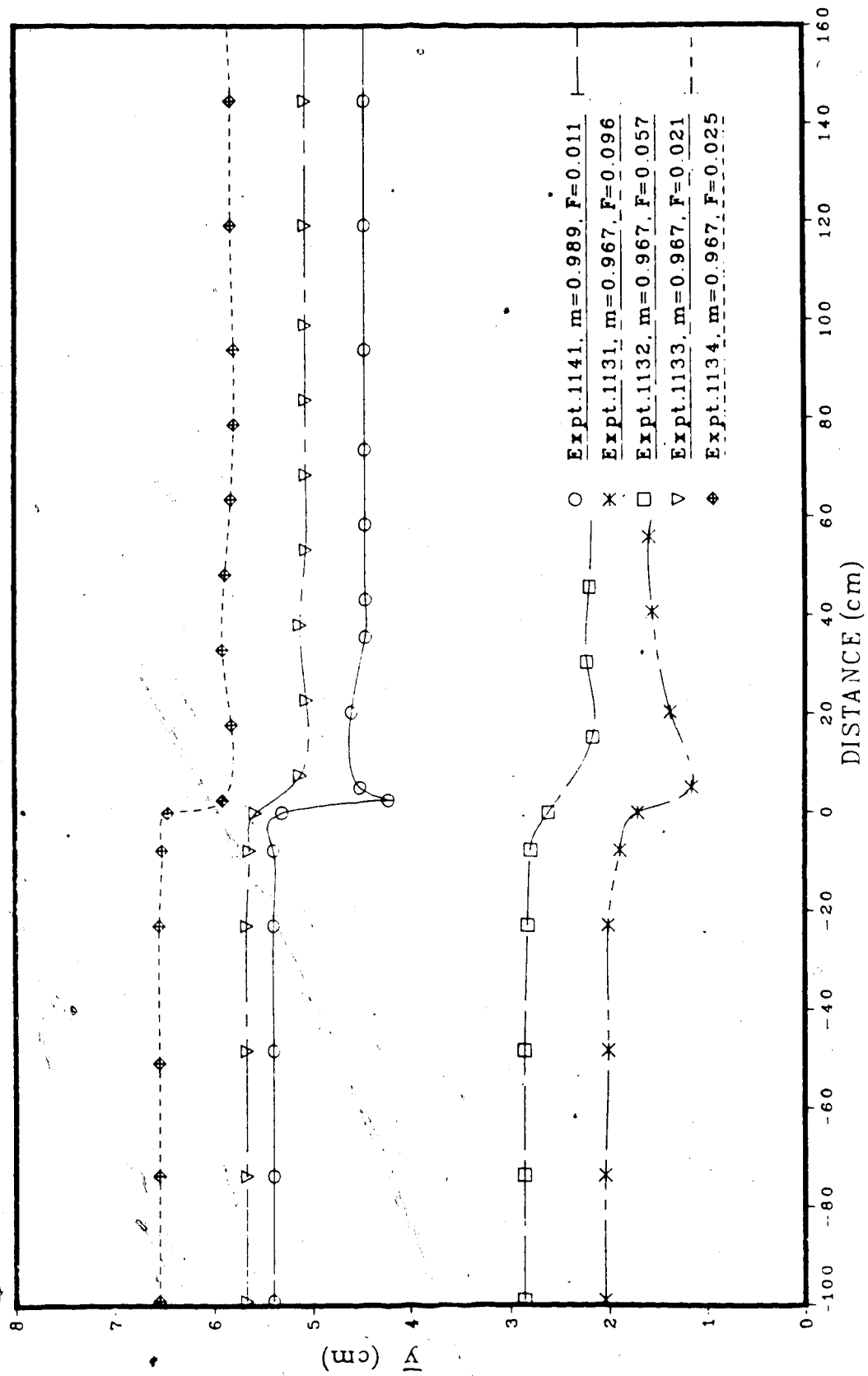
FIGURE 9 — WATER SURFACE PROFILES ALONG CHANNEL CENTRE

Expt.1141, m=0.989, F=0.011

Expt.1131, m=0.967, F=0.096

Expt.1132, m=0.967, F=0.057

Expt.1133, m=0.967, F=0.021

Expt.1134, m=0.967, F=0.025

a) Spur type constriction - There is no alteration in the shape of the stream lines near the center of the constriction but adjacent to each nose of the constriction lines are bent and close together. This indicates that the flow is concentrated near the noses. Thus, the scour occurs around each nose of the constriction. The scour act independently to each other and feels as the other end of the constriction does not exist. That is, the scour width at each end of the constriction across the constriction does not meet at each other. Plate I indicates this clearly. The maximum scour occurs at the nost of the constriction. The spur constriction is termed as constriction type I.

b) Interference spur type constriction - The stream lines are bent and close together near each nose of the constriction. The lines near the centre are also affected by these bends. This indicates that the flow is concentrated adjacent to the nose and lesser extent around the centre. Thus, across the constriction, the scour at each end of the constriction interferes at the other end. Due to this interference there will be always scour at the centre of constriction. This is shown in Plate II. In most cases the maximum scour occurs at or near the nose of constriction. The interference spur constriction is termed as
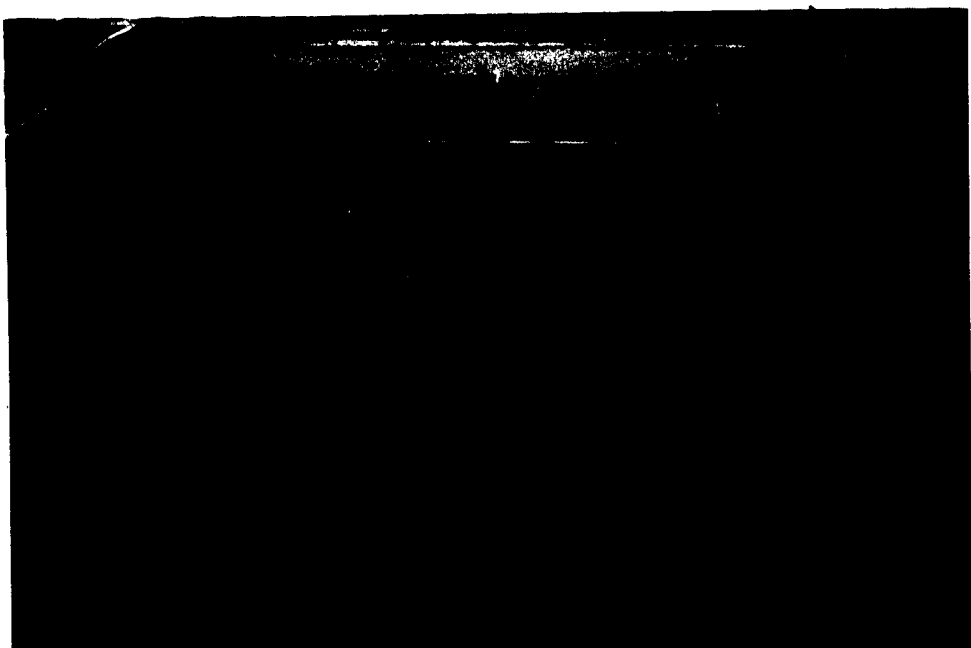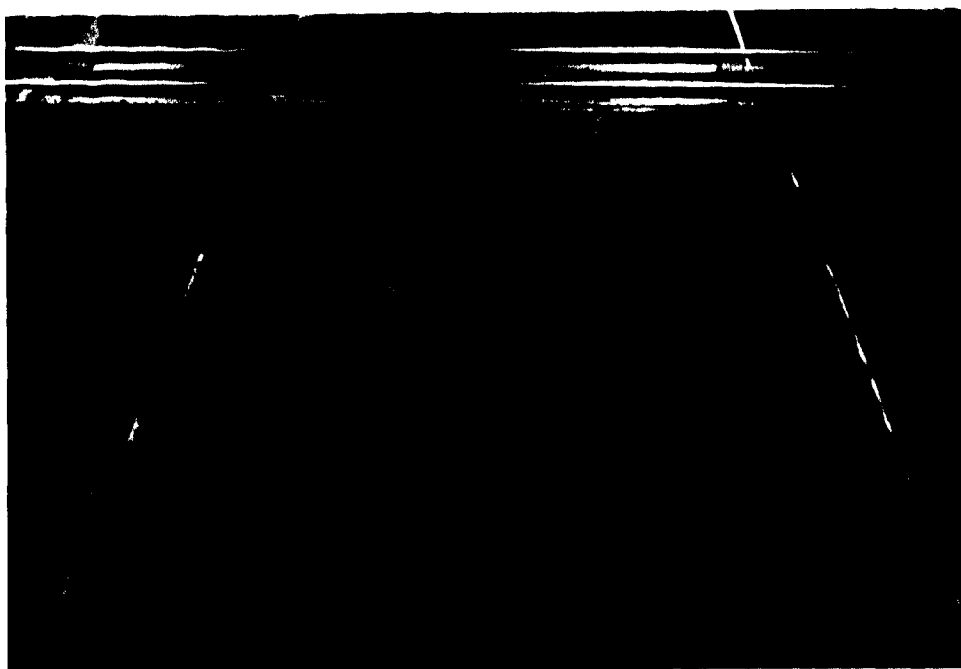
PLATE 1 – TYPICAL OF CONSTRICTION TYPE I
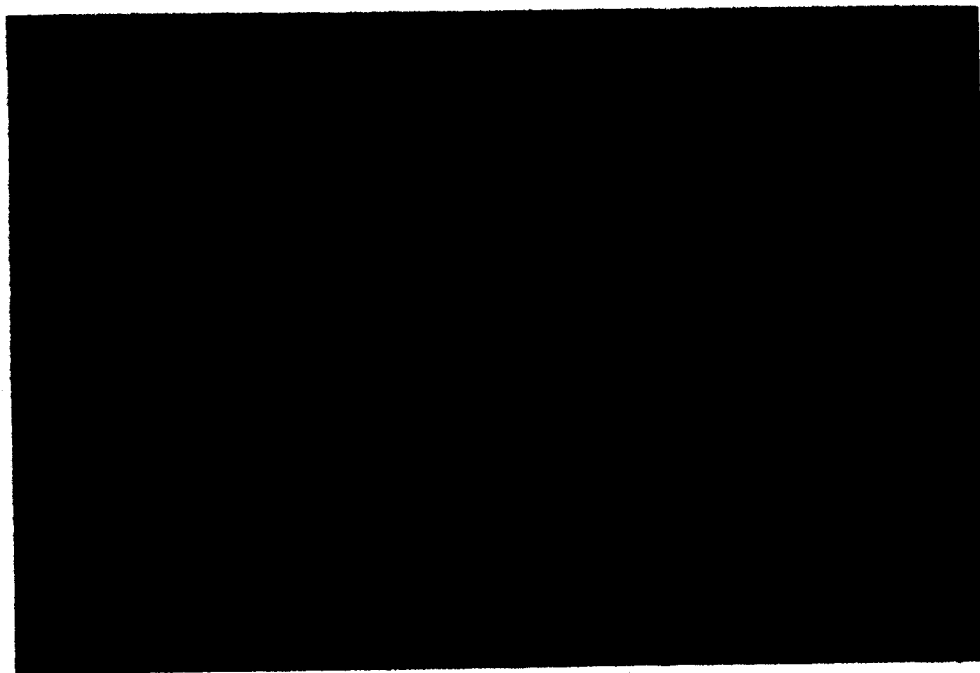
PLATE 2 -- TYPICAL OF CONSTRICTION TYPE II

constriction type II.

c) Jet type constriction - The constriction opening is
    generally very small. Thus, the velocity along the
    constriction opening is almost same. This makes the
    maximum scour to occur along the center line. Plate
    III shows a typical profile of this type. Jet
    constriction is termed as constriction type III.

Experiment numbers 11110, 11111, 11112, 1151, 1152,
1153, 1211, and 1212 fall into constriction type I,
experiment number 1141 falls into constriction type III and
others fall into constriction type II.
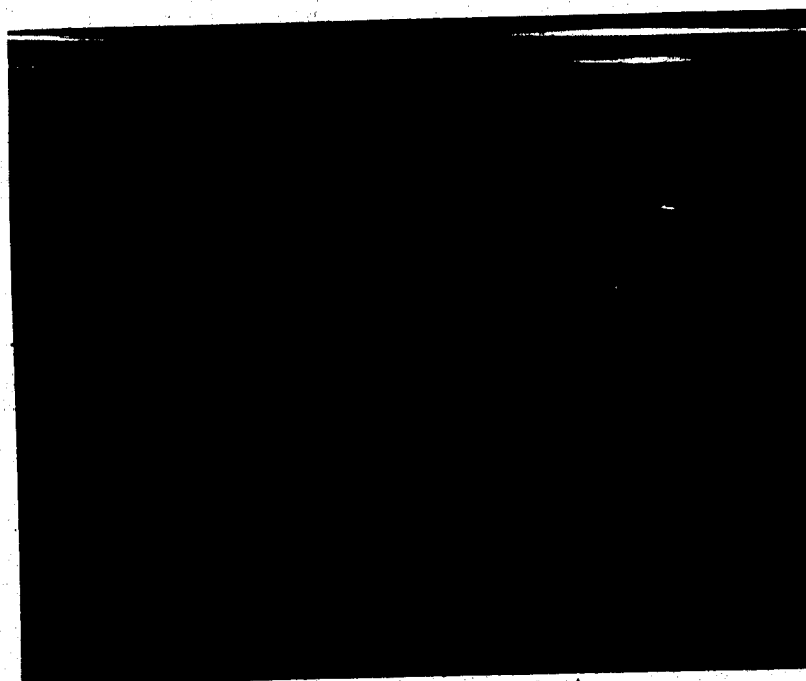
PLATE 3 – TYPICAL OF CONSTRICTION TYPE III

4. ANALYSIS OF EXPERIMENTAL RESULTS AND DISCUSSION

This chapter presents the analysis of the results and discussion. From dimensional considerations, a design chart to estimate the maximum clear water scour at constrictions is developed. The pattern of the scour development is also discussed. A brief study on backwater was also presented. A comparison of the results with regime theory concept is also included.

4.1 VELOCITY PROFILE

The velocity profile plot, Figure 5, indicates that the flow was fully developed upstream of the constriction. The non dimensional profile plot shows that it satisfies the Karman-Prandtl logarithmic law. From Figures 10 and 11, the following equations were obtained,

$$\frac{u}{u_*} = 5.75 \log\frac{y}{K_s} + 8.85 \qquad 4.1$$

and,

$$\frac{u}{u_*} = 5.75 \log\frac{y u_*}{\nu} + 5.87 \qquad 4.2$$
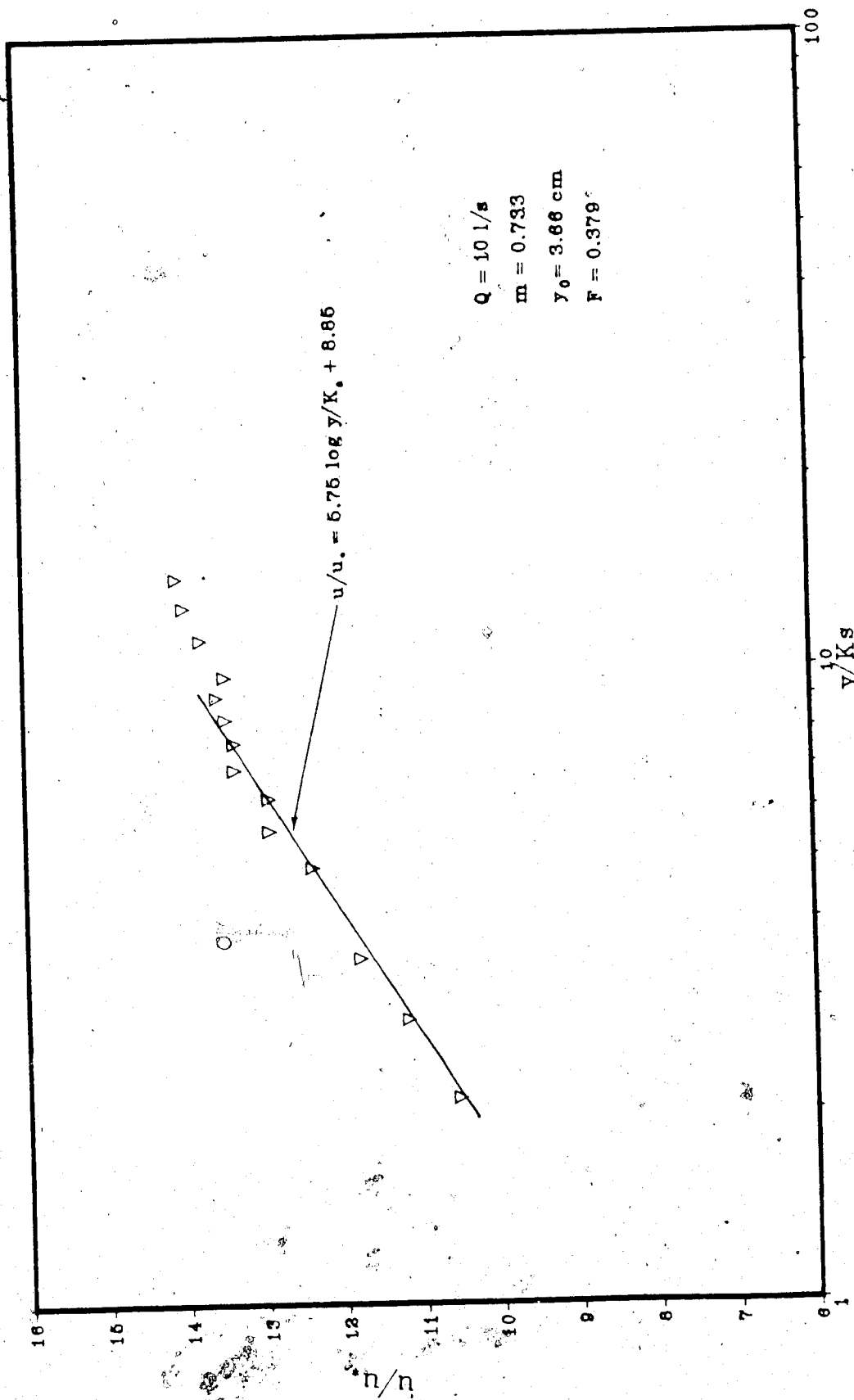
FIGURE 10 — NON–DIMENSIONAL VELOCITY PROFILE
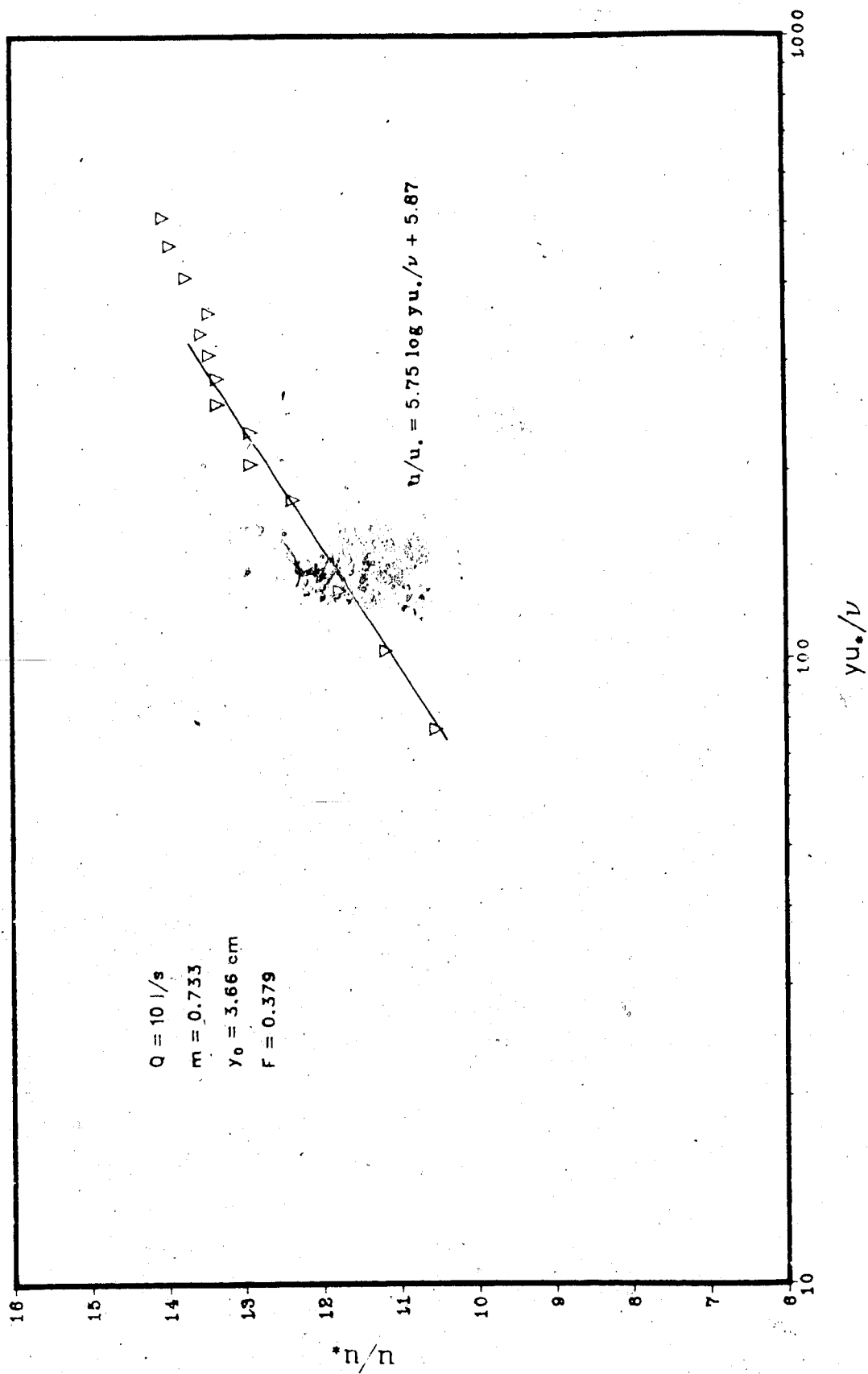
FIGURE 11 — NON–DIMENSIONAL VELOCITY PROFILE

$u/u_* = 5.75 \log y u_*/\nu + 5.87$

$Q = 10 \; l/s$

$m = 0.733$

$y_0 = 3.66 \; cm$

$F = 0.379$

yu_*/ν

u/u_*

where u is the approach velocity at y cm above the channel bed, u_* is the shear velocity, ν is the kinematic viscosity of water.

The ratio of bed shear stress to critical shear stress of bed material is 0.24, which indicates the bed materials in approach section were not in motion. Thus, the scour at constriction was clear water scour.

4.2 MAXIMUM CLEAR WATER SCOUR

It is reasonable to consider that the velocity at constriction causes the scour. To predict the velocity at constriction on an erodable bed is a difficult task.

Let us define a characteristic velocity V_* at constriction as Q/by_o, where all three parameters are known. This velocity will be referred to as the velocity scale.

4.2.1 Dimensional Analysis

From previous studies and our observations, the main variables causing clear water scour can be grouped into four categories, namely

a) Variables describing the constriction and channel geometry

channel width   B

constriction opening   b

b) Variables describing the flow

velocity scale	V_*
approach flow depth	y_0
maximum scour depth at	
equilibrium state	$\epsilon_{m\infty}$

c) Variables describing the fluid (water)

mass density	ρ
kinematic viscosity	ν

d) Variables describing the sediment

median size	D
mass density	ρ_s

Considering the equilibrium state, we can write

$$\epsilon_{m\infty} = f\left[V_*, \; y_0, \; \rho, \; g\Delta\rho, \; \nu, \; D, \; (B-b), \; B \right] \qquad 4.3$$

Choosing V_*, y_0, and ρ as repeating variables,

$$\frac{\epsilon_{max}}{y_0} = f_1 \left[\frac{V_*}{\sqrt{g(\Delta\rho/\rho)D}}, \frac{V_* y_0}{\nu}, \frac{(B-b)}{B}, \frac{y_0}{D}, \frac{B}{y_0} \right] \qquad 4.4$$

So long as B/y_0 is very large, it will not be an important parameter. Similarly, as long as y_0/D is very large, it appears that it will not be important. If the Reynolds number $V_* y_0^*/\nu$ is also very large, it is assumed to be of secondary importance. Then equation 4.4 may then be reduced to,

$$\frac{\epsilon_{max}}{y_0} = f_2 \left[F_* = \frac{V_*}{\sqrt{g(\Delta\rho/\rho)D}}, \quad m = \frac{B-b}{B} \right] \qquad 4.5$$

4.2.2 Classification of Experiments

Using constriction ratio and non-dimensional velocity scale, an attempt was made to prepare a chart (Figure 12) to draw a dividing line to separate Type I (spur) from Type II (interference spur) constrictions. Experiments on a constriction ratio of 0.867 gave a reasonable location of a point to draw the dividing line from constriction ratio of to 0.867. This is shown in Figure 12 by dashed lines. Additional experiments have to be carried out to complete this Figure.

constriction Type II

constriction Type I

○ Present work, interference spur
□ Present work, interference spur
✳ Present work, interference spur
▽ Present work, jet
◆ Present work, interference spur
◇ Present work, spur
▨ Present work, spur
⊕ Present work, spur
+ R.J.Garde 1961, spur
⊞ M.A.Gill 1972, spur
⊠ B.A.Nwachukwu 1980, spur
● H.K.Liu 1961, spur

m

F

FIGURE 12 -- STUDY ON SEPARATING CONSTRICTION TYPE I FROM TYPE II

4.2.3 Visual Observations of Scour Development

At the beginning in all experiments, a spiral type vortex was formed at the nose of the constriction. This caused the bed materials to move from the nose. The motion of the materials was mainly by rolling.

In the early stage, the eroded particles were piled up downstream of the scour hole and then pushed further as the scour progressed. Thus some bed zones moved from deposition to scour. The deposited particles eventually moved and were spread by the expansion of the jet. As the scour hole deepened, the bed particles from upstream and side slopes fell into the hole and then these particles were carried away downstream. The initial process of scour was rapid and then began to slow down. It indicates that as the scour depth increases the rate of scouring decreases. The rate of increase in scour depth was minimal after 4 to 6 hours. This could be seen in Figure 13, which is drawn with scour depth versus time.

As scour proceeded it expanded transversely and longitudinally. For smaller constriction ratios, the scour widths at constriction along transverse direction did not meet each other. The constriction ratio equal to 0.867 also behaved similarly when the discharge was low. When the discharge intensity was increased and the depth of water was kept constant, the scour widths met each other. For constriction ratios higher than 0.867, the scour widths met each other even for lesser discharges. A typical section is
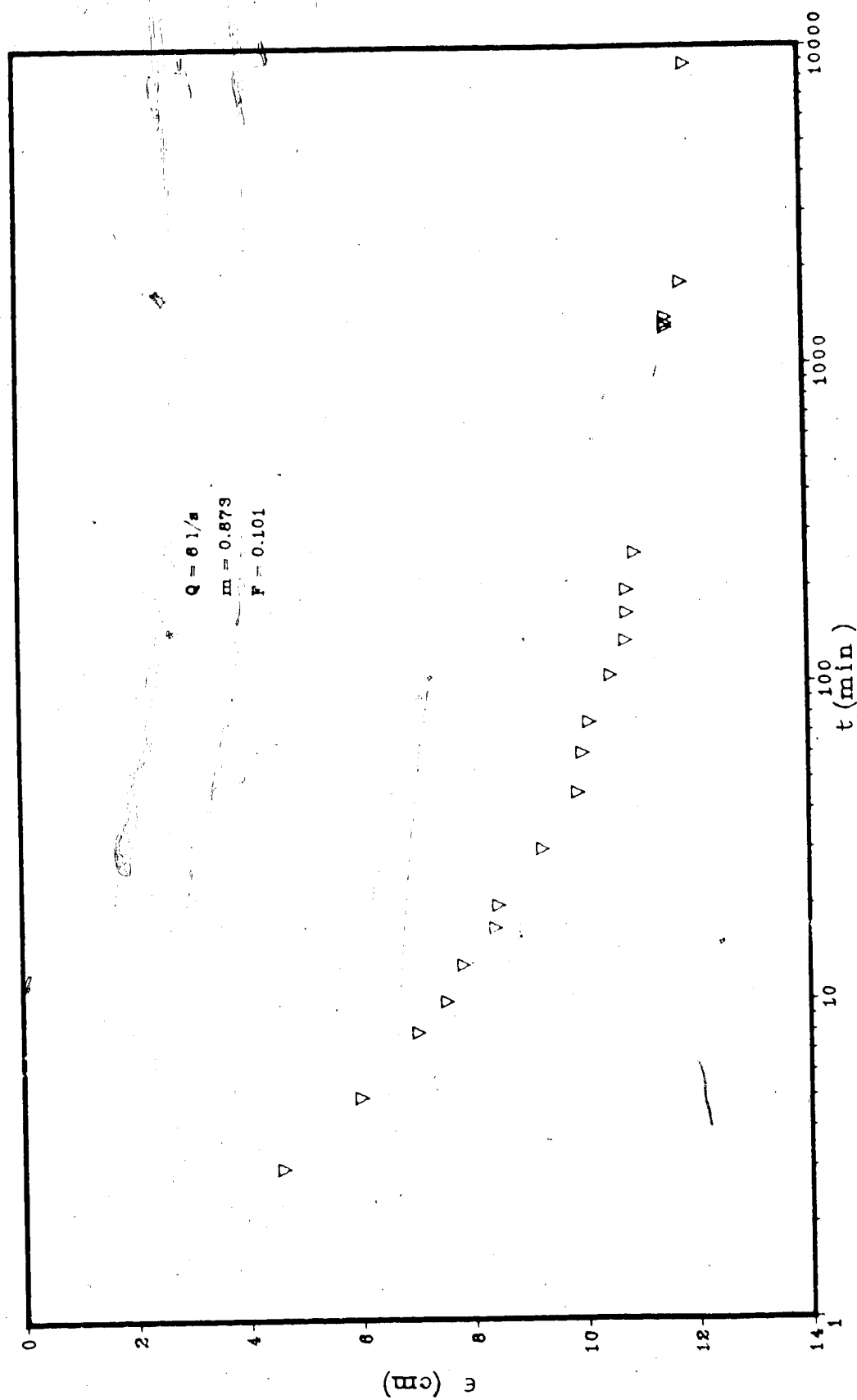
FIGURE 13 — VARIATION OF CLEAR WATER SCOUR DEPTH WITH TIME AT X = 0, Z = 0

shown in Figure 14 which shows the degree of interference of
each scour hole width by the indication of scour depth at
the centre of constriction. Additional Figures are
presented in Appendix B.

4.2.4 Location of Maximum Scour

For most of the experiments the maximum scour was at or
near the nose of constriction. For constriction type III,
the maximum scour was found to be downstream and along the
channel centerline.

Das (1972) concluded that the maximum scour was at
vena-contracta for clear water and sediment transporting
flow for end-dump closure. Das's constriction was different
from the present work because it was not an abrupt type
constriction. It was self formed and the flow made the ends
of constriction to form a curve (similar to a bell-mouth
opening) which created smoothed stream lines.

Garde et al. (1961), Liu et al. (1961), and Nwachukwu
(1980) concluded that maximum scour would occur at the nose
of spur type constriction. Laursen (1953) stated that the
deepest scour would occur adjacent to the upstream corner of
abutments and the shape of the abutment affects the scour to
a lesser extent.

Figure 15 shows the location of maximum scour measured
along the channel centre and from constriction type I. From
this diagram, the path of the maximum scour for spur type
constriction can be found.
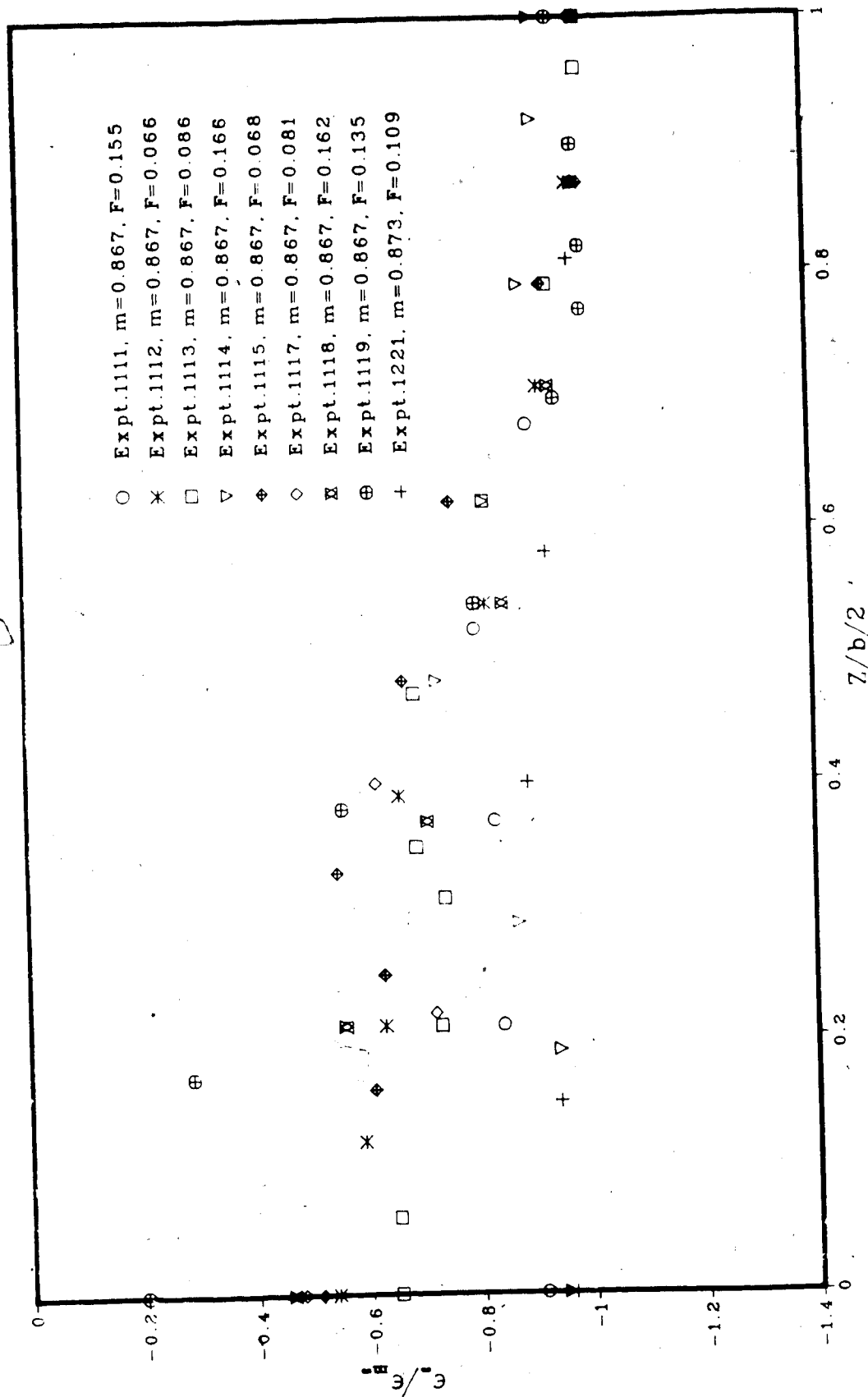
FIGURE 14 -- NON-DIMENSIONAL SCOUR PROFILES ACROSS CONSTRICTION
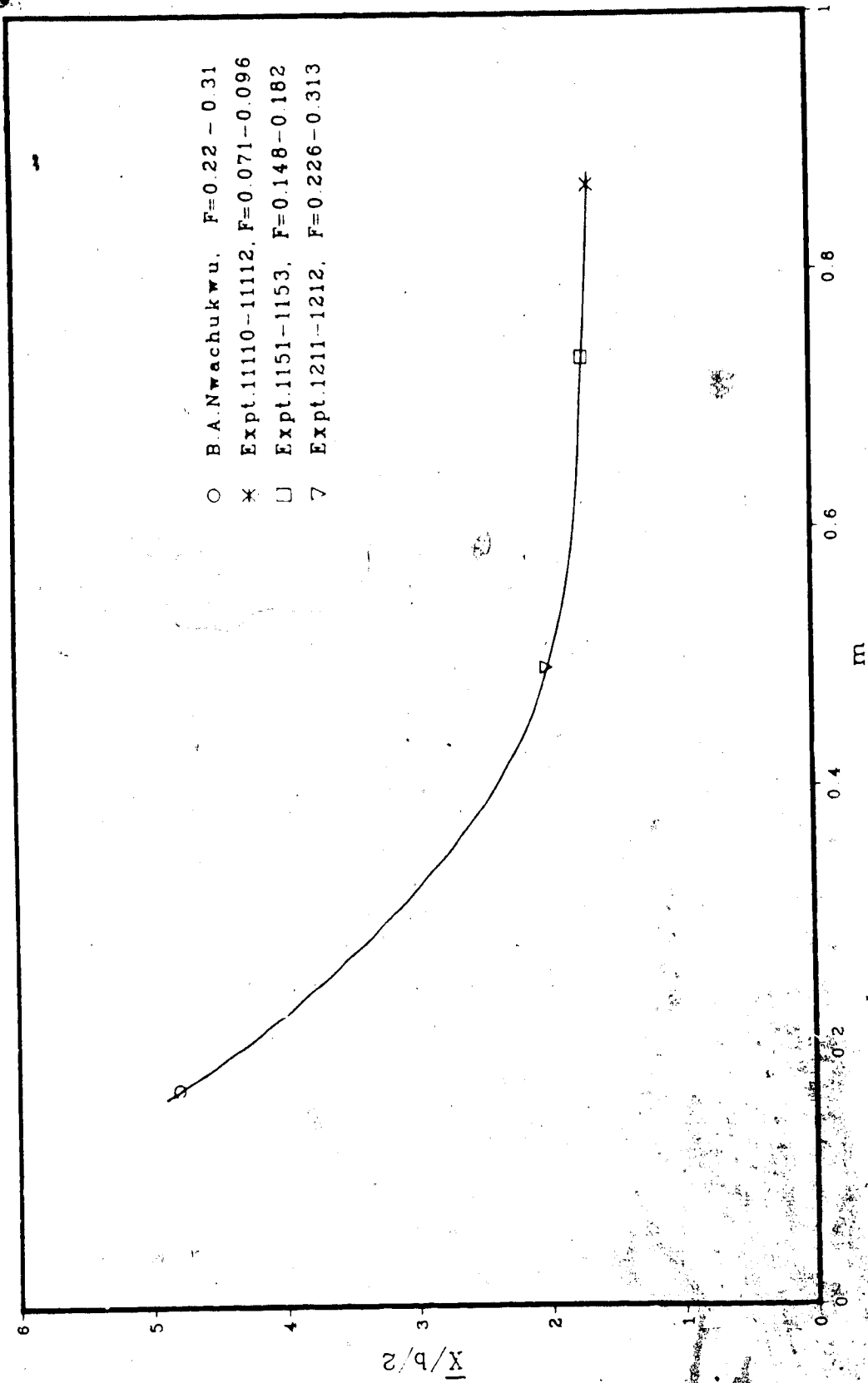
FIGURE 15 – LOCATION OF MAXIMUM SCOUR MEASURED ALONG CHANNEL CENTRE AND FROM CONSTRICTION TYPE I

Legend:

○ B.A. Nwachukwu.   F=0.22 – 0.31
✳ Expt.11110–11112.   F=0.071–0.096
▢ Expt.1151–1153,   F=0.148–0.182
▽ Expt.1211–1212.   F=0.226–0.313

Y-axis: $\overline{X}/b/2$

X-axis: m

4.2.5 Similarity in Scour

Longitudinal scour and ridge profiles along channel centre and at the nose of constriction show a similar trend of scour pattern to each other.

Let X_1 be the upstream length of scour hole from the constriction to the lip of the scour hole for constriction type II. A plot (Figure 16) was prepared for the upstream scour length versus maximum scour depth at channel center and from this plot the following relationship was developed as

$$\frac{X_1}{\epsilon_{mc\infty}} = 1.85 \qquad\qquad 4.6$$

Similarly, let X_2 be the upstream length of scour hole from the constriction to the lip of the scour hole for constriction type I. A plot (Figure 17) was prepared with X versus the maximum scour depth. From this Figure a similar relationship was developed as follows

$$\frac{X_2}{\epsilon_{m\infty}} = 1.75 \qquad\qquad 4.7$$

The upstream slope at channel centre and constriction makes an average angle of $28°$ and $30°$ respectively to the
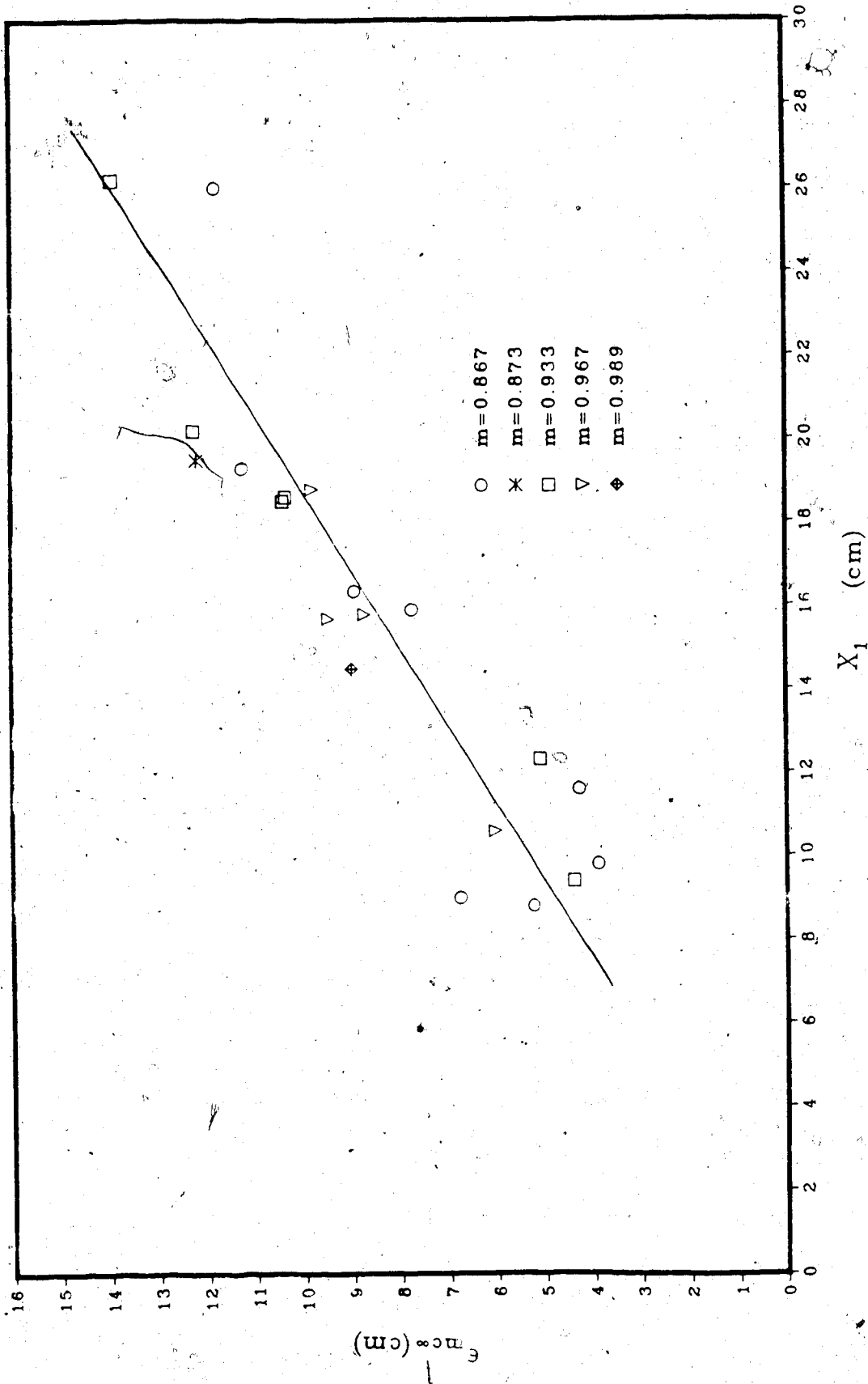
FIGURE 16 — MAXIMUM CLEAR WATER SCOUR VERSUS UPSTREAM
SCOUR HOLE LENGTH — CONSTRICTION TYPE II
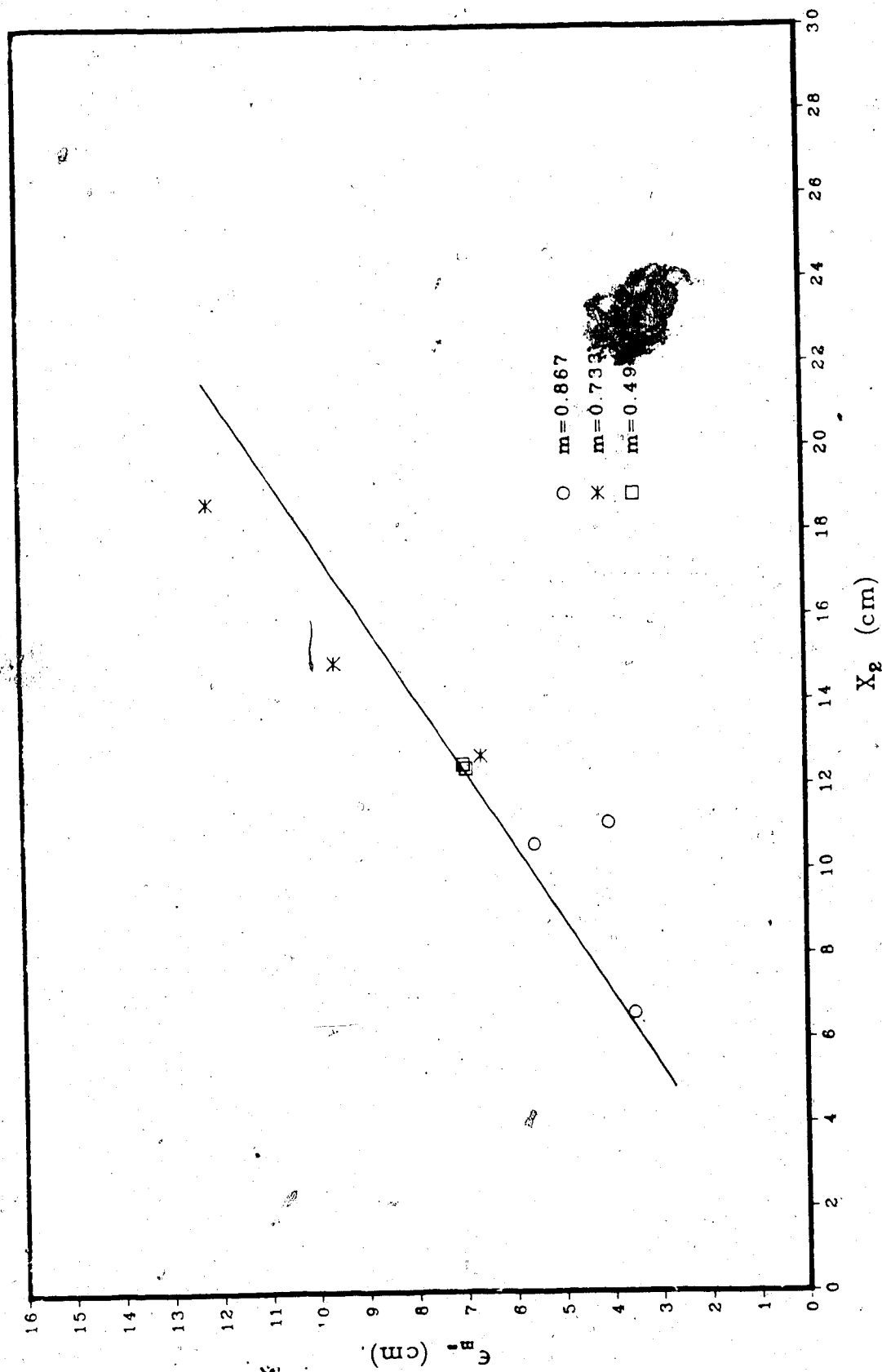
FIGURE 17 – MAXIMUM CLEAR WATER SCOUR VERSUS UPSTREAM
SCOUR HOLE LENGTH – CONSTRICTION TYPE I

horizontal. Let Z_1 is the scour hole width from the nose of the constriction to the lip of scour hole measured along the transverse direction. A plot was prepared with Z_1 versus maximum scour depth and is shown in Figure 18. From this Figure, an average value of $Z_1/\epsilon_{m\infty}$ was found to be 2. Laursen found this to be 2.75 and Garde et al. stated that it varies from 1.8 to 5.0.

Let X' be the length equal to the distance from the constriction to a point where the scour depth is equal to half the maximum scour depth at channel center for constriction type II. This was used as length scale for x axis and the maximum depth at channel center was used as length scale for y axis. Figure 1 shows the location of X' with respect to the constriction. Typical non-dimensional scour profile is shown in Figure 19.

Similarly for constriction type I, typical non-dimensional scour profile along the line passing through the nose of the constriction is shown in Figure 20. In this, let X" be the length equal to the distance from the constriction to a point where the scour depth is equal to half the maximum scour depth and this is used as x axis length scale. The maximum scour depth is used as length scale for y axis.

Additional Figures of non-dimensional scour profiles for Type I and II constrictions are presented in Appendix B.
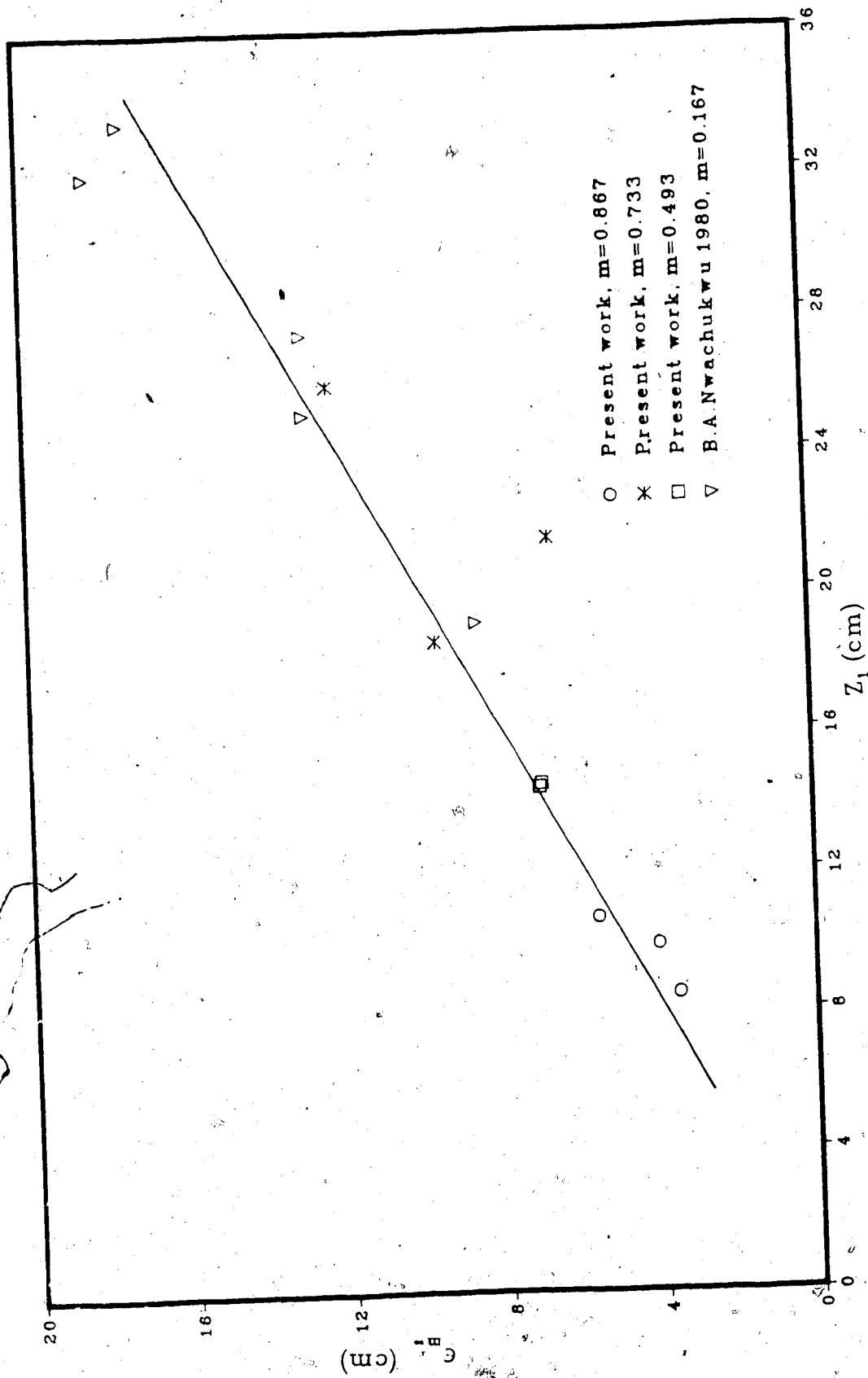
FIGURE 18 – MAXIMUM CLEAR WATER SCOUR VERSUS TRANSVERSE
SCOUR WIDTH -- CONSTRICTION TYPE I

Legend:

O   Present work, m=0.867
*   Present work, m=0.733
□   Present work, m=0.493
▽   B.A. Nwachukwu 1980, m=0.167

Axes: Z_1 (cm) (horizontal), ε_B (cm) (vertical)
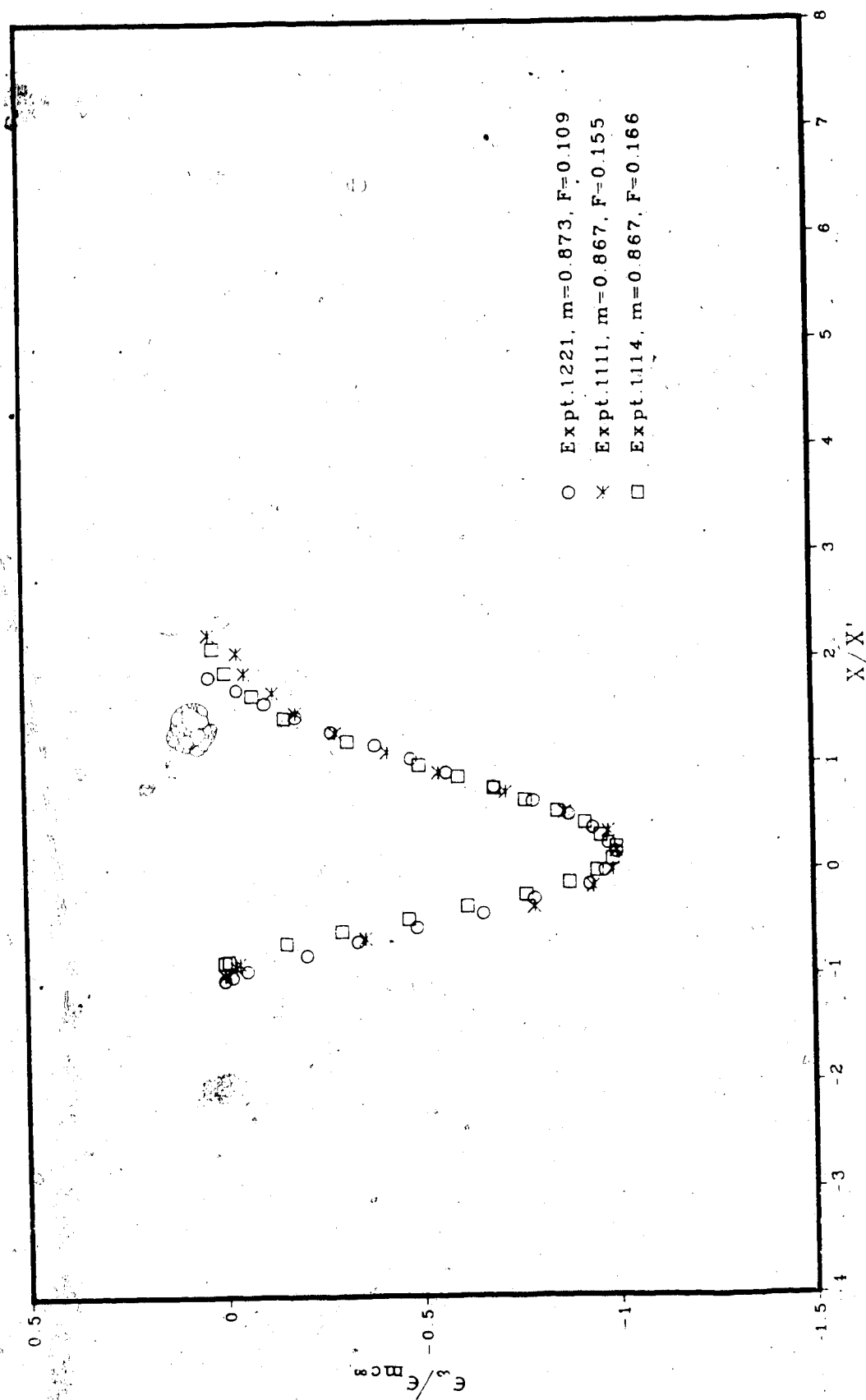
FIGURE 19 – NON–DIMENSIONAL SCOUR PROFILES ALONG CHANNEL CENTRE
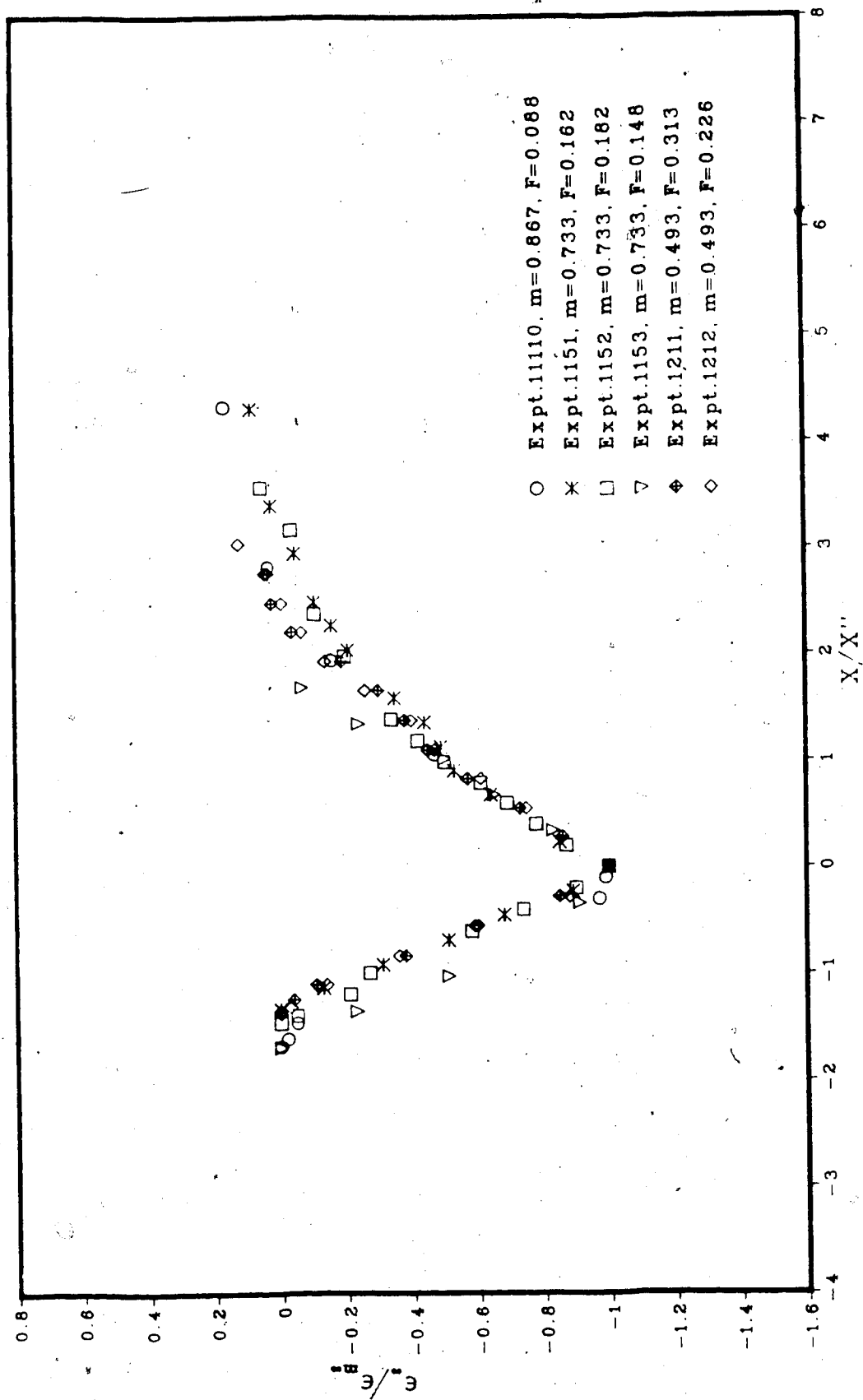
Legend:
- ○ Expt.1221, m=0.873, F=0.109
- ✳ Expt.1111, m=0.867, F=0.155
- □ Expt.1114, m=0.867, F=0.166

Axes: $\epsilon_s/\epsilon_{mc\infty}$ vs X/X'

FIGURE 20 – NON–DIMENSIONAL SCOUR PROFILES ALONG THE
LINE PASSING THROUGH THE NOSE OF CONSTRICTION

FIGURE 20 – NON–DIMENSIONAL SCOUR PROFILES ALONG THE
LINE PASSING THROUGH THE NOSE OF CONSTRICTION

Relationship's for X' and X" are established from Figures 21 and 22 and they are,

a) constriction type II,

$$\frac{X'}{b/2} = 0.69 \left[\frac{X_1}{b/2} \right] + 0.2 \qquad 4.8$$

b) constriction type I,

$$\frac{X''}{X_2} = 0.72 \qquad 4.9$$

It is possible to work out an aerial extent of the scour using the Figures and length scales discussed in this Section.

4.2.6 Design Charts

A non-dimensional plot (Figure 23) was prepared for spur type constrictions from the present work and studies of Garde et al. (1961), Liu et al. (1961), Gill (1972), Nwachukwu (1980) relating the maximum scour depth $\epsilon_{m\infty}$, approach depth of water y_o and non-dimensional velocity scale
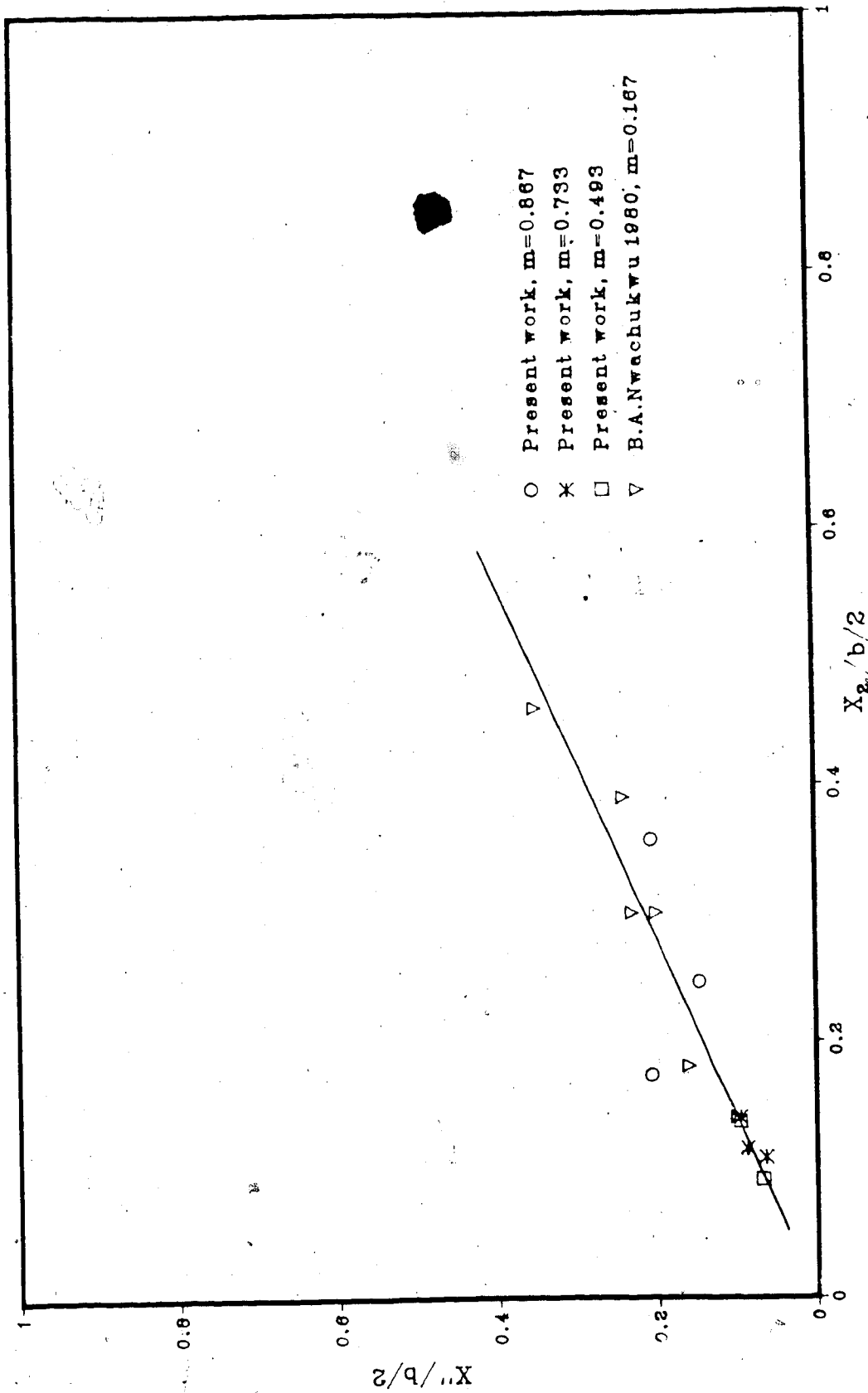
FIGURE 21 – SCALE OF SCOUR PROFILES FOR CONSTRICTION TYPE II

Legend:
○ Present work, m=0.867
✳ Present work, m=0.733
□ Present work, m=0.493
▽ B.A.Nwachukwu 1980, m=0.187

X-axis: $X_{2o}'/b/2$
Y-axis: $X''/b/2$
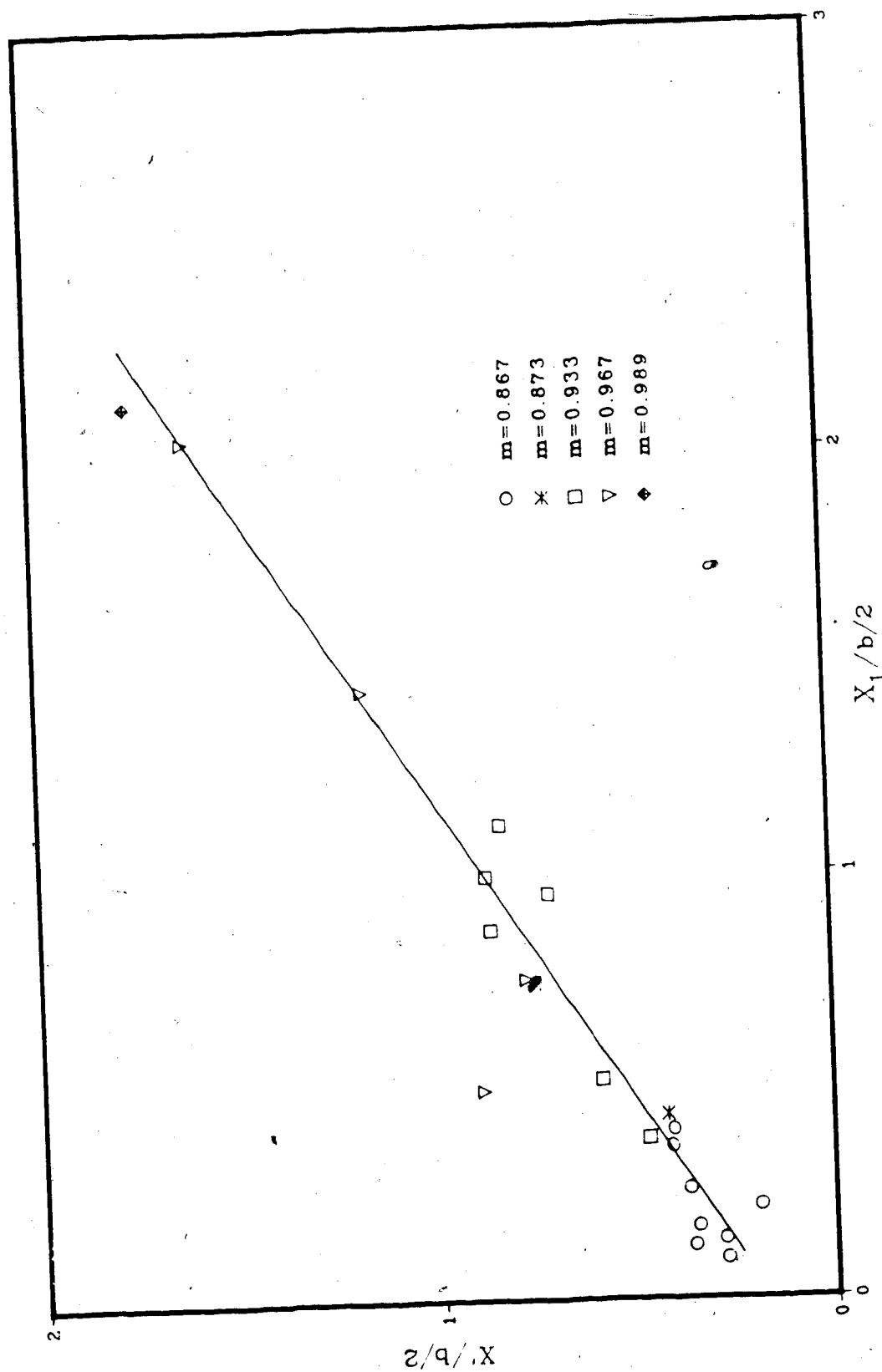
FIGURE 22 – SCALE OF SCOUR PROFILES FOR CONSTRICTION TYPE I
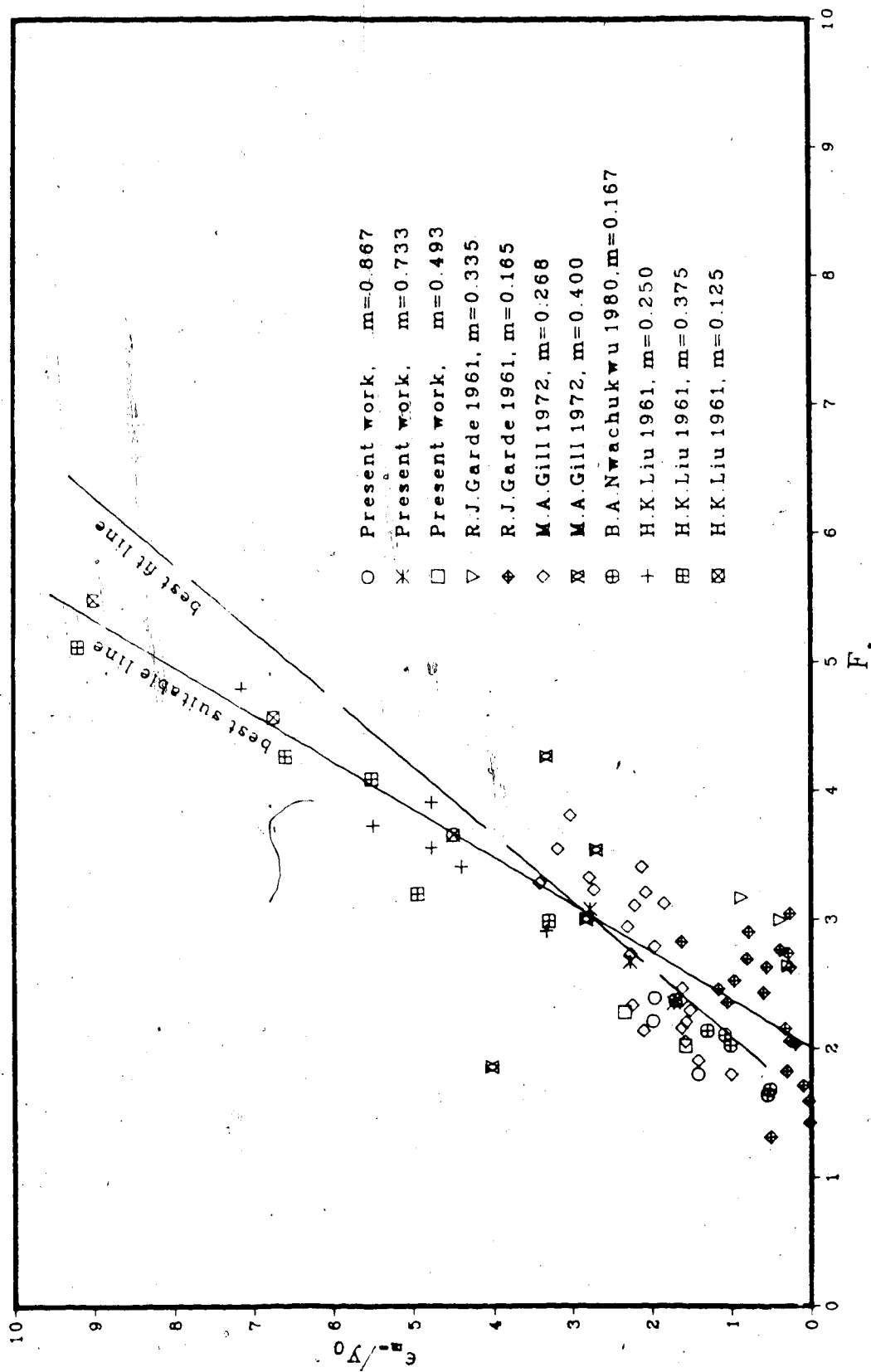
FIGURE 23 — MAXIMUM CLEAR WATER SCOUR — CONSTRICTION TYPE I

V_*. In this plot, the best fit line which was obtained by linear regression is drawn in dashed line and the most suitable line which was considered appropriate from visual inspection of the data, is drawn as a solid line. Similar plots for Type II (interference spur) constrictions were prepared for the maximum scour and maximum scour at channel center respectively. These plots are presented in Figures 24 and 25. Data for Figures 23 to 25 are tabulated in Table 2 and is presented in Appendix A.

A non-dimensional design chart (Figure 26) was prepared using Figures 23 and 24. The non-dimensional plot which was developed by Rajaratnam and Diebel (1981) for estimating the maximum scour for jet type constriction is also included in the chart. From this chart, the maximum scour depth could be estimated for constriction type I (spur), type II (interference spur) and type III (jet), if the approach depth of water, constriction opening, discharge, mass density of water and median size of sand grain are known.

4.3 STUDY OF THE RIDGE

A diagram was prepared for non-dimensional crest of ridge versus non-dimensional velocity scale and is shown in Figure 27. This Figure indicates that for F_* ranges from 2 to 6, the data for ridge crest are scattered badly and for F_* greater than 6, the non-dimensional crest of ridge appears to reach a constant value of 0.57. Similar experiments with increased F have to be carried out to confirm this. Data
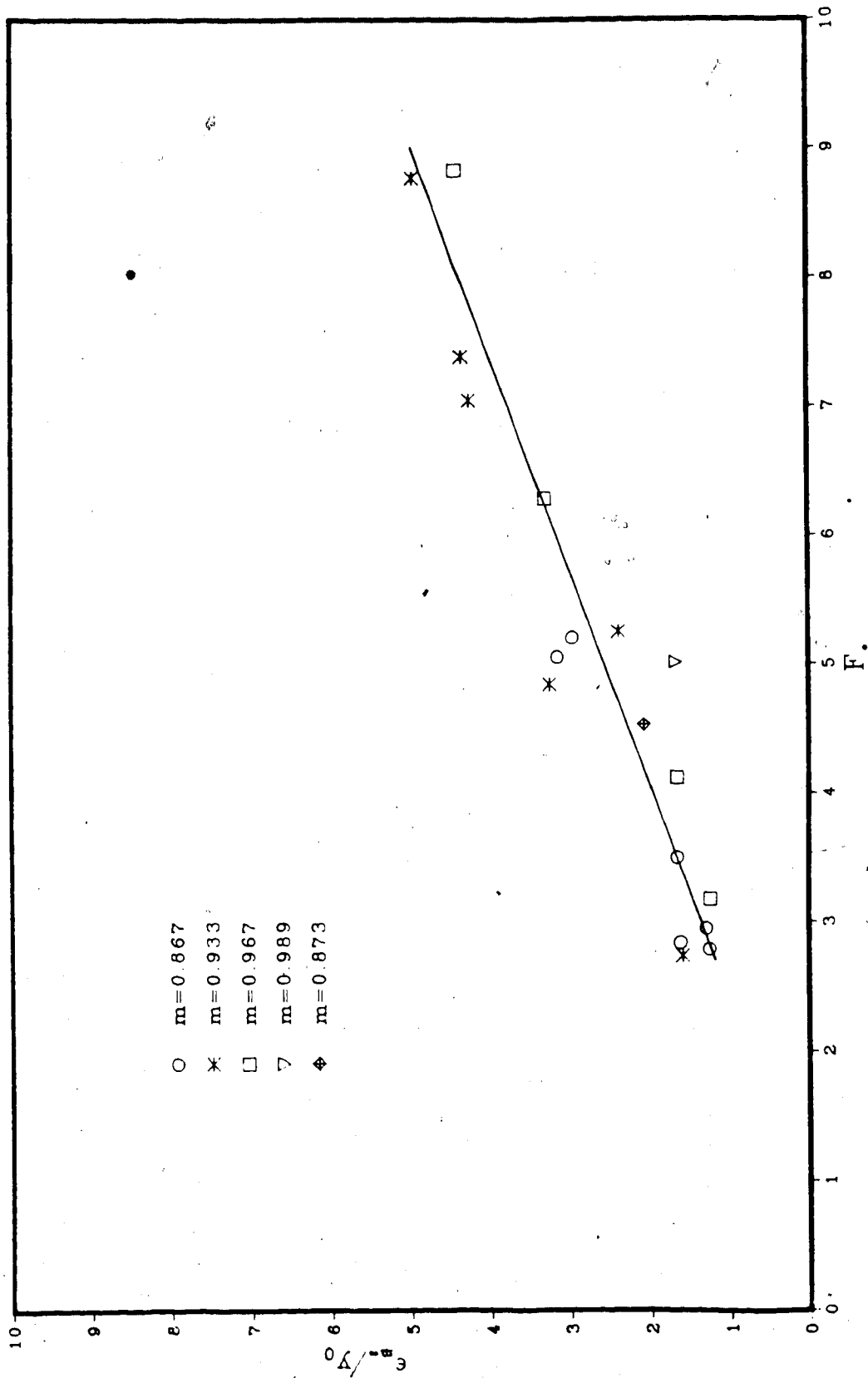
FIGURE 24 — MAXIMUM CLEAR WATER SCOUR — CONSTRICTION TYPE II
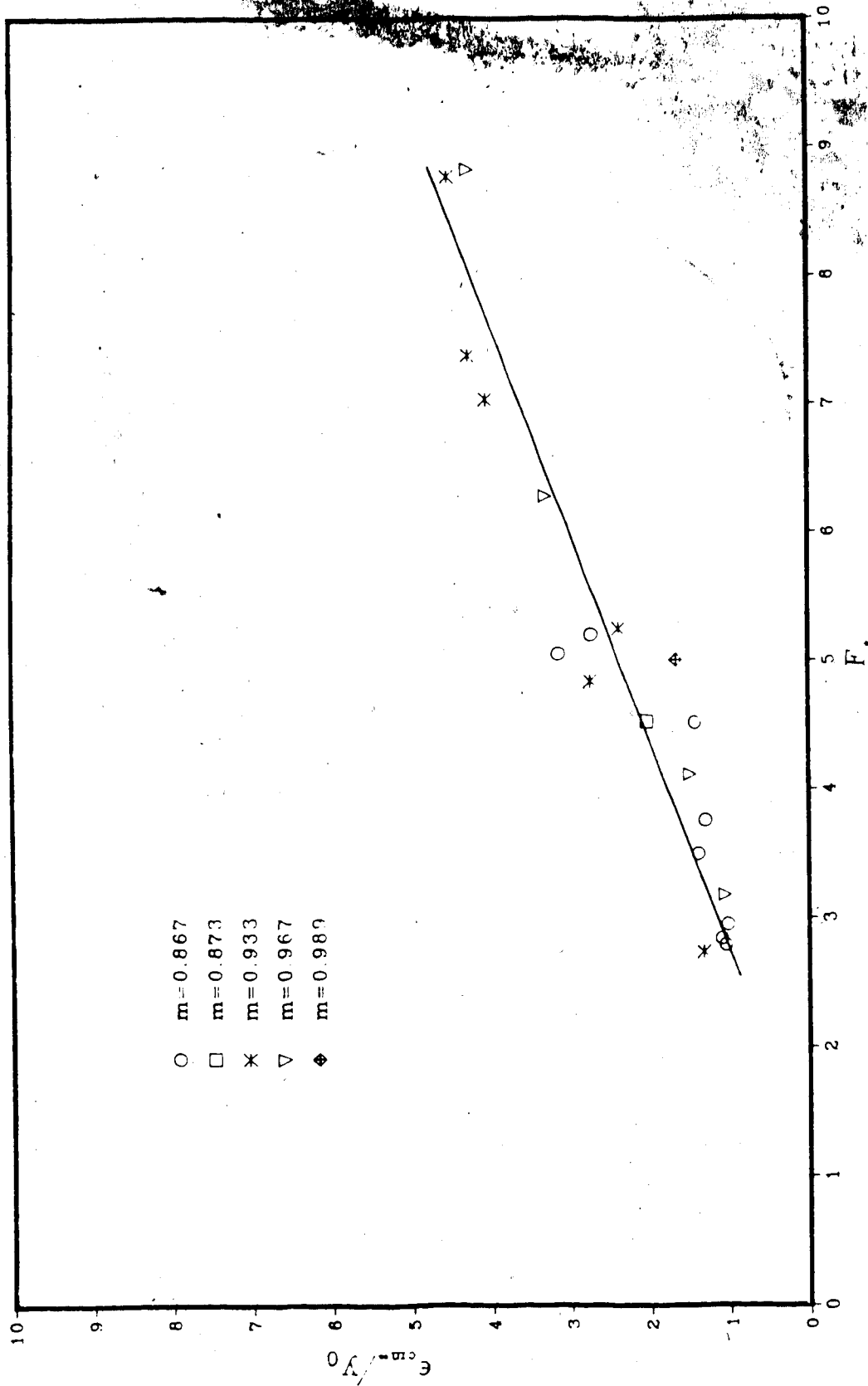
FIGURE 25 -- MAXMIUM CLEAR WATER SCOUR AT
CHANNEL CENTRE -- CONSTRICTION TYPE II

63
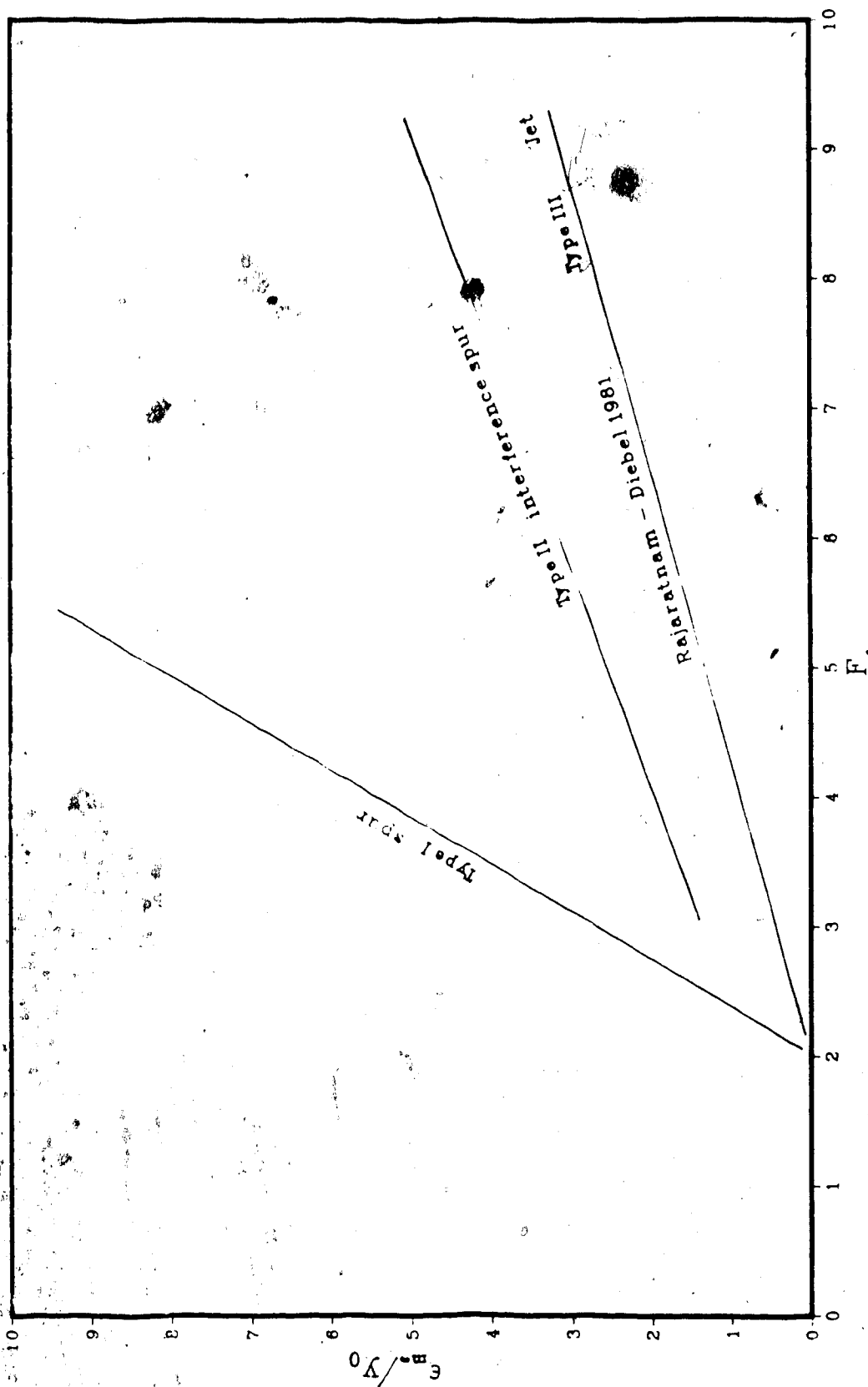
FIGURE 26 – DESIGN CHART FOR MAXIMUM CLEAR WATER SCOUR
FOR CONSTRICTION TYPE I, II, III

Legend:
- ○ m=0.867
- □ m=0.867
- ✳ m=0.933
- ▷ m=0.967
- ✦ m=0.989
- ◇ m=0.733
- ⬔ m=0.493
- ⊕ m=0.873
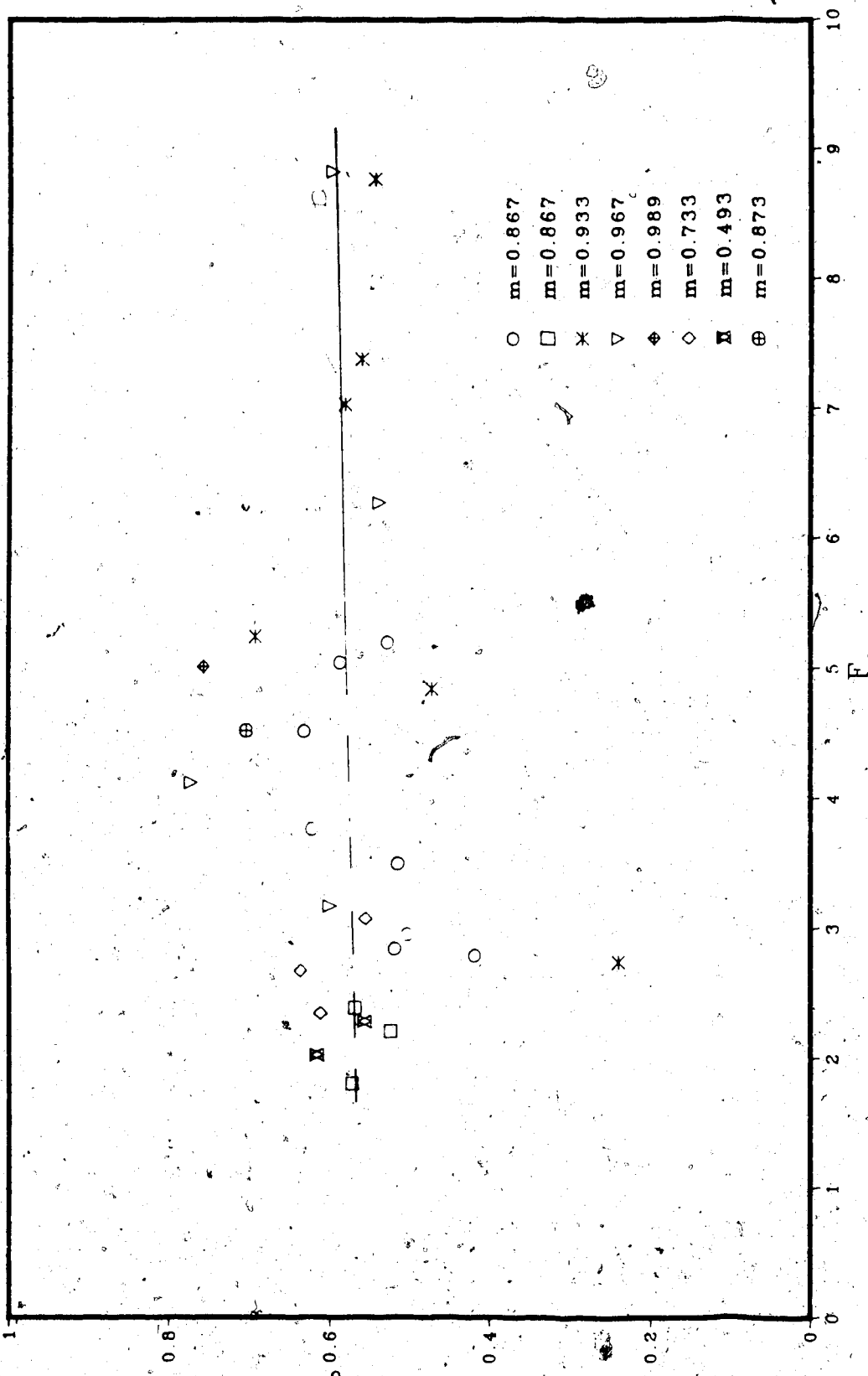
FIGURE 27 -- STUDY OF CREST OF RIDGE

for Figure 27 is tabulated in Table 3 and is presented in Appendix A.

During experiments for the same discharge and constriction ratio it was observed that the deposit spread widely for higher Froude numbers than for low Froude numbers.

An attempt to plot non-dimensional location of maximum ridge failed because the data points were scattered. Thus, no acceptable length scales were obtained.

4.4 MAXIMUM BACKWATER

From the previous studies using dimensional analysis it could be concluded that,

$$\frac{\Delta y}{y_0} = f\left[\frac{V_0}{gy_0}, \frac{b}{B}\right]$$ 4.10

where Δy is maximum backwater, y_0 is the approach flow depth, V_0 is the approach mean velocity, b is constriction opening, B is the channel bed width and g is the acceleration due to gravity.

Vallentine (1958) and Das (1972) assumed weir flow through the constriction and used the discharge equation in the form

$$Cd = Q/bH^{3/2} \qquad\qquad 4.11$$

where Cd is the coefficient of discharge and H is the
water depth in the upstream stagnation zone.

In this thesis, an orifice formula is used to describe
the flow through the constriction and the relative discharge
equation is given by

$$Q = C'bh\sqrt{2g\Delta y} \qquad\qquad 4.12$$

in which C' is the coefficient of discharge at
constriction, h is the depth of water at constriction.

Referring to dimension sketch in Figure 1, the equation 4.12
is modified as,

$$Q = Cby_t\sqrt{2g\Delta y} \qquad\qquad 4.13$$

where C is the new coefficient of discharge which
includes the depth $(h - y_t)$.

$$Q = BV_t y_t \qquad\qquad 4.14$$

Substituting F_t for V_t,

$$Q = By_t F_t\sqrt{gy_t} \qquad\qquad 4.15$$

By combining equations 4.13 and 4.15 an equation for backwater was obtained. That is,

$$\frac{\Delta y}{y_t} = 1/2 \left[\frac{F_t}{C} \frac{B}{b}\right]^2$$

By substituting m for B/b in equation 4.16, the backwater equation becomes,

$$\frac{\Delta y}{y_t} = 1/2 \left[\frac{1}{1-m} \frac{F_t}{C}\right]^2$$

Figure 28 represents a plot of coefficient of discharge versus tail end Froude number with constriction ratio as a third parameter. From this, Δy could be computed from equation 4.17, if the flow parameters before the constriction were known. Alternatively from Figure 29, which gives a non-dimensional relationship of backwater versus tail end Froude number, the maximum backwater could be found. Data for Figures 28 and 29 are tabulated in Tables 4A and 4B respectively and are presented in Appendix A.

Figure 30 is a reprint of Das's plot which relates the coefficient of discharge and Froude number. Das also
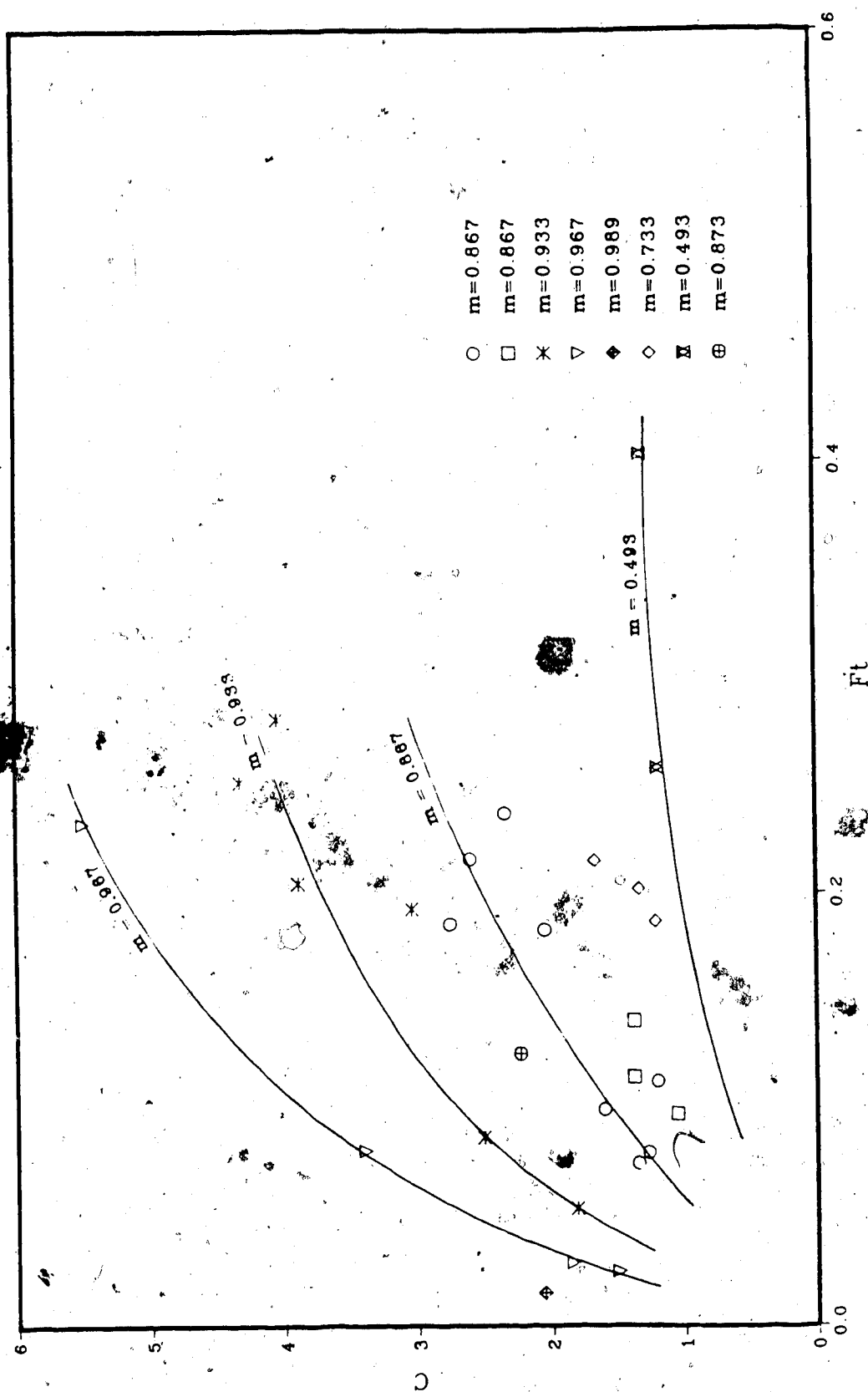
FIGURE 28.— MAXIMUM BACKWATER ON MOBILE BEDS CORRELATING C, F_t AND m
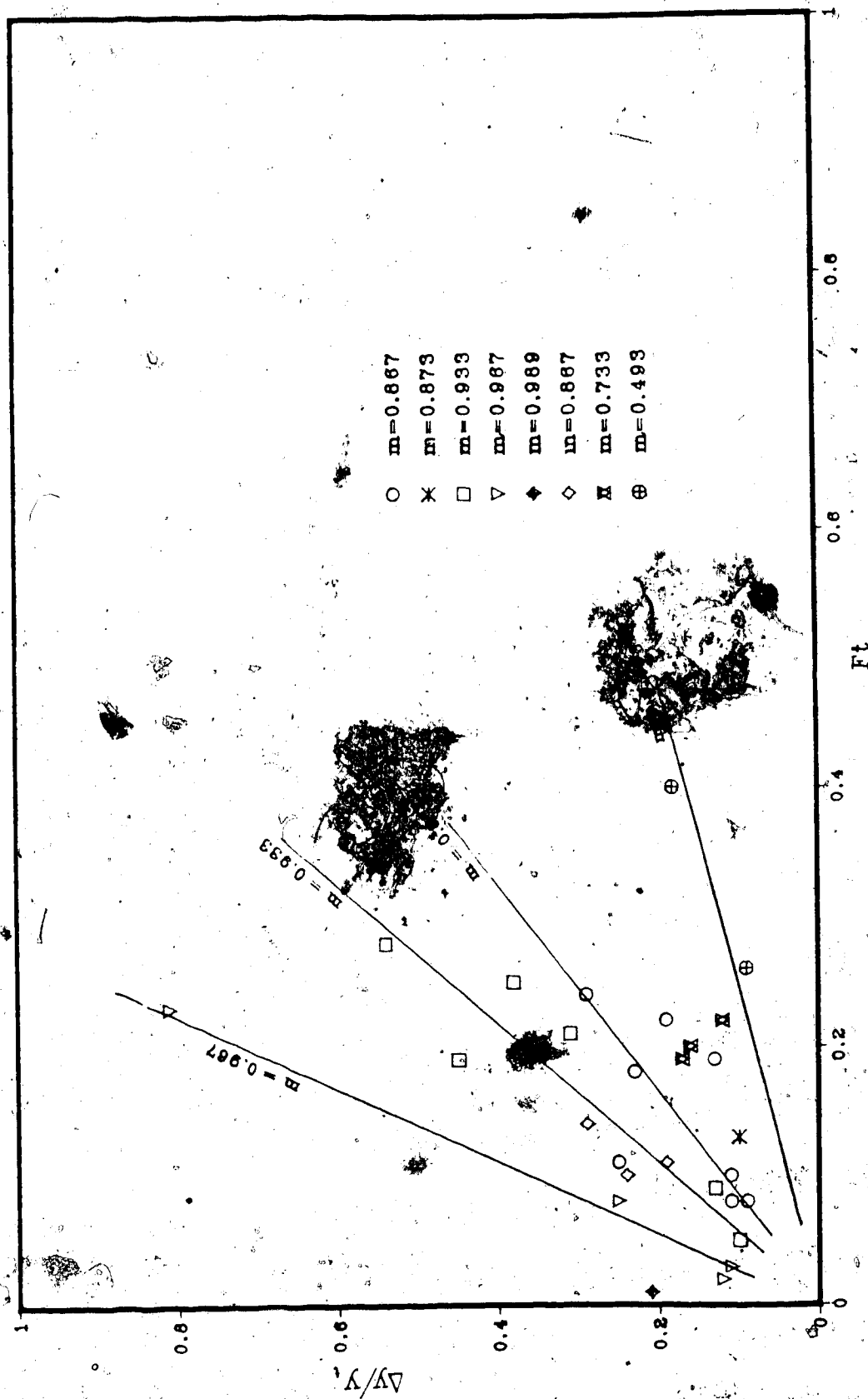
FIGURE 29 — MAXIMUM BACKWATER ON MOBILE BEDS CORRELATING Δy, F_t, AND m
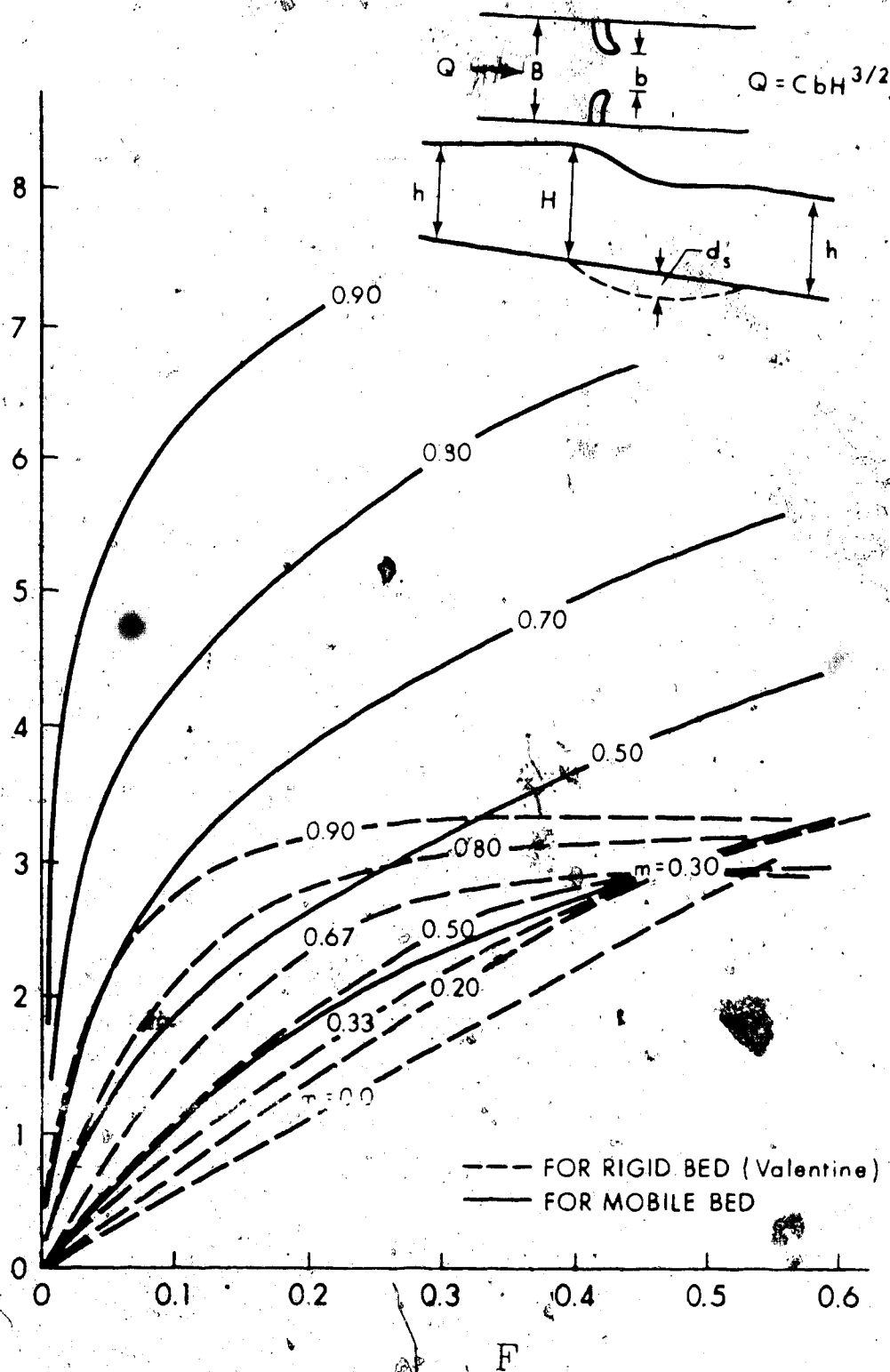
FIGURE 30 — MAXIMUM BACKWATER ON MOBILE BEDS
BY B.P. DAS, 1972

included the corresponding plot for flow on a rigid bed by
Vallentine.

4.5 UNIVERSAL FLOW DIAGRAM METHOD

Tutt (1972) modified the equations for plots of the
basic sediment transport developed by Cooper and Peterson
(1968) as

$$\frac{\rho q^2}{\gamma_{sub} D^3} = f\left[C, \frac{h}{D} \right]$$

4.18

where q is the discharge intensity, ρ is the mass
density of water, $\gamma_{sub} = (SG - 1)\rho g$, SG is specific
gravity of the material, g is acceleration due to
gravity, C is the sediment discharge or concentration,
D is median size of sand grain.

In the present studies, there is no sediment discharge
in the approach flow. A plot was prepared in Figure 31
relating Q Factor $(q/\sqrt{(\gamma_{sub}/\rho)D^3})$ and h/D. Quazi and
Peterson (1973) prepared chart for Q-Factor versus h/D for
rip rap for piers. They also prepared similar charts from a
compendium of sediment transport data for flumes and from
the studies of Das (1972) for end-dump closure and included
these in one plot. This plot is included in Figure 31.
Data for Figure 31 are tabulated in Table 5 and additional
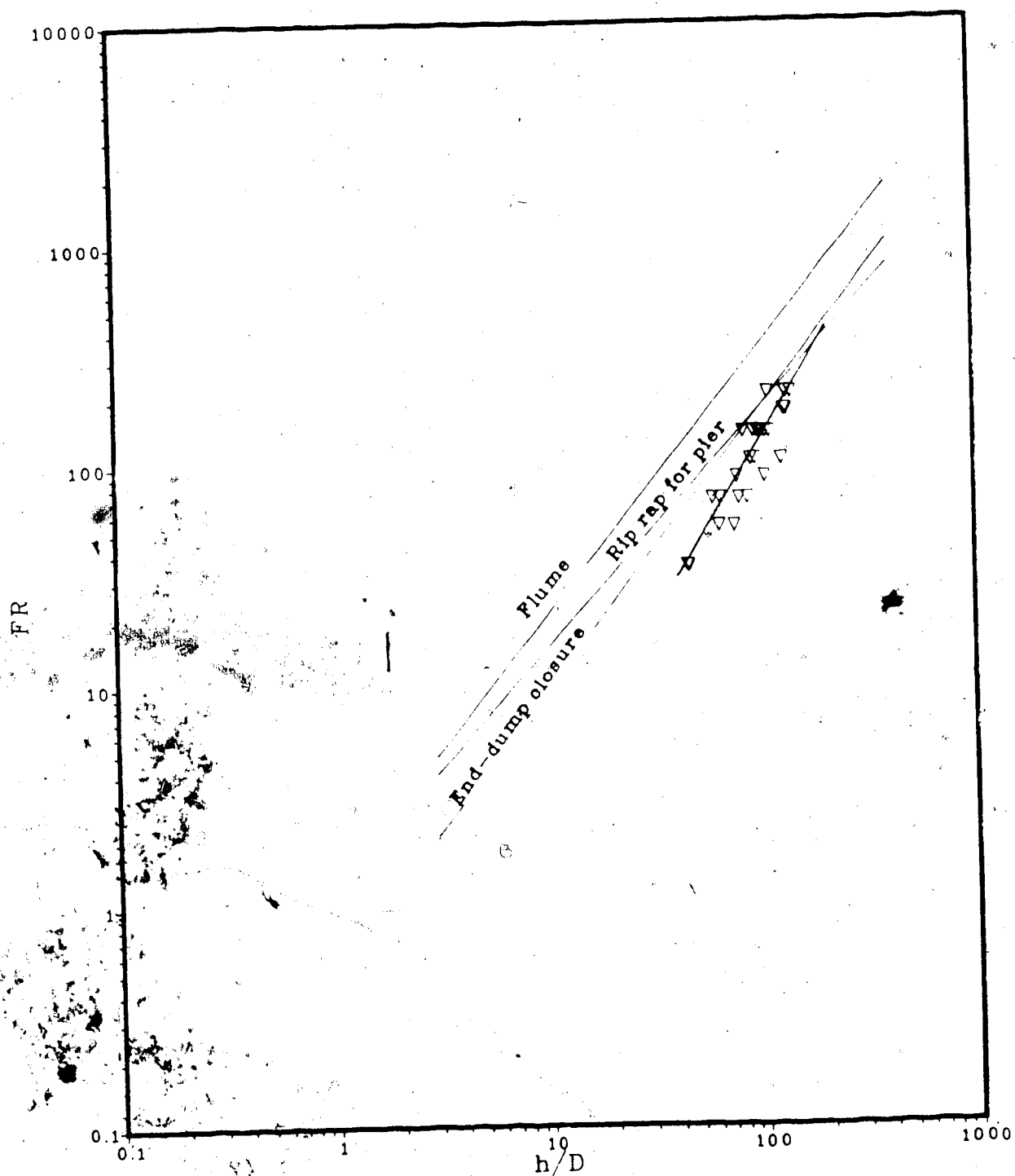
FIGURE 31 — COMPARATIVE PLOT OF h/D VERSUS C — FACTOR (FR)

data in Table 6 are presented in Appendix A.

From Figure 31, the mean clear water scour depth can be estimated. Q-Factor at constriction is calculated by replacing q by q/(1-m) where q is the discharge intensity at approach section. The calculated average scour depth is tabulated in Table 7 and is presented in Appendix A. Table 7 also includes the measured maximum scour depth. From this, it can be concluded that the sediment transport analysis yields a conservative estimates for maximum scour depth.

Figure 31 shows that the charts for rip-rap, end-dump closure and present studies respectively to the right of the chart for flumes. The sketch of these four cases are shown in Figure 32.

The flume situation is shown in Figure 32a. The flow is axial. The stream lines are parallel to the side walls and the velocity is unchanged. There is an average charge of 0.2 ppht and it can be considered that there is no bed movement.

In bridge piers, the stream lines adjacent to the piers are curved as indicated in Figure 32b. Due to this curvature of stream lines, the velocity is increased adjacent to the piers. Thus, scour takes place.

Figure 32c indicates the end-dump closure situation. In this, the stream lines are smoothed at the constriction. This is because of the self formed opening which also causes the maximum scour to occur at vena-contracta.
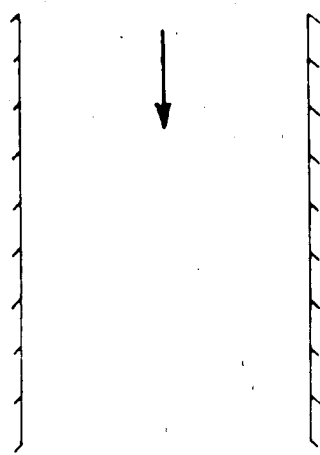
a) FLUME
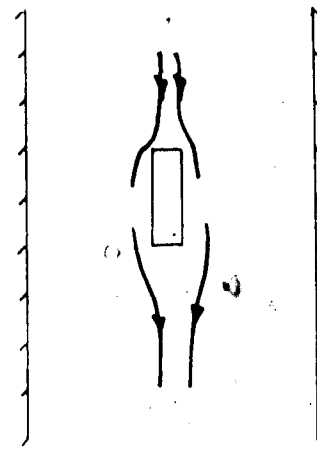
b) BRIDGE PIER
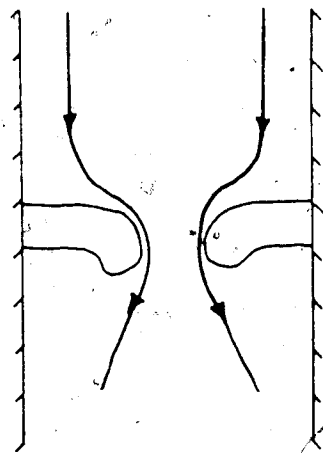
c) END–DUMP CLOSURE
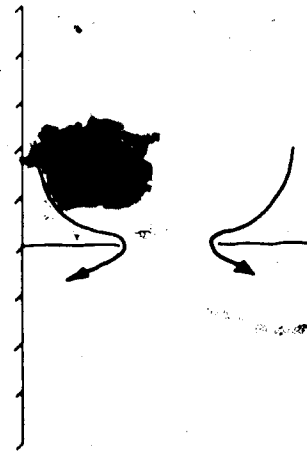
d) ABRUPT TYPE CONSTRICTION

FIGURE 32 – TYPICAL SKETCH OF FLUME, BRIDGE PIER, END–DUMP CLOSURE AND ABRUPT TYPE CONSTRICTION

The present studies were similar to end-dump closure situation but the constriction was abrupt and is shown in Figure 32d. For this type of constrictions, the stream lines are bent and close together indicating concentration of flow near the nose of the constriction. Usually the maximum scour occurs adjacent to the constrictions.

From above, it is clear that the geometry of the constriction is the main factor for the difference. Thus, for different situations the initiation of motion will also differ.

5. CONCLUSIONS AND RECOMMENDATIONS

5.1 CONCLUSIONS

The objective of this research was to continue to develop more understanding on scour depth and scour profiles in abrupt type constrictions and also to develop a design chart for maximum clear water scour. Finally it was also to compare the results from the present studies with regime theory concept. The following conclusions are formulated from the limited experimental observations made.

- Maximum clear water scour due to constriction type I (spur), type II (interference spur) and type III (jet) can be estimated from the design chart, Figure 26.

- Maximum clear water scour at the channel centre for interference spur type constriction can also be estimated from Figure 25.

- The location of the maximum scour for spur and interference type constriction was found to be at the nose of constriction. The location of maximum scour for jet type constriction was at the downstream along the channel centre. From the figures 16 to 22 and length scales discussed in an

77

earlier chapter, it is possible to establish the
scour pattern.

- The maximum backwater can be determined from Figure
28 or 29 which correlates the coefficient of
discharge and Froude number at tail end F, for
different constriction ratios.

- The averaged scoured depth can also be predicted
from sediment transport analysis which gives
conservative estimates.

Although considerable understanding of scour, caused by
flow at constrictions has been obtained as a result of this
research, a more thorough understanding of the scour
mechanics, measurements of scour and backwater is still
lacking.

5.2 RECOMMENDATION

It is recommended to,

- carry out similar experiments with varying sediment
sizes and constriction ratio.

- carry out similar experiments to measure the
velocity at constriction when the scour is at

equilibrium state.

- modify the outlet of the experiments to provide free
  fall so that there will be no asymmetry.

- carry out more laboratory experiments to complete
  the classification of interference spur and spur in
  Figure 12.

6. LIST OF REFERENCES

AHMAD, M., "Experiments on Design and Behaviour of
Spur-Dikes", Proceedings, Minnesota International
Hydraulics Convention, 1953, pp. 145-159.

ANDRU, P., "Study of Scour at Obstructions in Non-cohesive
Bed", thesis presented to the University of Alberta,
Edmonton, Canada in 1956, in partial fulfilment of the
requirement for the degree of Master of Science.

BREUSERS, N.H.C., NICOLLET, G., SHEN, H.W., "Local scour
around cylindrical Piers", (IAHR Task Force on Local
Scour around Piers) Journal of Hydraulic Research,
1977, No.3, pp. 211-253.

CARSTENS, M.R., "Similarity Laws for Localized scour",
Journal of the Hydraulics Division, ASCE. Vol. 92,
No.Hy3, May 1966, pp. 13-36.

CHOW, V.T., "Open Channel Hydraulics", McGraw-Hill, New
York, 1959, pp.475-490.

DAS, B.P., "Hydraulics of End-Dump closure of Alluvial
channels", thesis presented to the University of
Alberta, Edmonton, Canada in 1972, in partial

fulfilment of the requirements for the degree of Doctor
of Philosophy.

GARDE, R.J., SUBRAMANYA, K., and NAMBUDRIPAD, K.D., "Study
of scour Around Spur-Dikes", Journal of Hydraulics
Division, ASCE, Vol. 87, No.Hy6, Proc., November 1961,
pp. 23-37.

GARDE, R.J., SUBRAMANYA, K., and NAMBUDRIPAD, K.D., Closure
of "Study of Scour Around Spur Dikes", Journal of
Hydraulics Division, ASCE, Vol. 89, No.Hy1, Proc.,
January 1963, pp. 167-175.

GILL, M., "Erosion of Sand Beds Around Spur Dikes", Journal
of Hydraulics Division, ASCE, Vol. 98, No.Hy9, Proc.,
September 1972, pp. 1587-1601.

HOLLINGSHEAD, A.B., and RAJARATNAM, N., "A Calibration Chart
for the Preston Tube", Journal of Hydraulic Reasearch
18 (1980) No. 4, pp. 313-326.

IZZARD, C.F., and BRADLEY, J.N., "Field Verification of
Model Tests on Flow Through and Culverts", Proceedings,
7th Hydraulics Conference, Iowa, 1957, pp. 225-243.

KINDSVATER, C.E., and CARTER, R.W., "Tranquil Flow Through
Open Channel Constrictions", Transactions ASCE, Vol.

120, 1953, pp. 955-980.

KOMURA, S., "Equilibrium Depth of Scour in Long
    Constrictions", Journal of the Hydraulics Division,
    ASCE, Vol. 92, No.Hy5, Proc., September 1966, pp.
    17-37.

LANE, E.W., "Experiments on the Flow of Water Through
    Constrictions in an Open Channel", Transactions ASCE,
    Vol. 83, pp. 1149-1219.

LAURSEN, E.M., "Observations on the Nature of Scour",
    Proceedings, 5th Hydraulics Conference, Iowa City,
    Iowa, Bulletin No.34, 1952, pp. 179-197.

LAURSEN, E.M., and TOCH, A., "A Generalized Model Study of
    Scour Around Bridge Piers and Abutments", Proceedings
    5th IAHR Congress at Minneapolis, Minnesota, 1953, pp.
    123-131.

LAURSEN, E.M., "Scour at Bridge Crossings", Transactions,
    ASCE, Vol. 127, Part I, 1962, pp. 166-209.

LAURSEN, E.M., "An Analysis of Relief Bridge Scour", Journal
    of the Hydraulics Division, ASCE, Vol. 89, No.Hy3,
    Proc., May 1963, pp. 93-118.

LIU, H.K., CHANG, F.M., and SKINNER, M.M., "Effect of Bridge
    Constrictions on Scour and Backwater", Colorado State
    University, Civil Engineering Section, prepared for
    Bureau of Public Roads, February 1961.

NEILL, C.R., "River Bed Scour", Technical Publication No.23,
    Canadian Good Roads Association, March 1970.

PETERSON, A.W., "Universal Flow Diagrams for Mobile Boundary
    Channels", presented at 2nd Canadian Hydrotechnical
    Conference, Burlington, Ontario, May 14-16, 1975.

PETERSON, A.W., and HOWELLS, R.F., "A Compendium of solids
    transport data for mobile boundary channels." Environ.
    Can., Inland Waters Div., Ottawa, Report No.
    HY-1973-ST3.

QUAZI, M.E., and PETERSON, A.W., "A Method For Bridge Pier
    Rip Rap Design", Proc. 1st Can. Hydraulic Conf.,
    Edmonton, Alberta 1973.

RAUDKIVI, A.J., "Loose Boundary Hydraulics", Pergamon Press.
    1976, pp. 282-305.

RAJARATNAM, N., "Erosion By Plane Turbulent Jets", Journal
    of Hydraulic Research 19(1981), No.4, pp. 339-358.

RAJARATNAM, N., BERRY, B., "Erosion By Circular Turbulent

    Wall Jets" Journal of Hydraulic Research, 15(1977),

    No.3, pp. 277-289.

RAJARATNAM, N., and HUMPHRIES, J.A., "Diffusion of Bluff

    Wall Jets in Finite Depth Tailwater", Journal of

    Hydraulic Engineering, Vol. 109, No .11, November 1983,

    pp. 1487-1504.

RAJARATNAM, N., NWACHUKWU, B.A., "Erosion Near Groyne-Like

    Structure", Journal of Hydraulic Research 21(1983),

    No.4, pp. 277-287.

SCHLICHTING, H.,"Boundary Layer Theory", McGraw-Hill Book

    Company, 7th edition, 1979, pp. 618-624.

Task Committee on Preparation of Sedimentation Manual,

    Committee on Sedimentation, "Sediment Transportation

    Mechanics-Initiation of Motion", Journal of the

    Hydraulics Division, ASCE, Vol. 92, No.Hy2, Proc.

    March 1966, pp. 291-314.

TUTT, D.B., "The Determination of Scour Between Bridge

    Embankments on Gravel Bed Rivers", thesis presented to

    the University of Alberta, Edmonton, Canada in 1972, in

    partial fulfilment of the requirement for the degree of

    Master of Science.

VALLENTINE, H.R., "Flow in Rectangular Channels with Lateral
    Constriction Plates", La Houille Blanche No.1, January/
    February 1958, pp. 75-84.

VANONI, A., "Sedimentation Engineering", ASCE-Manuals and
    Reports on Engineering Practice No.54, 1975, pp.
    96-100.

7. APPENDIX A

EXPERIMENTAL & ANALYSIS DATA

TABLE 1 - BASIC EXPERIMENTAL DATA

Expt No.	G (1/s)	F (cm)	b (cm)	Yo (cm)	y+ (cm)	T (°C)	t (hrs)	$\epsilon_{m\alpha}$ (cm)	$\epsilon_{mc\alpha}$ (cm)	$\Delta\epsilon_\alpha$ (cm)
1111	10.0	228.60	30.48	4.33	3.84	25.7	30.0	13.08	11.80	2.29
1112	10.0	228.60	30.48	7.62	7.01	24.5	23.0	9.94	7.74	3.84
1113	10.0	228.60	30.48	6.43	5.79	21.0	24.0	10.70	8.95	3.35
1114	9.0	228.60	30.48	5.50	2.60	22.8	24.0	11.25	11.25	2.10
1115	8.0	228.60	30.48	6.46	5.82	27.1	5.0	8.14	6.77	2.71
1117	6.0	228.60	30.48	4.75	3.81	21.7	21.0	7.68	5.23	2.47
1118	6.0	228.60	30.48	2.99	2.33	21.6	24.0	8.93	4.27	1.89
1119	5.0	228.60	30.48	2.99	2.44	21.7	20.0	7.28	3.96	1.86
1201	6.0	120.20	15.24	5.97	5.43	18.2	29.0	12.35	12.19	1.61
1121	6.0	228.60	15.24	3.08	2.23	25.1	16.0	13.95	13.91	1.07
1122	6.0	228.60	15.24	5.15	4.54	21.6	20.0	12.25	12.25	1.43
1123	4.0	228.60	15.24	2.50	1.95	18.7	20.5	10.88	10.30	1.68
1124	4.0	228.60	15.24	2.44	1.58	22.8	22.0	10.58	10.42	3.57
1125	2.0	228.60	15.24	3.29	2.99	20.8	15.5	5.24	4.34	1.49
1126	2.0	228.60	15.24	1.86	1.28	25.4	18.0	6.01	5.09	1.37
1131	2.0	228.60	7.62	2.04	1.13	15.5	5.0	8.99	8.72	0.79
1132	2.0	228.60	7.62	2.87	2.29	18.2	17.0	9.46	9.18	0.88
1133	2.0	228.60	7.62	5.67	5.06	18.3	24.0	7.10	6.03	1.22
1134	3.0	228.60	7.62	6.55	5.88	18.9	23.0	10.85	9.51	1.55
1141	1.0	228.60	3.54	5.39	4.45	16.9	23.0	8.99	8.99	3.41
1149	3.0	228.60	30.48	2.83	2.37	21.7	20.5	5.58	0.0	5.06
1111	2.0	228.60	30.48	2.04	1.58	23.0	5.0	4.05	0.0	4.08
1112	2.0	228.60	30.48	2.50	2.01	21.7	5.0	3.54	0.0	2.68
1151	10.0	228.60	60.96	4.21	3.63	17.0	24.0	9.60	0.0	2.44
1152	12.0	228.60	60.96	4.39	3.93	17.6	23.0	12.19	0.0	2.35
1153	8.0	228.60	60.96	3.84	3.29	17.7	24.0	6.64	0.0	1.65
1211	6.0	120.20	60.96	2.96	2.50	16.7	10.0	6.95	0.0	2.74
1212	5.0	120.20	60.96	4.45	4.08	15.5	21.0	7.01	0.0	4.21

We

TABLE 2 — DATA FOR DESIGN CHARTS

Expt No.	Q (1/s)	R (cm)	L (cm)	(cm)	ϵ_{ms}	$\epsilon_{mc s}$	m	V* (cm)	F*	ϵ_{mcs}/Y_c	ϵ_{ms}/Y_c
1111	10 0	228 60	30 18	4 22	13 05			75	5 20		2
1112	10 0	228 60	30 18	7 60	9 41	31	0 867	43 86	95		1 79
1113	10 0	228 60	30 18	6 12	10 26	9 25	0 867	51	7 50	1 66	1 75
1114	8 0	228 60	30 18	3 57	11 35	11 25	0 867	73	7 05	3 15	3 15
1115	8 0	228 60	30 18	6 16	8 11	6 77	0 867	49 66	7 79	26	1
1117	6 0	228 60	30 18	4 35	7 48	5 21	0 867	41 11	7 84	62	1
1118	6 0	228 60	30 18	2 79	8 87	4 27	0 867	65 81	7 52	99	1 43
1119	5 0	228 60	30 18	2 99	7 29	7 99	861	51 86	3 76	43	1 70
1221	6 0	120 30	15 21	4 91	12 35	12 19	0 873	65 05	1 53	07	2 03
1121	6 0	228 60	15 21	7 08	15 25	13 91	0 933	127 82	8 77	64	1 52
1122	6 0	228 60	15 24	5 15	12 35	12 25	0 933	76 15	5 25	38	2 74
1123	4 0	228 60	15 21	2 55	10 86	10 36	0 933	102 53	7 00	25	1 05
1124	4 0	228 60	15 21	2 11	10 58	42	33	107 55	7 38	21	1 27
1125	2 0	228 60	15 21	3 29	5 21	39	0 933	39 80	2 74	59	1
1126	2 0	228 60	15 21	1 65	6 03	5 03	0 967	70 55	1 84	25	2 71
1131	2 0	228 60	7 62	2 03	8 30	6 18	0 967	129 65	8 83	30	1 27
1132	2 0	228 60	7 62	2 87	9 18	63	0 967	91 15	6 28	30	3
1133	2 0	228 60	7 62	5 61	7 10	7	0 967	46 29	7 18	25	1 05
1134	3 0	228 60	7 62	6 35	10 85	8 81	0 967	60 11	4 12	66	1 50
1141	1 0	228 60	2 51	5 30	8 04	8 09	0 989	73	5 01	67	1 67

TABLE 2 - DATA FOR DESIGN CHARTS CONTINUED ....

Exit No.	Q (l/s)	R (cm)	b (cm)	y_o (cm)	e_{ma} (cm)	e_{mcb} (cm)	m	(cm²)	f	e_{ma}/y_o	e_{mcb}/y_o
11110	3.0	228.60	30.48	2.83	1.58	0.0	0.867	31.78	2.20	1.97	0.0
11111	2.0	228.60	30.48	2.04	1.05	0.0	0.867	32.17	2.21	1.99	0.0
11112	2.0	228.60	30.48	2.50	3.51	0.0	0.867	26.25	1.81	1.42	0.0
1151	10.0	228.60	60.96	4.21	9.60	0.0	0.733	38.96	2.67	2.28	0.0
1152	12.0	228.60	60.96	4.39	12.19	0.0	0.733	44.84	3.09	2.78	0.0
1153	8.0	228.60	60.96	3.84	6.61	0.0	0.733	34.18	2.35	1.73	0.0
1211	6.0	120.20	60.96	2.96	6.95	0.0	0.493	33.25	2.28	2.35	0.0
1212	8.0	120.20	60.96	4.45	7.01	0.0	0.493	29.49	2.02	1.58	0.0

TABLE 3 - DATA FOR CREST OF RIDGE

Expt No	Q (1/s)	P (cm)	b (cm)	y_o (cm)	Δε_∞ (cm)	m	F	Δε_∞/y_o
1111	10.0	228.60	30.48	4.33	2.29	0.867	5.20	0.53
1112	10.0	228.60	30.48	7.62	3.84	0.867	2.95	0.50
1113	10.0	228.60	30.48	6.43	3.32	0.867	3.51	0.52
1114	8.0	228.60	30.48	3.57	2.10	0.867	5.05	0.59
1115	8.0	228.60	30.48	6.46	2.71	0.867	2.79	0.42
1117	6.0	228.60	30.48	4.75	2.47	0.867	2.84	0.52
1118	6.0	228.60	30.48	2.99	1.89	0.867	4.52	0.63
1119	5.0	228.60	30.48	2.99	1.89	0.867	3.77	0.62
11110	3.0	228.60	30.48	2.83	1.61	0.867	2.39	0.57
11111	2.0	228.60	30.48	2.04	1.07	0.867	2.21	0.52
11112	2.0	228.60	30.48	2.50	1.43	0.867	1.80	0.57
1121	6.0	228.60	15.24	3.08	1.68	0.933	8.77	0.55
1122	6.0	228.60	15.24	5.15	3.57	0.933	5.25	0.69
1123	4.0	228.60	15.24	2.56	1.49	0.933	7.03	0.58
1124	4.0	228.60	15.24	2.44	1.37	0.933	7.38	0.56
1125	2.0	228.60	15.24	3.29	0.79	0.933	2.74	0.24
1126	2.0	228.60	15.24	1.86	0.88	0.933	4.84	0.47
1131	2.0	228.60	7.62	2.04	1.22	0.967	8.83	0.60
1132	2.0	228.60	7.62	2.87	1.55	0.967	6.28	0.54
1133	2.0	228.60	7.62	5.67	3.41	0.967	3.18	0.60
1134	3.0	228.60	7.62	6.55	5.06	0.967	4.13	0.77
1141	1.0	228.60	2.54	5.39	4.08	0.989	5.01	0.76
1151	10.0	228.60	60.96	4.21	2.68	0.733	2.67	0.64
1152	12.0	228.60	60.96	4.39	2.44	0.733	3.08	0.56
1153	8.0	228.60	60.96	3.84	2.35	0.733	2.35	0.61
1211	6.0	120.20	60.96	2.96	1.65	0.493	2.28	0.56
1212	8.0	120.20	60.96	4.45	2.74	0.493	2.02	0.62
1221	6.0	120.20	15.24	5.97	4.21	0.873	4.52	0.71

TABLE 4A - DATA FOR BACKWATER ANALYSIS

Expt No	Q (l/s)	B (cm)	b (cm)	Yt (cm)	m	Vt (cm/s)	Ft	C
1111	10.0	228.60	30.48	3.84	0.867	11.39	0.186	2.76
1112	10.0	228.60	30.48	7.01	0.867	6.24	0.075	1.35
1113	10.0	228.60	30.48	5.79	0.867	7.56	0.100	1.60
1114	8.0	228.60	30.48	2.99	0.867	11.70	0.246	2.60
1115	8.0	228.60	30.48	5.82	0.867	6.01	0.080	1.27
1117	6.0	228.60	30.48	3.81	0.867	6.89	0.113	1.20
1118	6.0	228.60	30.48	2.32	0.867	11.31	0.237	2.34
1119	5.0	228.60	30.48	2.44	0.867	8.96	0.183	2.05
1221	6.0	120.20	15.24	5.43	0.873	9.19	0.126	2.23
1121	6.0	228.60	15.24	2.23	0.933	11.77	0.251	4.02
1122	6.0	228.60	15.24	4.54	0.933	5.78	0.087	2.51
1123	4.0	228.60	15.24	1.95	0.933	8.97	0.205	3.89
1124	6.0	228.60	15.24	1.58	0.933	11.07	0.281	4.04
1125	2.0	228.60	15.24	2.99	0.933	2.93	0.054	1.81
1126	2.0	228.60	15.24	1.28	0.933	6.84	0.193	3.04
1131	2.0	228.60	7.62	1.13	0.967	7.74	0.233	5.50
1132	2.0	228.60	7.62	2.29	0.967	3.82	0.081	3.40
1133	2.0	228.60	7.62	5.06	0.967	1.73	0.025	1.50
1134	3.0	228.60	7.62	5.88	0.967	2.23	0.029	1.85
1141	1.0	228.60	2.54	4.45	0.989	0.98	0.015	2.06
11110	3.0	228.60	30.48	2.37	0.867	5.54	0.115	1.38
11111	2.0	228.60	30.48	1.58	0.867	5.54	0.141	1.38
11112	2.0	228.60	30.48	2.01	0.867	4.35	0.098	1.05
1151	10.0	228.60	60.96	3.63	0.733	12.05	0.202	1.34
1152	12.0	228.60	60.96	3.93	0.733	13.36	0.215	1.67
1153	8.0	228.60	60.96	3.29	0.733	10.64	0.187	1.21
1211	6.0	120.20	60.96	2.50	0.493	19.97	0.403	1.31
1212	8.0	120.20	60.96	4.08	0.493	16.31	0.258	1.13

TABLE 4B - DATA FOR BACKWATER ANALYSIS

Expt No	Q (l/s)	B (cm)	b (cm)	Yt (cm)	m	Vt (cm/s)	Ft	Δv (cm)	Δv/yt
1111	10.0	228.60	30.48	3.84	0.867	11.39	0.186	0.49	0.13
1112	10.0	228.60	30.48	7.01	0.867	6.24	0.075	0.61	0.09
1113	10.0	228.60	30.48	5.79	0.867	7.56	0.100	0.64	0.11
1114	8.0	228.60	30.48	2.99	0.867	11.70	0.216	0.58	0.19
1115	8.0	228.60	30.48	5.82	0.867	6.01	0.080	0.64	0.11
1117	6.0	228.60	30.48	3.81	0.867	6.89	0.113	0.94	0.25
1118	6.0	228.60	30.18	2.32	0.867	11.31	0.237	0.67	0.29
1119	5.0	228.60	30.48	2.44	0.867	8.96	0.183	0.55	0.23
1221	6.0	120.20	15.24	5.43	0.873	9.19	0.126	0.54	0.10
1121	5.0	228.60	15.24	2.23	0.933	11.77	0.252	0.85	0.38
1122	5.0	228.60	15.24	4.54	0.933	5.78	0.087	0.61	0.13
1123	4.0	228.60	15.24	1.95	0.933	8.97	0.205	0.61	0.31
1124	4.0	228.60	15.24	1.58	0.933	11.07	0.281	0.86	0.54
1125	2.0	228.60	15.24	2.99	0.933	2.93	0.054	0.3	0.10
1126	2.0	228.60	15.24	1.28	0.933	6.84	0.193	0.58	0.45
1131	2.0	228.60	7.62	1.13	0.967	7.74	0.233	0.91	0.81
1132	2.0	228.60	7.62	2.29	0.967	3.82	0.081	0.58	0.25
1133	2.0	228.60	7.62	5.06	0.967	1.73	0.025	0.61	0.12
1134	3.0	228.60	7.62	5.88	0.967	2.23	0.029	0.07	0.11
1141	1.0	228.60	2.54	4.45	0.989	0.98	0.015	0.94	0.21
11110	3.0	228.60	30.48	2.37	0.867	5.54	0.115	0.46	0.19
11111	2.0	228.60	30.48	1.58	0.867	5.54	0.141	0.46	0.29
11112	2.0	228.60	30.48	2.01	0.867	4.35	0.098	0.49	0.24
1151	10.0	228.60	60.96	3.63	0.733	12.05	0.202	0.58	0.16
1152	12.0	228.60	60.96	3.93	0.733	13.36	0.215	0.46	0.12
1153	8.0	228.60	60.96	3.29	0.733	10.64	0.187	0.55	0.17
1211	6.0	120.20	60.96	2.50	0.493	19.97	0.403	0.46	0.18
1212	8.0	120.20	60.96	4.08	0.493	16.31	0.258	0.37	0.09

TABLE 5 - DATA FOR SEDIMENT TRANSPORT ANALYSIS

Expt. No.	Q (1/s)	B (cm)	b (cm)	YO (cm)	Y (cm)	ε_B (cm)	m	h (cm)	q0 (cm/s)	q1 (cm/s)	FR0	FR1	h
1111	10.0	228.60	30.48	4.33	4.06	13.08	0.867	17.41	43.7	328.1	22.7	170.6	131.9
1112	10.0	228.60	30.48	7.62	7.35	9.94	0.867	17.56	43.7	328.1	22.7	170.6	133.0
1113	10.0	228.60	30.48	6.43	6.16	10.70	0.867	17.13	43.7	328.1	22.7	170.6	129.8
1114	8.0	228.60	30.48	3.57	3.29	11.25	0.867	14.82	35.0	262.5	18.2	136.4	112.3
1115	8.0	228.60	30.48	6.46	6.19	8.14	0.867	14.60	35.0	262.5	18.2	136.1	110.6
1117	6.0	228.60	30.48	4.75	4.15	7.68	0.867	12.43	26.2	196.9	13.6	102.3	91.2
1118	6.0	228.60	30.48	2.99	2.71	8.93	0.867	11.92	26.2	196.9	13.6	102.3	90.3
1119	5.0	228.60	30.48	2.99	2.74	7.28	0.862	10.27	21.9	164.0	11.4	85.3	77.8
1221	6.0	120.20	15.24	5.97	5.70	12.35	0.873	18.32	49.0	393.7	25.9	204.7	138.8
1121	6.0	228.60	15.24	3.08	2.74	15.25	0.933	18.33	26.2	393.7	13.6	204.7	138.9
1122	6.0	228.60	15.24	5.15	4.88	12.25	0.933	17.40	26.2	393.7	13.6	204.7	134.8
1123	4.0	228.60	15.24	2.56	2.26	10.88	0.933	13.44	17.5	262.5	9.1	136.4	101.8
1124	4.0	228.60	15.24	2.44	2.10	10.58	0.933	13.02	17.5	262.5	9.1	136.4	98.6
1125	2.0	228.60	15.24	3.29	3.14	5.21	0.933	8.53	8.7	131.2	4.5	68.2	61.6
1126	2.0	228.60	15.24	1.86	1.55	6.04	0.933	7.90	8.7	131.2	4.5	68.2	59.8

TABLE 5 - DATA FOR SEDIMENT TRANSPORT ANALYSIS CONTINUED .....

Expt No	Q (1/s)	B (cm)	b (cm)	yo (cm)	y (cm)	c_{max} (cm)	m	h (cm)	q_p (cm/s)	q_t (cm/s)	FRO	FRI	h/D
1131	2.0	228.60	7.62	2.03	1.71	8.99	0.967	11.03	8.7	262.5	4.5	136.4	87.6
1132	2.0	228.60	7.62	2.87	2.62	9.18	0.967	12.35	8.7	262.5	4.5	136.4	93.6
1133	2.0	228.60	7.62	5.67	5.58	7.10	0.967	12.77	8.7	262.5	4.5	136.4	96.7
1134	3.0	228.60	7.62	6.55	6.29	10.85	0.967	17.40	13.1	393.7	6.8	204.7	131.8
1141	1.0	228.60	2.54	5.39	5.24	8.99	0.989	14.38	4.4	393.7	2.3	204.7	108.9
11110	3.0	228.60	30.48	2.83	2.58	5.58	0.867	8.41	13.1	98.4	6.8	51.2	63.7
11111	2.0	228.60	30.48	2.04	1.89	4.05	0.867	6.09	8.7	65.6	4.5	34.1	46.1
11152	2.0	228.60	30.48	2.50	2.26	3.51	0.867	6.04	8.7	65.6	-1.5	34.1	45.8
1151	10.0	228.60	60.96	4.21	3.96	9.60	0.733	13.81	43.7	164.0	22.7	85.3	104.6
1152	12.0	228.60	60.96	4.39	4.11	12.19	0.733	16.58	52.5	196.9	27.3	102.3	125.6
1153	8.0	228.60	60.96	3.84	3.60	6.61	0.733	10.48	35.0	131.2	18.2	68.2	79.1
1211	6.0	120.20	60.96	2.96	2.74	6.95	0.493	9.91	19.9	98.4	25.9	51.2	75.1
1212	8.0	120.20	60.96	4.45	4.24		0.493	11.45	65.6	131.2	31.6	68.2	86.2

TABLE 6 - ADDITIONAL INFORMATION

Expt. No.	Q (1/s)	B (cm)	h (cm)	yo (cm)	ym (cm)	Ao (cm)	A1 (cm)	Vo (cm/s)	V1 (cm/s)	Fo	V1/Vo	y' (cm)
1111	10.0	228.60	30.48	4.33	13.08	999.8	150.7	10.10	21.75	0.155	2.15	17.11
1112	10.0	228.60	30.48	7.62	9.94	1741.2	465.5	5.74	21.48	0.066	3.74	17.29
1113	10.0	228.60	30.48	6.43	10.70	1460.0	416.0	6.80	22.12	0.086	3.30	16.86
1114	8.0	228.60	30.48	3.57	11.25	816.1	401.5	9.80	19.92	0.166	2.03	14.51
1115	8.0	228.60	30.48	6.46	8.14	1476.8	375.0	5.42	21.33	0.068	3.94	14.33
1117	6.0	228.60	30.48	4.75	7.68	1085.8	289.3	5.53	20.74	0.081	3.75	11.83
1118	6.0	228.60	30.48	2.99	8.93	683.5	294.5	8.78	20.38	0.162	2.32	11.64
1119	5.0	228.60	30.48	2.99	7.28	683.5	233.6	7.32	21.40	0.135	2.93	10.02
11110	3.0	228.60	30.48	2.83	5.58	646.9	131.1	4.64	22.87	0.088	4.93	8.16
11111	2.0	228.60	30.48	2.04	4.05	466.3	108.4	4.29	18.44	0.096	4.30	5.94
11112	2.0	228.60	30.48	2.50	3.54	571.5	97.9	3.50	20.42	0.071	5.84	5.80
1121	6.0	228.60	15.24	3.08	15.25	704.1	213.5	8.52	24.64	0.155	2.89	17.99
1122	6.0	228.60	15.24	5.15	12.25	1177.3	246.8	5.10	21.31	0.072	4.77	17.13
1123	4.0	228.60	15.24	2.56	10.88	585.2	137.5	6.84	21.33	0.136	3.12	13.14
1124	4.0	228.60	15.24	2.44	10.58	557.1	178.1	7.17	22.46	0.147	3.13	12.68
1125	2.0	228.60	15.24	3.29	5.21	752.1	111.4	2.66	17.49	0.047	6.58	8.38
1126	2.0	228.60	15.24	1.86	6.01	425.2	104.8	4.70	19.08	0.110	4.06	7.59

TABLE 6 - ADDITIONAL INFORMATION CONTINUED . . . .

Exnt No.	Q (1/s)	R (cm)	b (cm)	Yo (cm)	c_mo (cm)	Ao (cm)	A1 (cm)	Vo (cm/s)	V1 (cm/s)	To	V1/Vo	y'
1131	2.0	228.60	7.62	3.04	8.94	1466.9	79.3	4.39	25.21	0.006	5.88	10.70
1132	2.0	228.60	7.62	2.87	9.48	656.1	89.1	3.05	22.36	0.057	7.34	12.10
1133	2.0	228.60	7.52	5.67	7.10	1296.2	92.0	1.54	21.71	0.021	14.09	12.68
1134	3.0	228.60	7.62	6.55	10.85	1197.3	125.8	2.09	23.81	0.025	11.90	17.11
1141	1.0	228.60	2.51	5.79	8.99	1232.2	35.7	0.81	28.02	0.011	34.53	13.23
1151	10.0	228.60	60.96	4.21	9.60	962.4	437.2	10.39	22.88	0.162	2.20	13.56
1152	12.0	228.60	60.96	4.39	12.19	1003.6	553.2	11.96	21.69	0.182	1.81	16.30
1153	8.0	228.60	60.96	3.84	6.64	877.8	384.8	9.11	20.79	0.148	2.28	10.31
1211	6.0	120.20	60.96	2.96	6.95	355.8	281.7	16.86	21.30	0.313	1.26	9.69
1212	8.0	120.20	60.96	4.45	7.01	594.9	373.3	14.96	21.12	0.226	1.43	11.25
1221	6.0	120.20	15.24	5.97	12.35	717.6	264.0	8.36	22.73	0.109	2.72	18.05

TABLE 7 - COMPARISION OF CALCULATED AVERAGE SCOUR BY SEDIMENT TRANSPORT ANALYSIS AND MEASURED MAXIMUM SCOUR

Expt.	Q-Factor at unconst	Q-Factor at const.	h/D flume chart	h/D present chart	Scour dep. calculated (cm)	Scour dep. measured (cm)
1111	22.70	170.60	11.13	121.00	14.50	13.08
1112	22.70	170.60	11.13	121.00	14.50	9.94
1113	22.70	170.60	11.13	121.00	14.50	10.70
1114	18.20	136.40	9.30	98.00	11.70	11.25
1115	18.20	136.40	9.30	98.00	11.70	8.14
1117	13.60	102.30	7.30	85.00	10.30	7.68
1118	13.60	102.30	7.30	85.00	10.30	8.93
1119	11.40	85.30	6.30	80.00	9.70	7.28
11110	6.80	51.20	4.10	56.00	6.90	5.58
11111	4.50	34.10	3.00	43.00	5.30	4.05
11112	4.50	34.10	3.00	43.00	5.30	3.54
1121	13.60	204.70	7.30	139.00	17.40	15.25
1122	13.60	204.70	7.30	139.00	17.40	12.25
1123	9.10	136.40	5.30	98.00	12.20	10.88
1124	9.10	136.40	5.30	98.00	12.20	10.58
1125	4.50	68.20	3.00	68.00	8.60	5.24
1126	4.50	68.20	3.00	68.00	8.60	6.04
1131	4.50	136.40	3.00	98.00	12.50	8.99
1132	4.50	136.40	3.00	98.00	12.50	9.48
1133	4.50	136.40	3.00	98.00	12.50	7.10
1134	6.80	204.70	4.10	139.00	17.80	10.85
1141	2.30	204.70	1.70	139.00	18.10	8.99
1151	22.70	85.30	11.10	80.00	9.10	9.60
1152	27.30	102.30	13.00	85.00	9.50	12.19
1153	18.20	68.20	9.30	68.00	7.70	6.64
1211	25.90	51.20	12.40	56.00	5.80	6.95
1212	34.60	68.20	15.70	68.00	6.90	7.01
1221	25.90	204.70	12.40	139.00	16.70	12.35

8. APPENDIX B

ADDITIONAL FIGURES
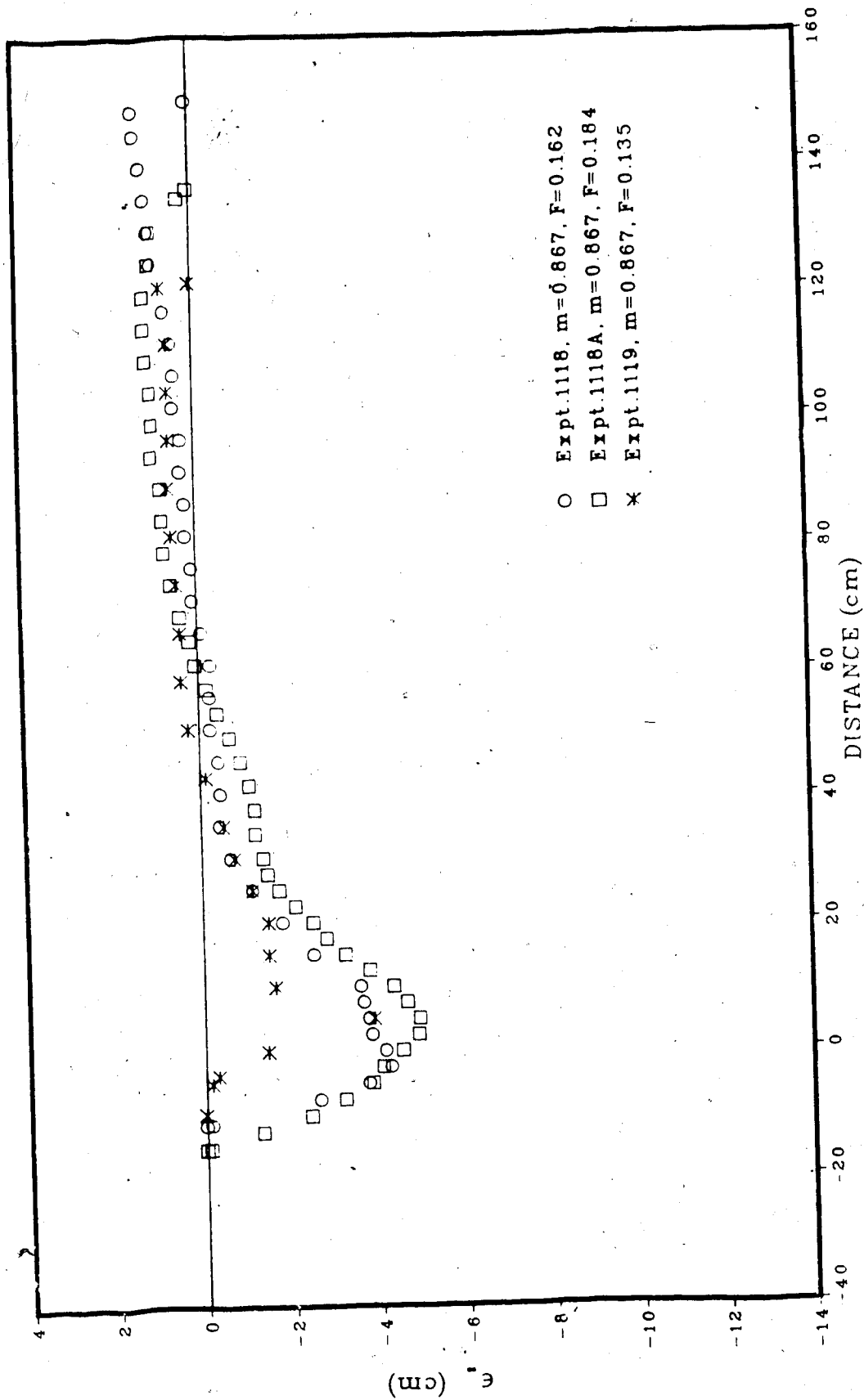
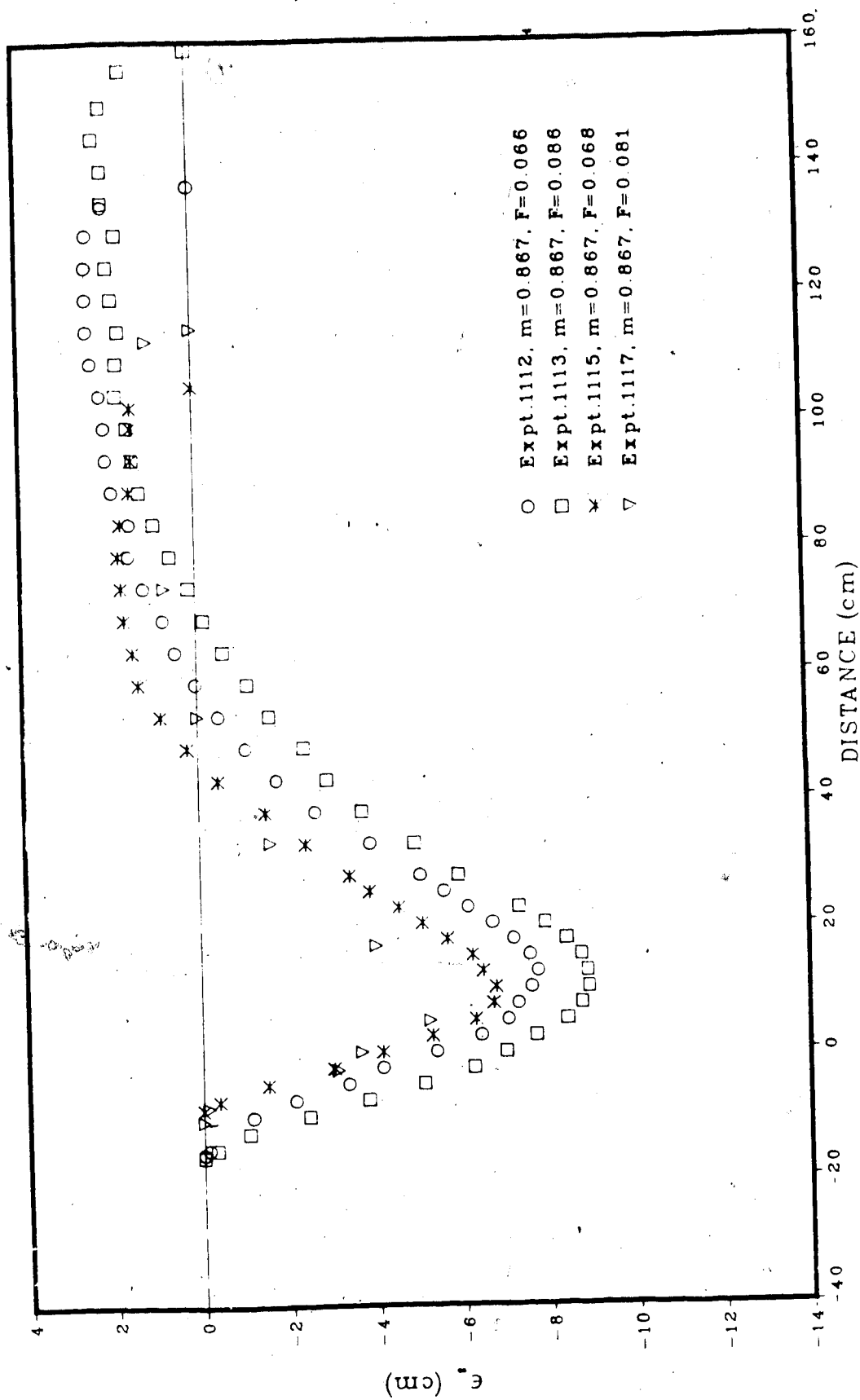FIGURE 33.— SCOUR AND RIDGE PROFILES ALONG CHANNEL CENTRE
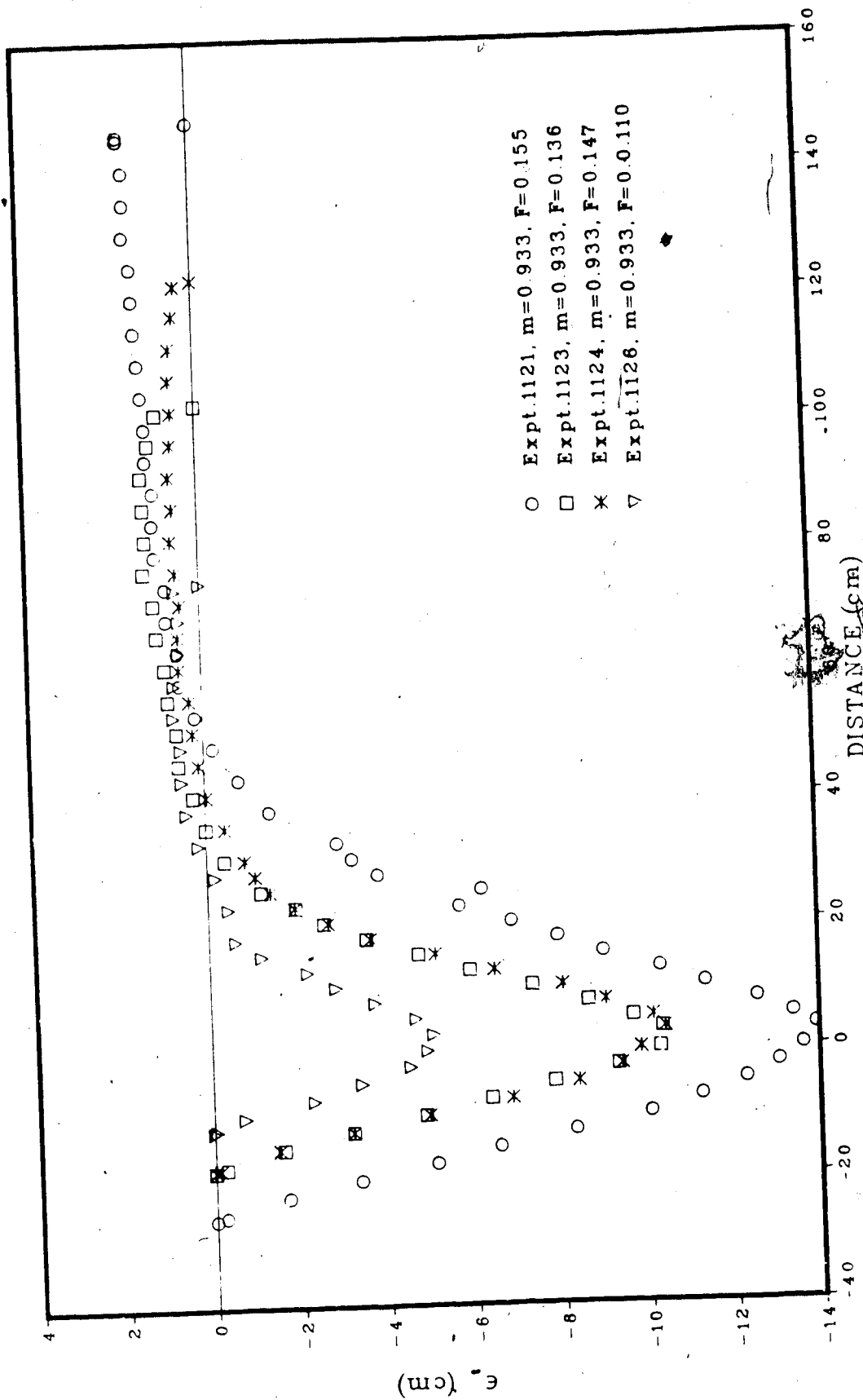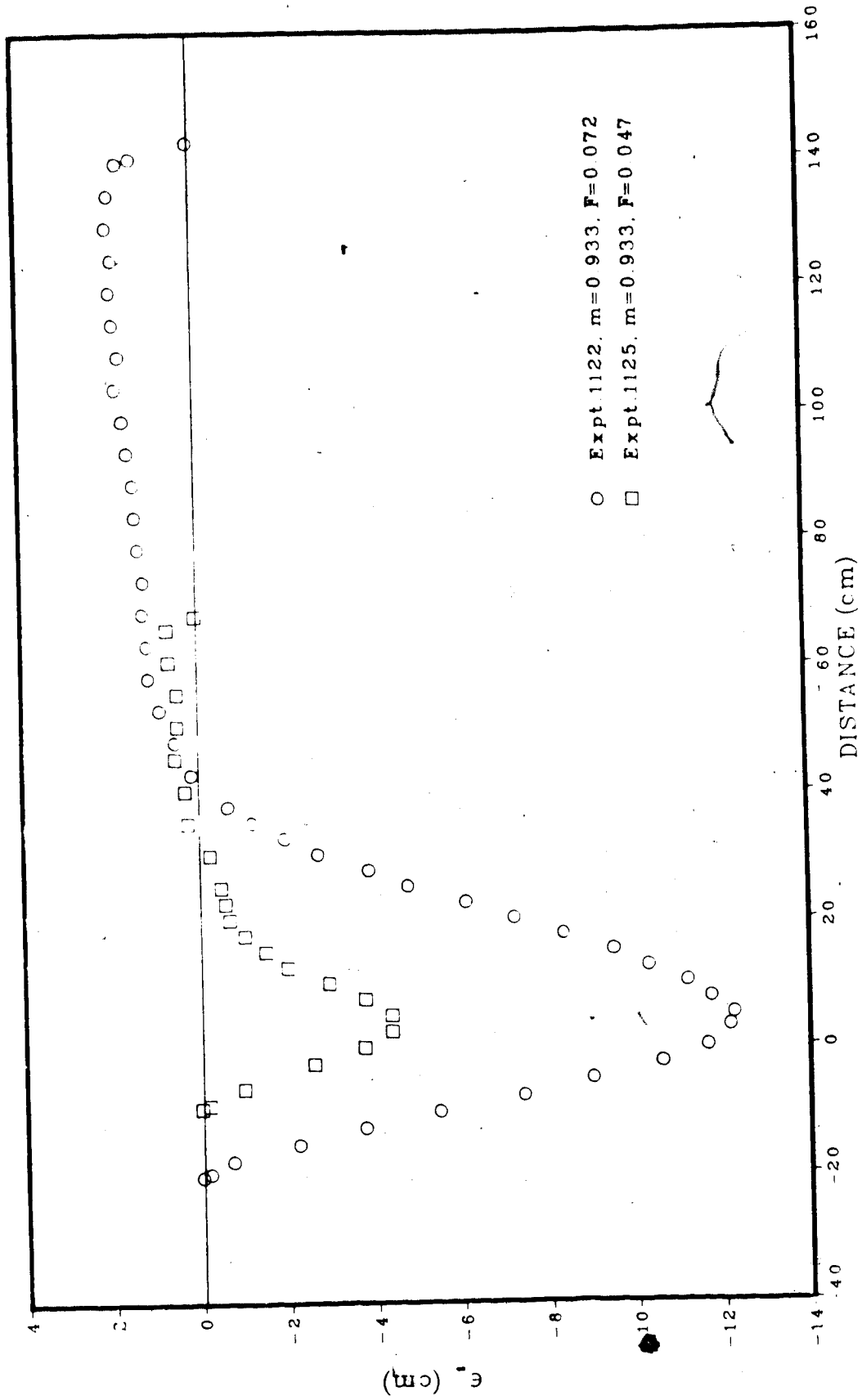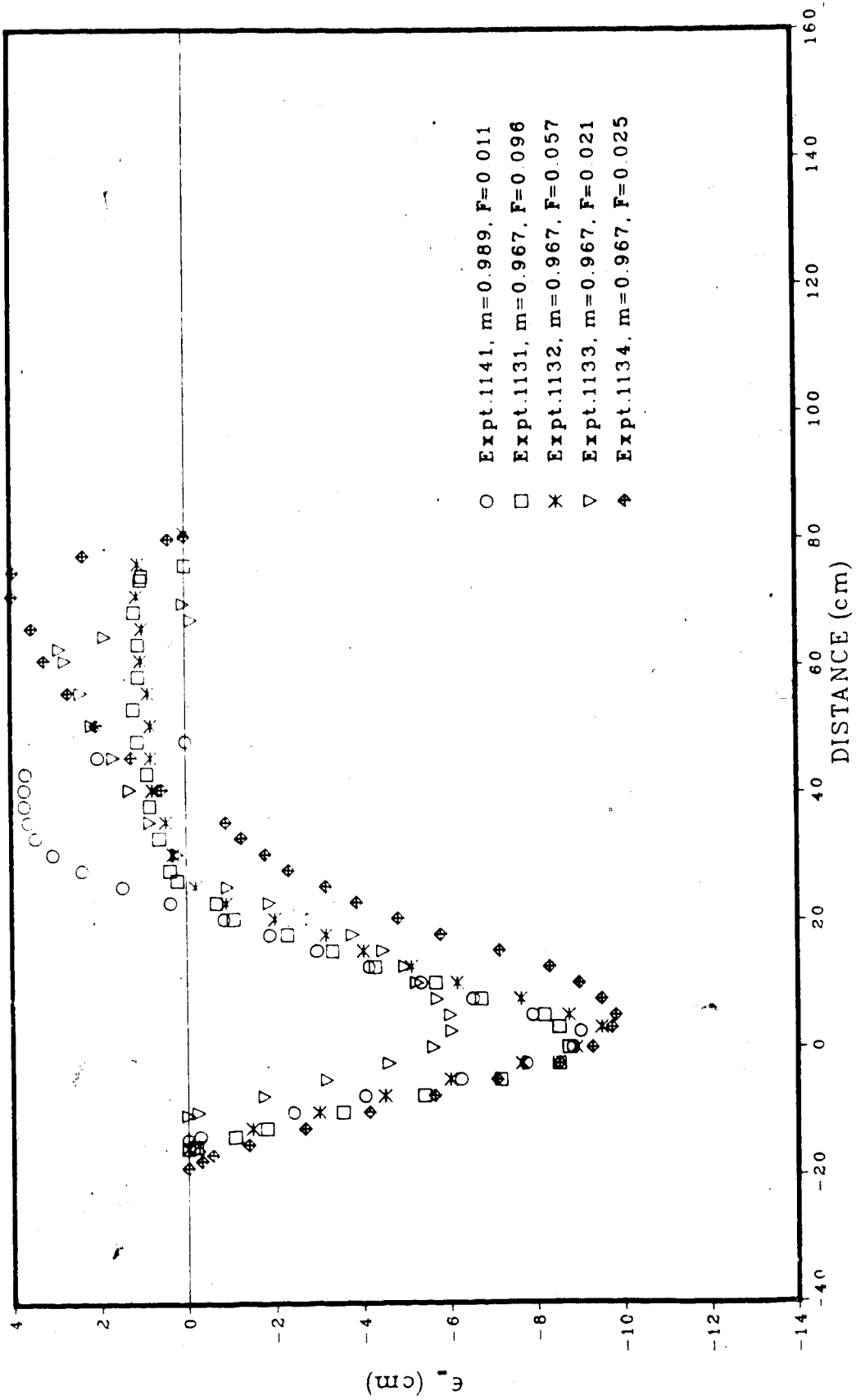
FIGURE 34 — SCOUR AND RIDGE PROFILES ALONG CHANNEL CENTRE

Legend:
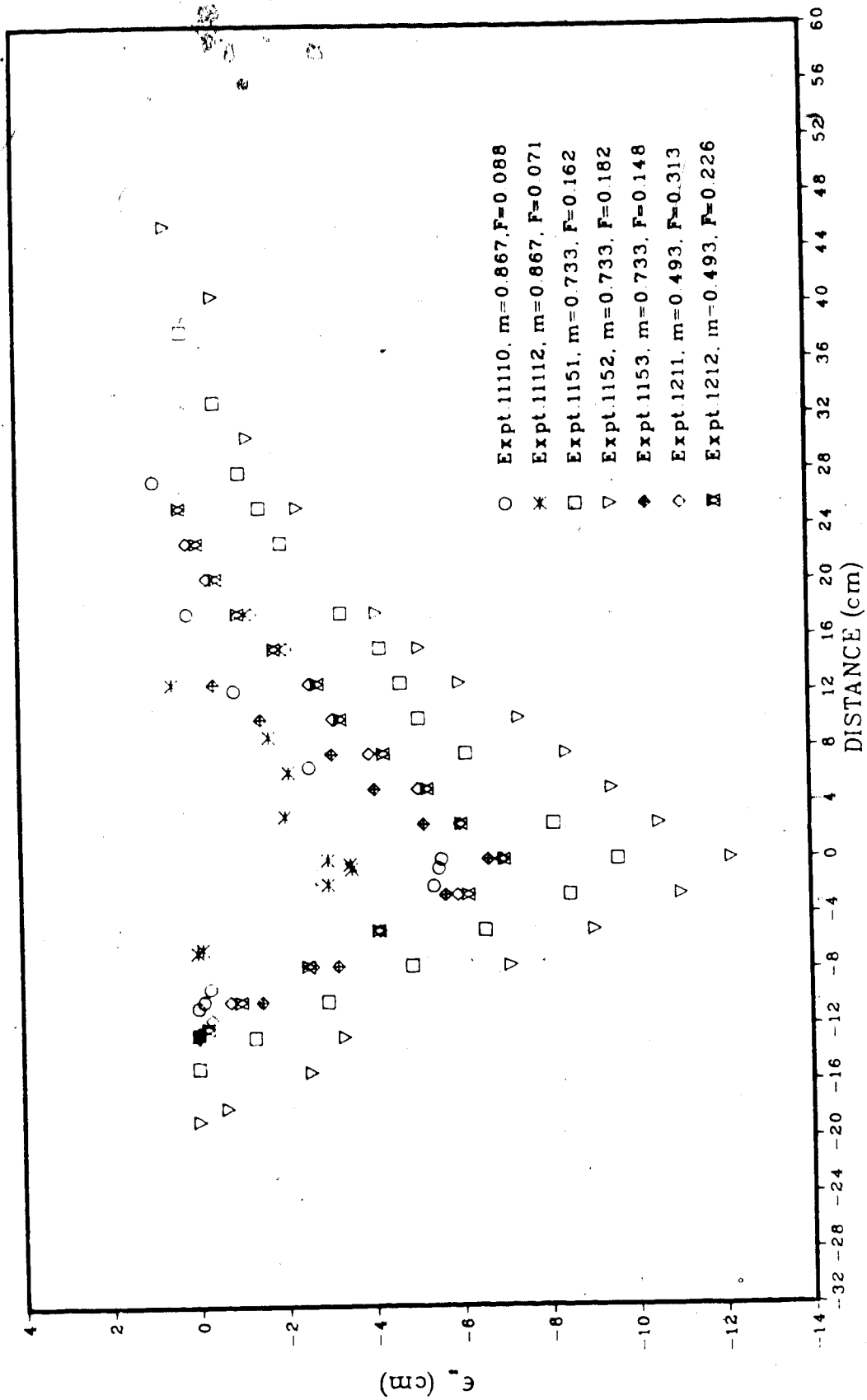○ Expt.1112. m=0.867. F=0.066
□ Expt.1113. m=0.867. F=0.086
✳ Expt.1115. m=0.867. F=0.068
▽ Expt.1117. m=0.867. F=0.081

Axis labels:
DISTANCE (cm)
e_* (cm)

DISTANCE (cm)

ϵ_m (cm)

Expt.1121, m=0.933, F=0.155
Expt.1123, m=0.933, F=0.136
Expt.1124, m=0.933, F=0.147
Expt.1126, m=0.933, F=0.0.110

FIGURE 35 – SCOUR AND RIDGE PROFILES ALONG CHANNEL CENTRE

FIGURE 36 – SCOUR AND RIDGE PROFILES ALONG CHANNEL CENTRE

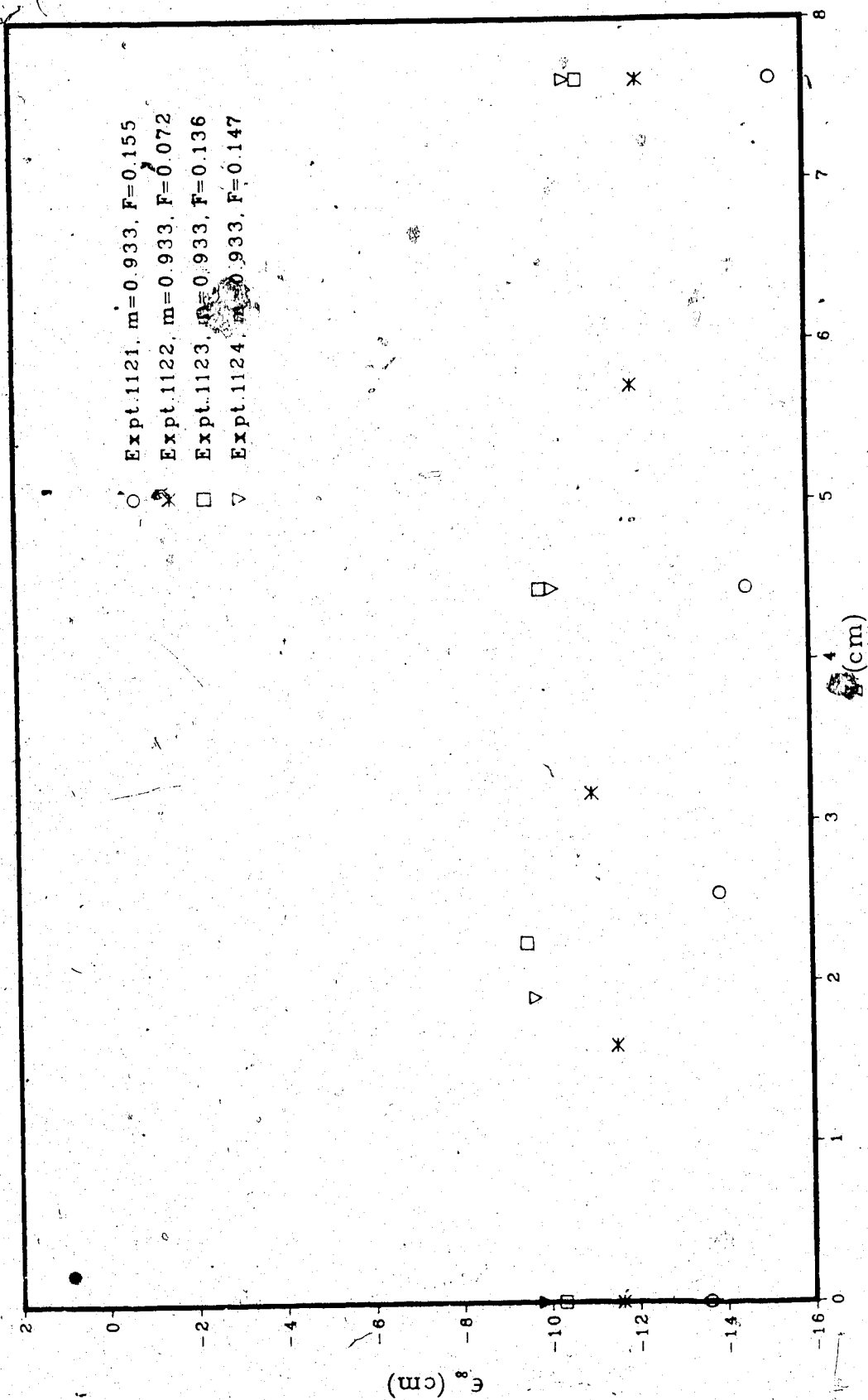FIGURE 37 — SCOUR AND RIDGE PROFILES ALONG CHANNEL CENTRE

Legend:

○ Expt.1141, m=0.989, F=0.011
□ Expt.1131, m=0.967, F=0.098
✳ Expt.1132, m=0.967, F=0.057
▽ Expt.1133, m=0.967, F=0.021
⬥ Expt.1134, m=0.967, F=0.025

FIGURE 38 – SCOUR PROFILES ALONG THE LINE PASSING
THROUGH THE NOSE OF CONSTRICTION

Legend:

○ Expt.11110. m=0.867, F=0.088
✳ Expt.11112. m=0.867, F=0.071
▢ Expt.1151. m=0.733, F=0.162
▽ Expt.1152. m=0.733, F=0.182
◆ Expt.1153. m=0.733, F=0.148
◇ Expt.1211. m=0.493, F=0.313
▣ Expt.1212. m=0.493, F=0.226

DISTANCE (cm)

e_s (cm)
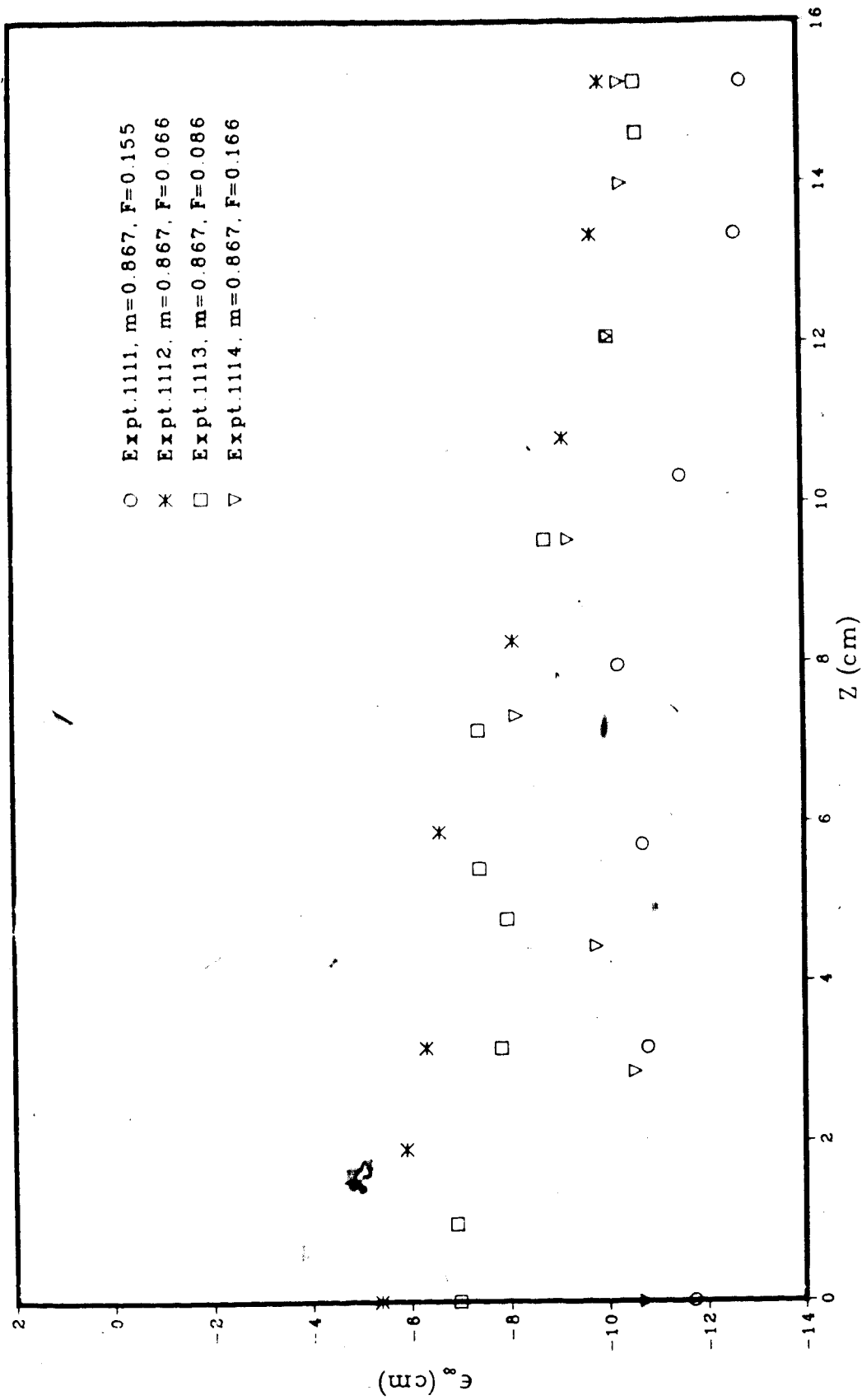
FIGURE 39 — SCOUR PROFILES ALONG THE CONSTRICTION; X = 0

Legend:
- ○ Expt.1111, m=0.867, F=0.155
- ✳ Expt.1112, m=0.867, F=0.066
- ☐ Expt.1113, m=0.867, F=0.086
- ▽ Expt.1114, m=0.867, F=0.166

Axes: e_∞ (cm) vs Z (cm)

FIGURE 40 – SCOUR PROFILES ALONG THE CONSTRICTION; X = 0

○ Expt.1121, m=0.933, F=0.155
✳ Expt.1122, m=0.933, F=0.072
□ Expt.1123, m=0.933, F=0.136
▽ Expt.1124, m=0.933, F=0.147

Axes: horizontal axis x (cm) from 0 to 8; vertical axis e_∞ (cm) from 2 to -16.
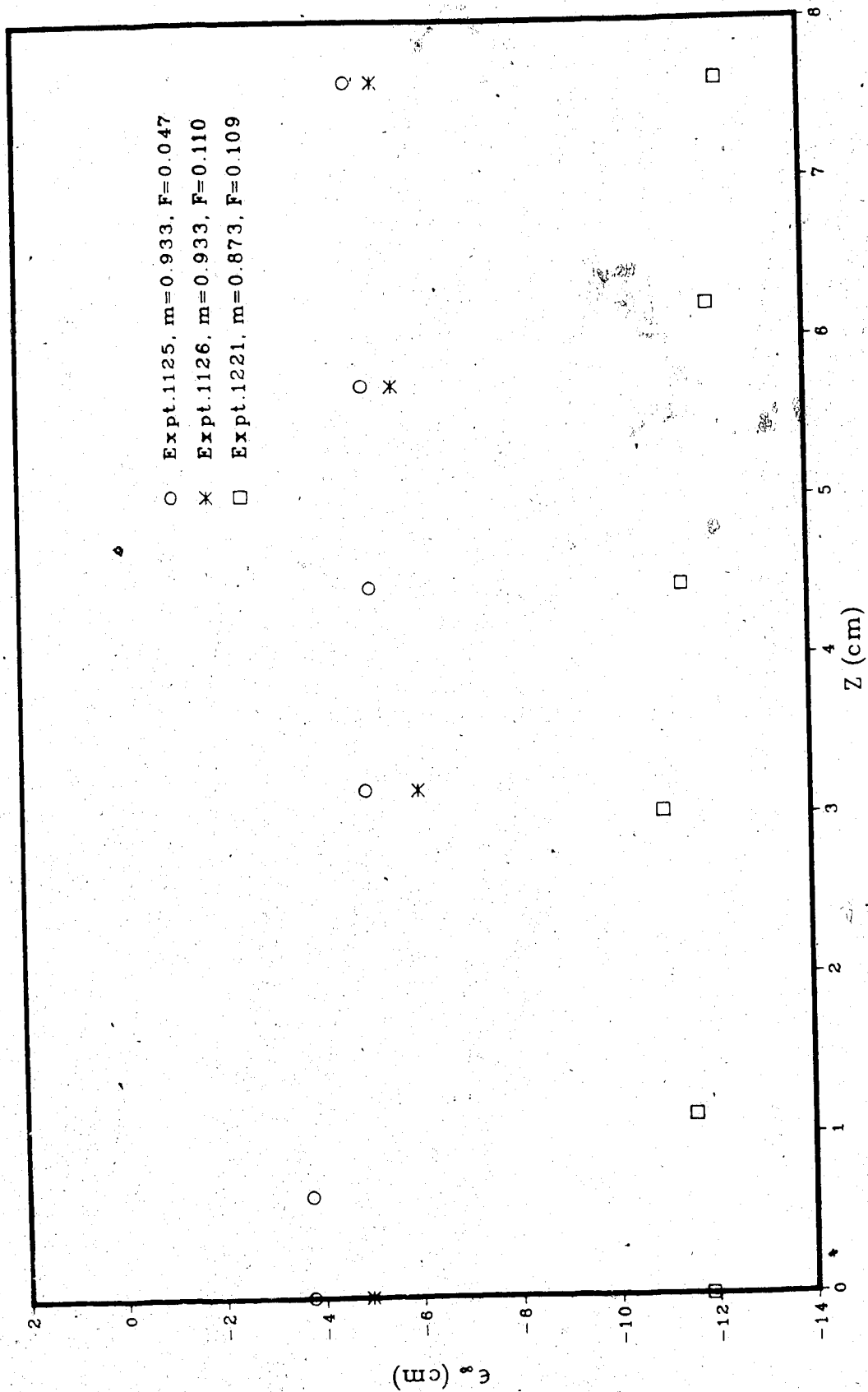
FIGURE 41 – SCOUR PROFILES ALONG THE CONSTRICTION; X = 0

Legend:
- ○ Expt.1125. m=0.933, F=0.047
- ✳ Expt.1126. m=0.933, F=0.110
- □ Expt.1221. m=0.873, F=0.109

Axes: Z (cm) (horizontal), ε_∞ (cm) (vertical)
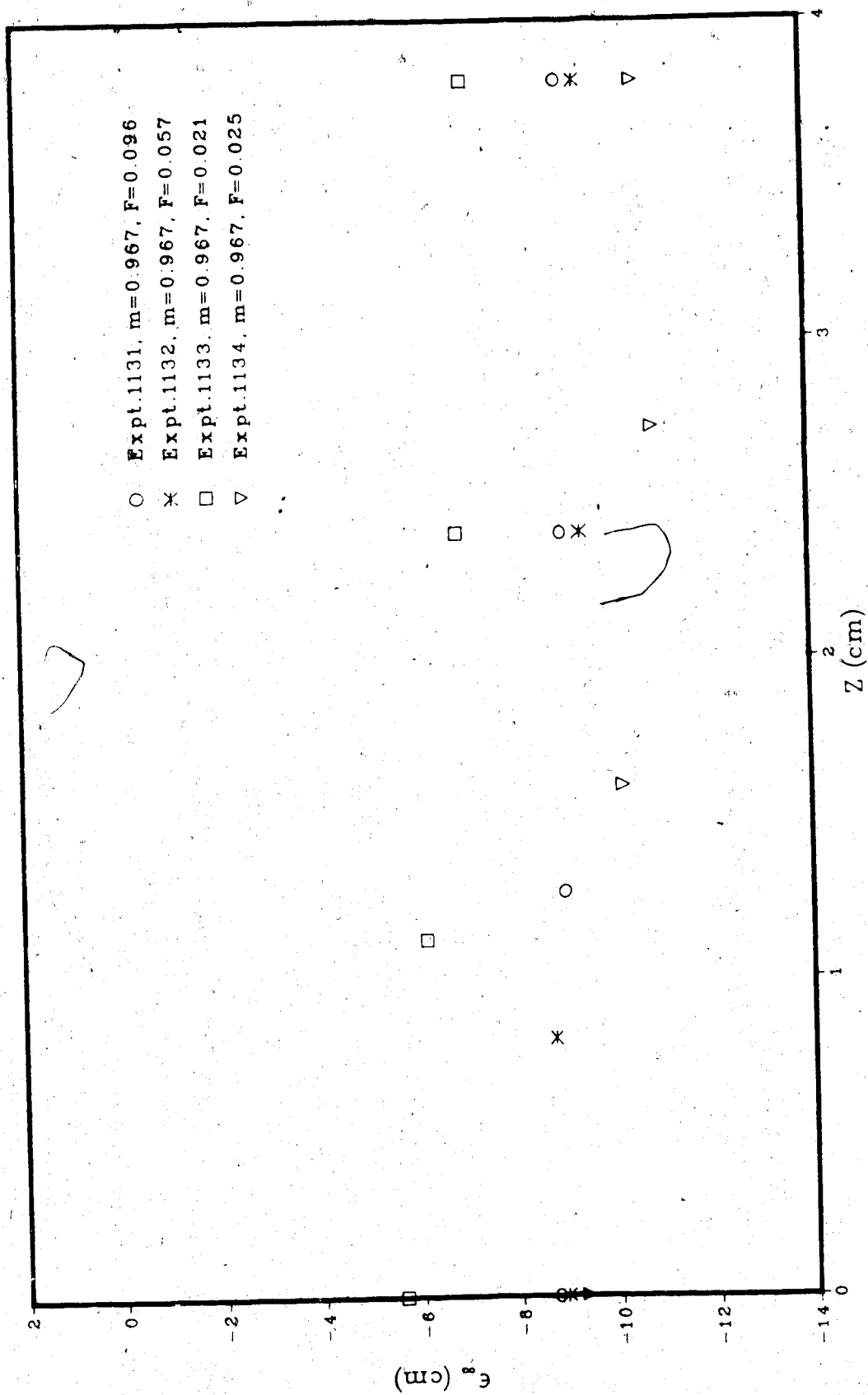
FIGURE 42 – SCOUR PROFILES ALONG THE CONSTRICTION; X = 0
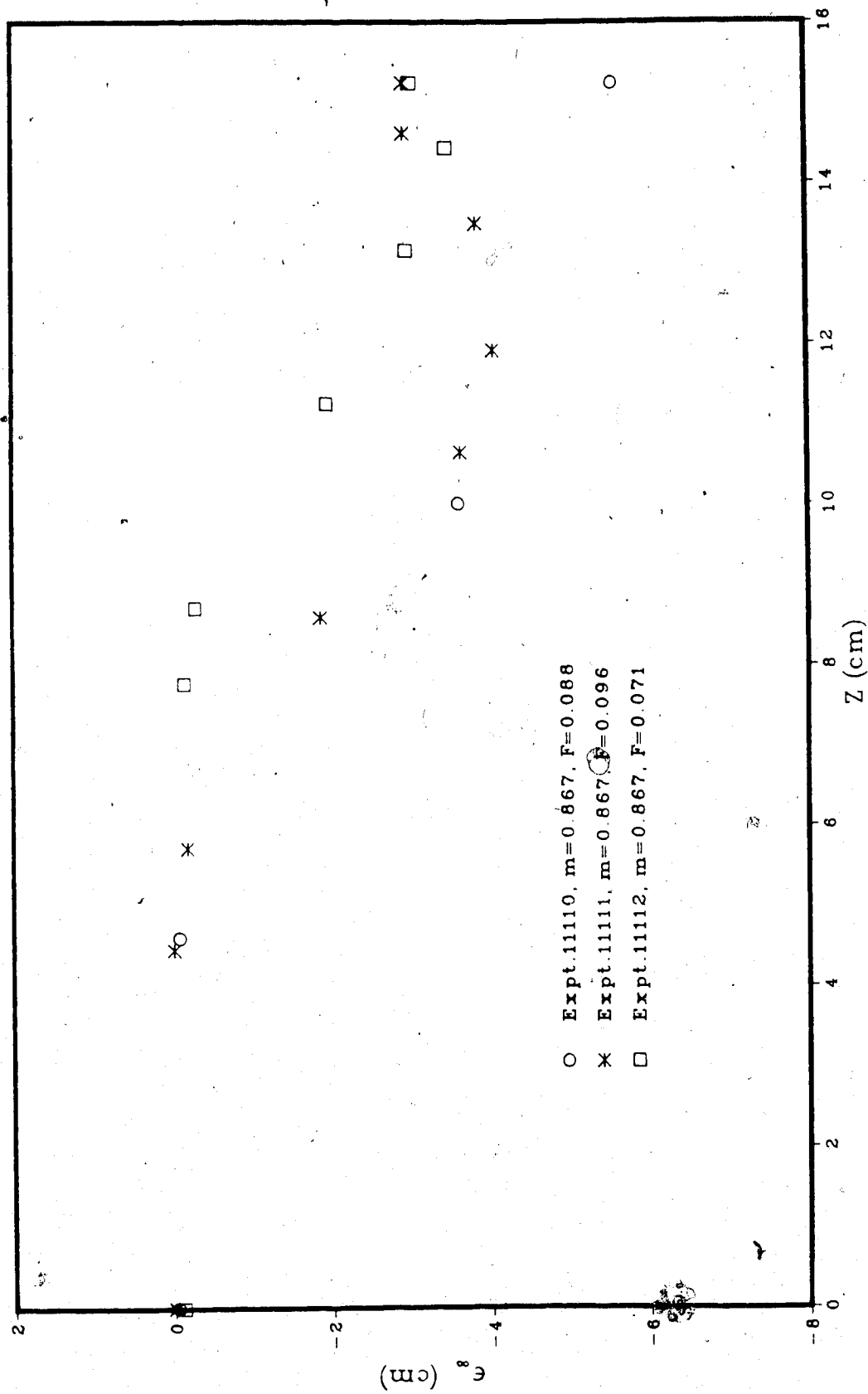
FIGURE 43 – SCOUR PROFILES ALONG THE CONSTRICTION; X = 0

O   Expt.11110, m=0.867, F=0.088
✳   Expt.11111, m=0.867, F=0.096
□   Expt.11112, m=0.867, F=0.071
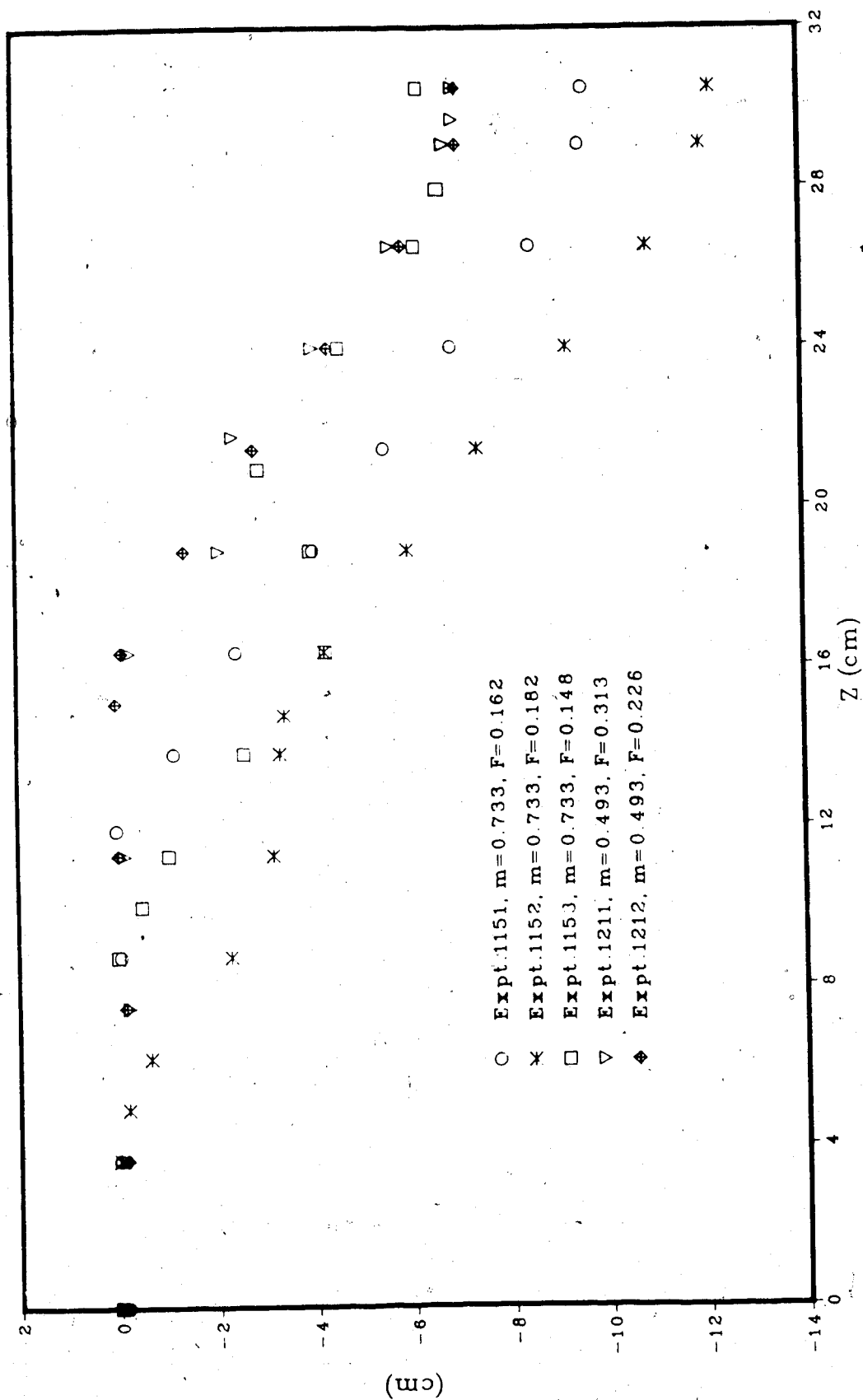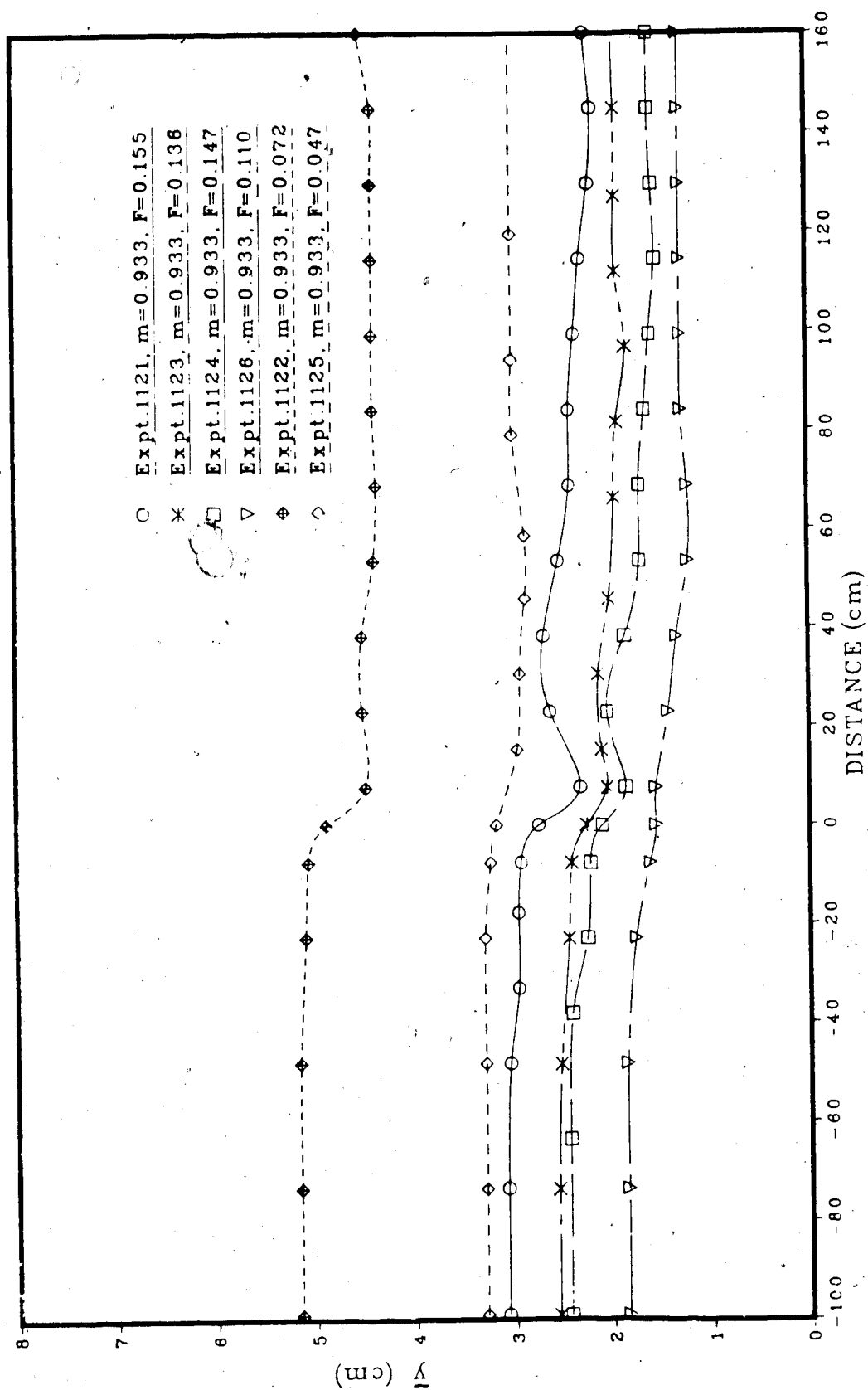
FIGURE 44 – SCOUR PROFILES ACROSS THE CONSTRICTION; X = 0
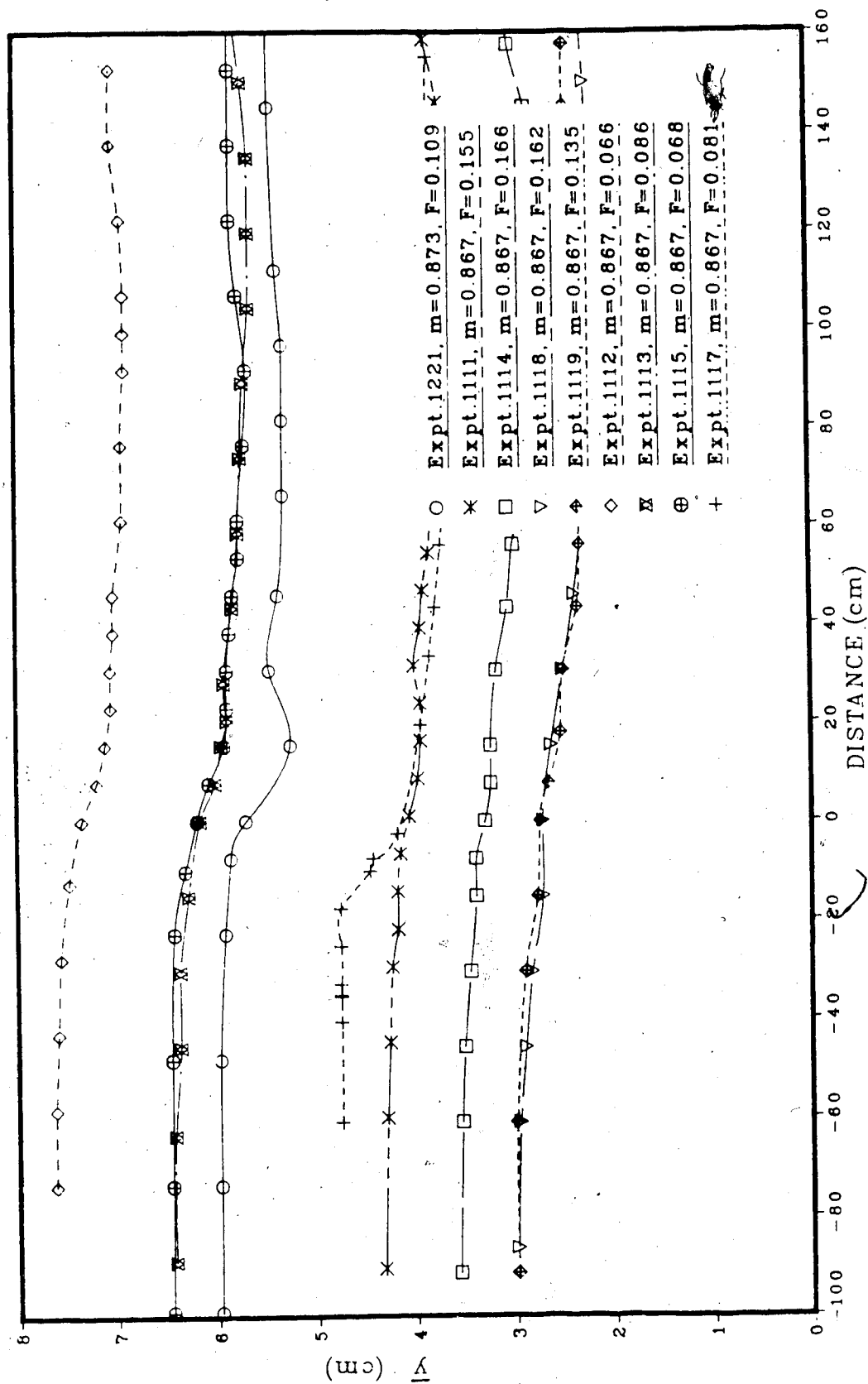
FIGURE 45 – WATER SURFACE PROFILES ALONG CHANNEL CENTRE
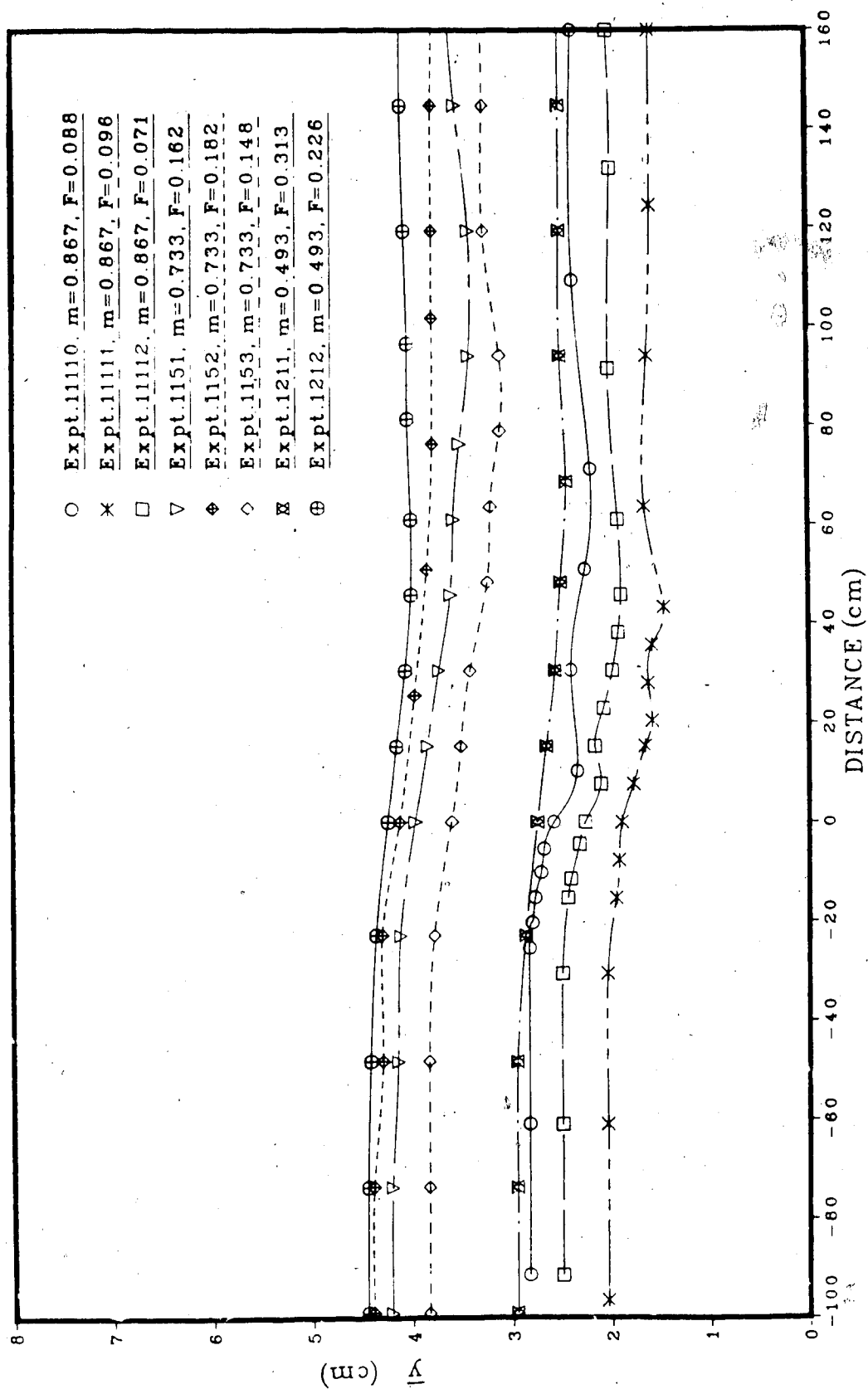
FIGURE 46 — WATER SURFACE PROFILES ALONG CHANNEL CENTRE

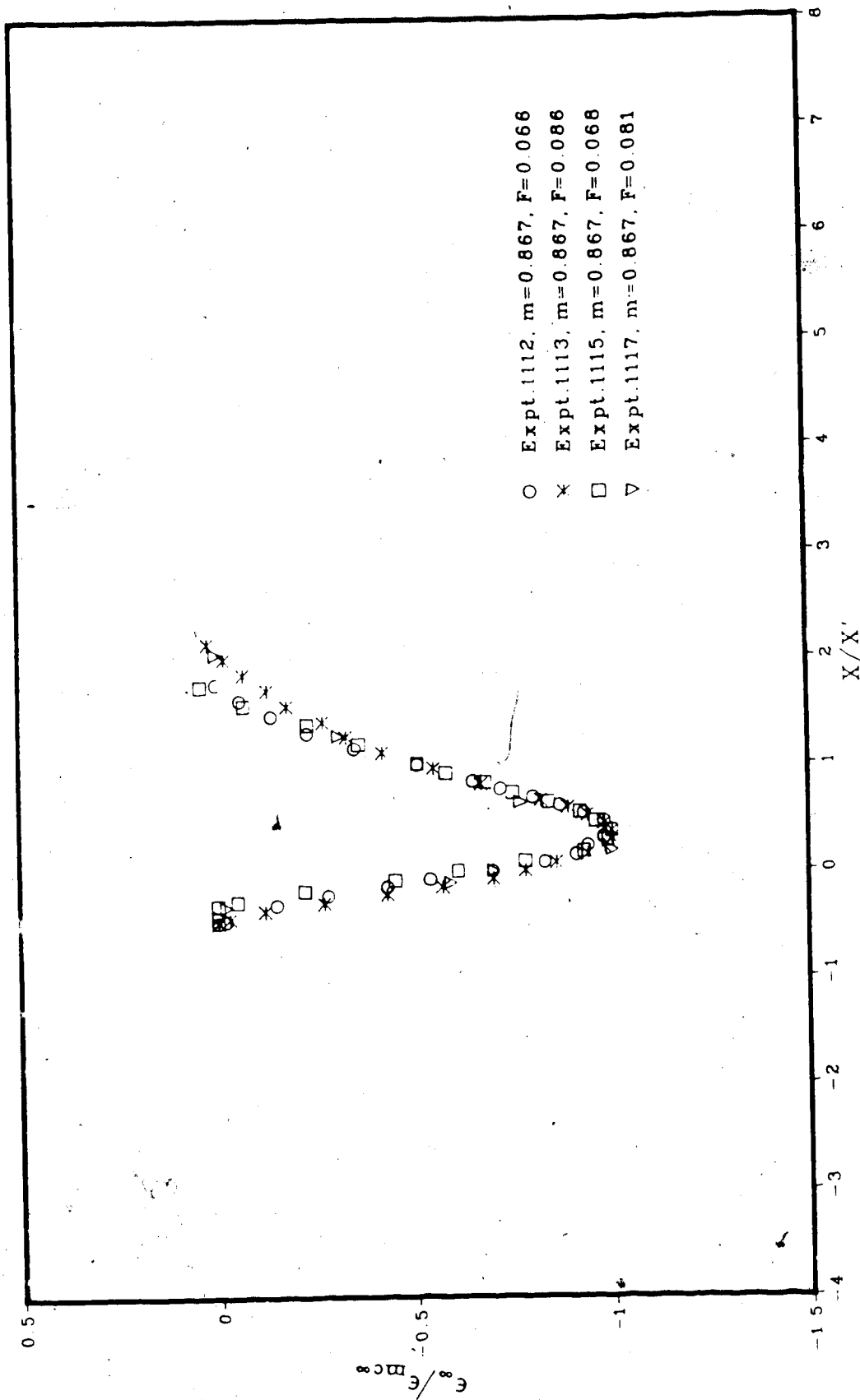FIGURE 47 — WATER SURFACE PROFILES ALONG CHANNEL CENTRE

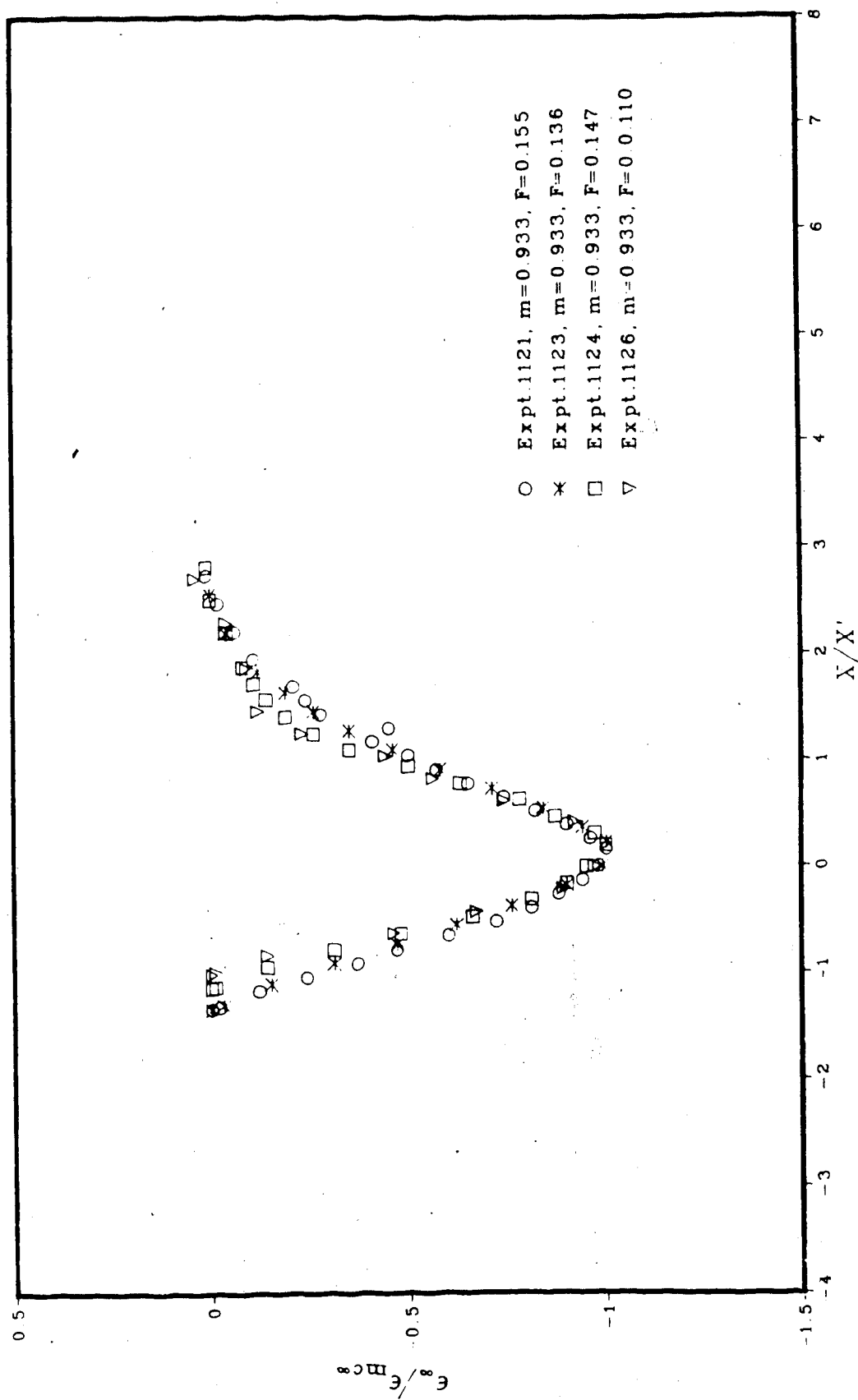FIGURE 48 – NON–DIMENSIONAL SCOUR PROFILES ALONG CHANNEL CENTER

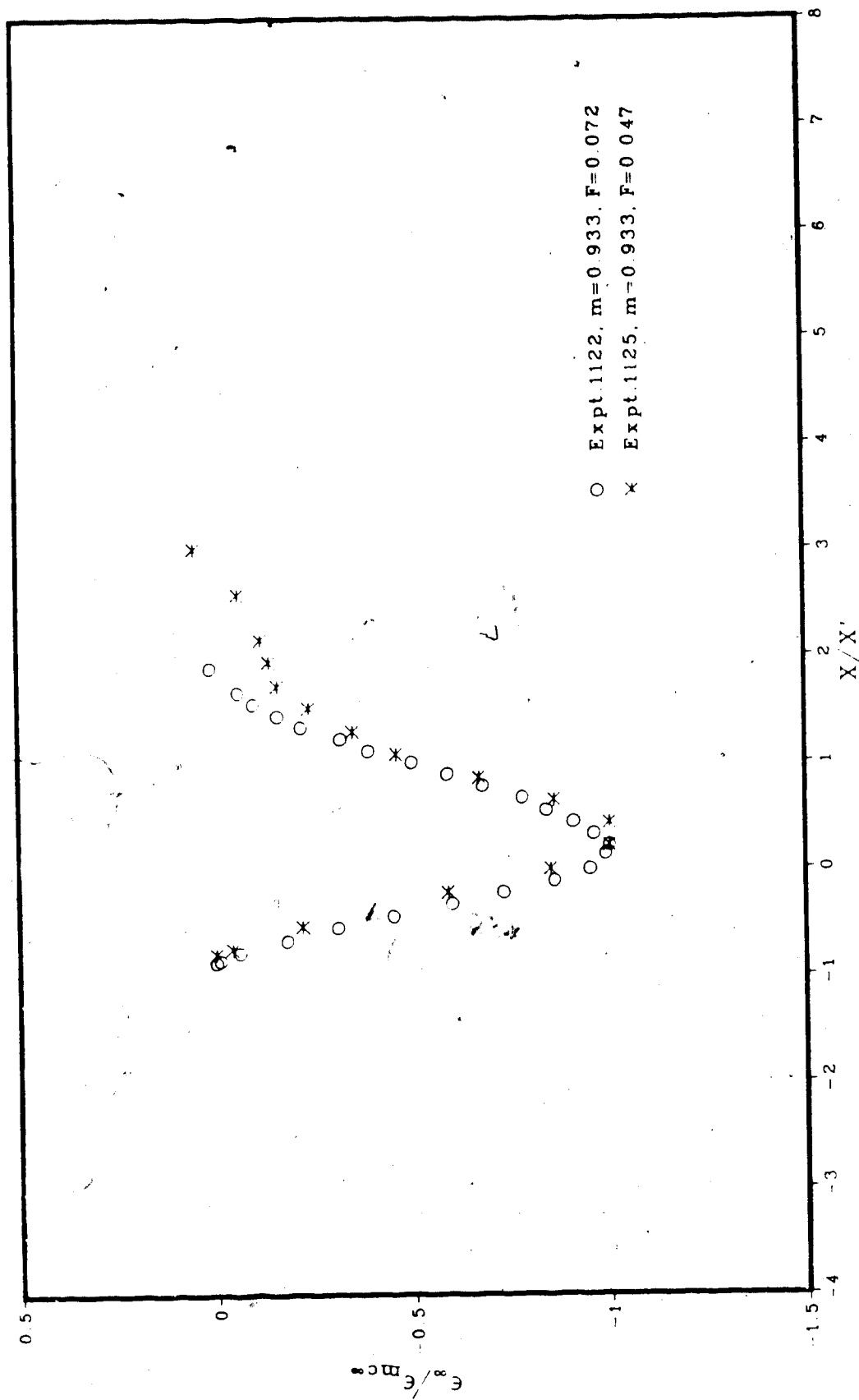FIGURE 49 – NON–DIMENSIONAL SCOUR PROFILES ALONG CHANNEL CENTRE

Legend (within figure):

○   Expt.1121, m=0.933, F=0.155
＊   Expt.1123, m=0.933, F=0.136
□   Expt.1124, m=0.933, F=0.147
▽   Expt.1126, m=0.933, F=0.0.110

Axis labels: X/X' (horizontal), $\epsilon_s/\epsilon_{mc\infty}$ (vertical)

FIGURE 50 -- NON-DIMENSIONAL SCOUR PROFILES ALONG CHANNEL CENTRE

○ Expt.1122. m=0.933. F=0.072
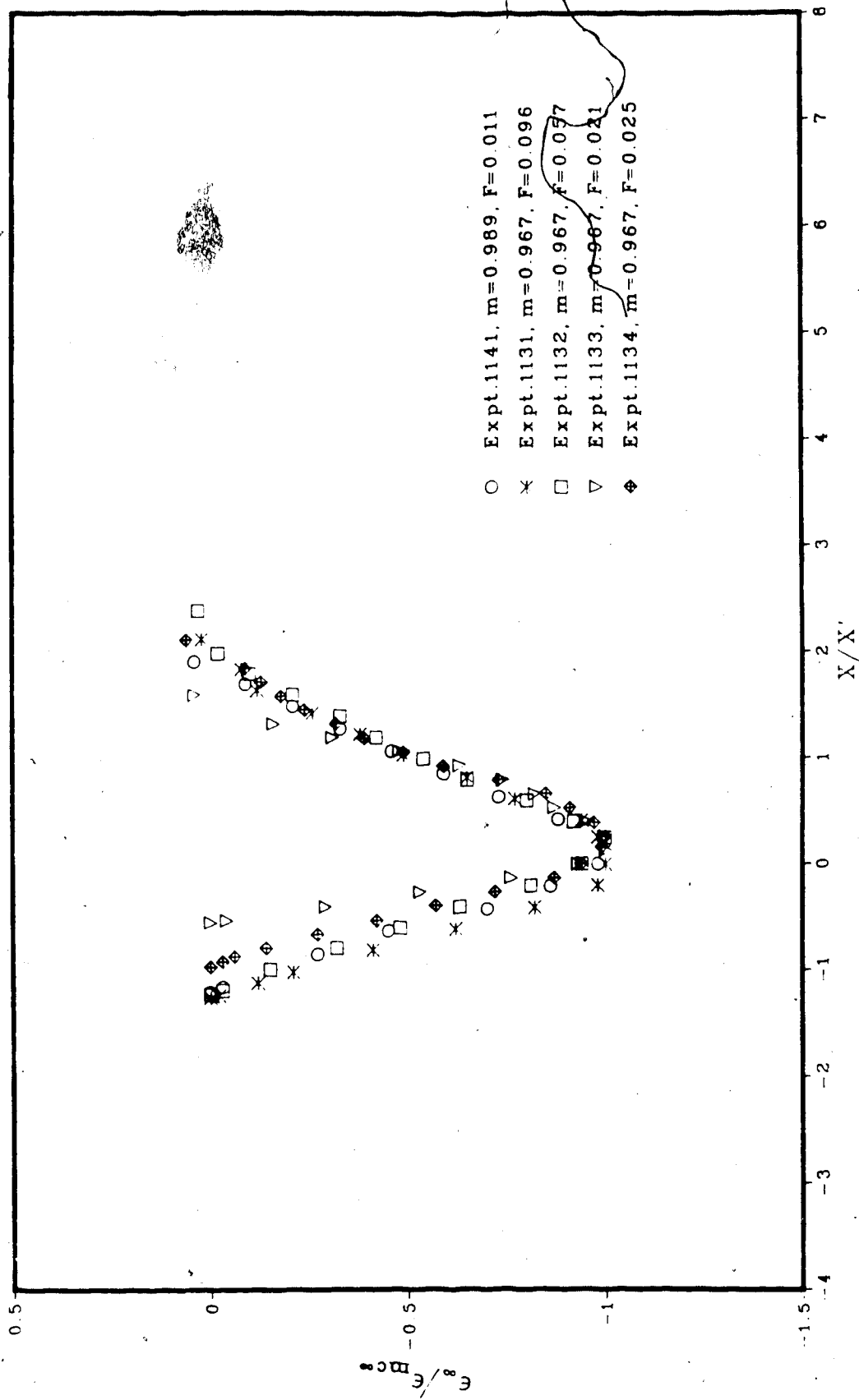✳ Expt.1125. m=0.933. F=0 047

X/X'

$\epsilon_s/\epsilon_{mc8}$

117

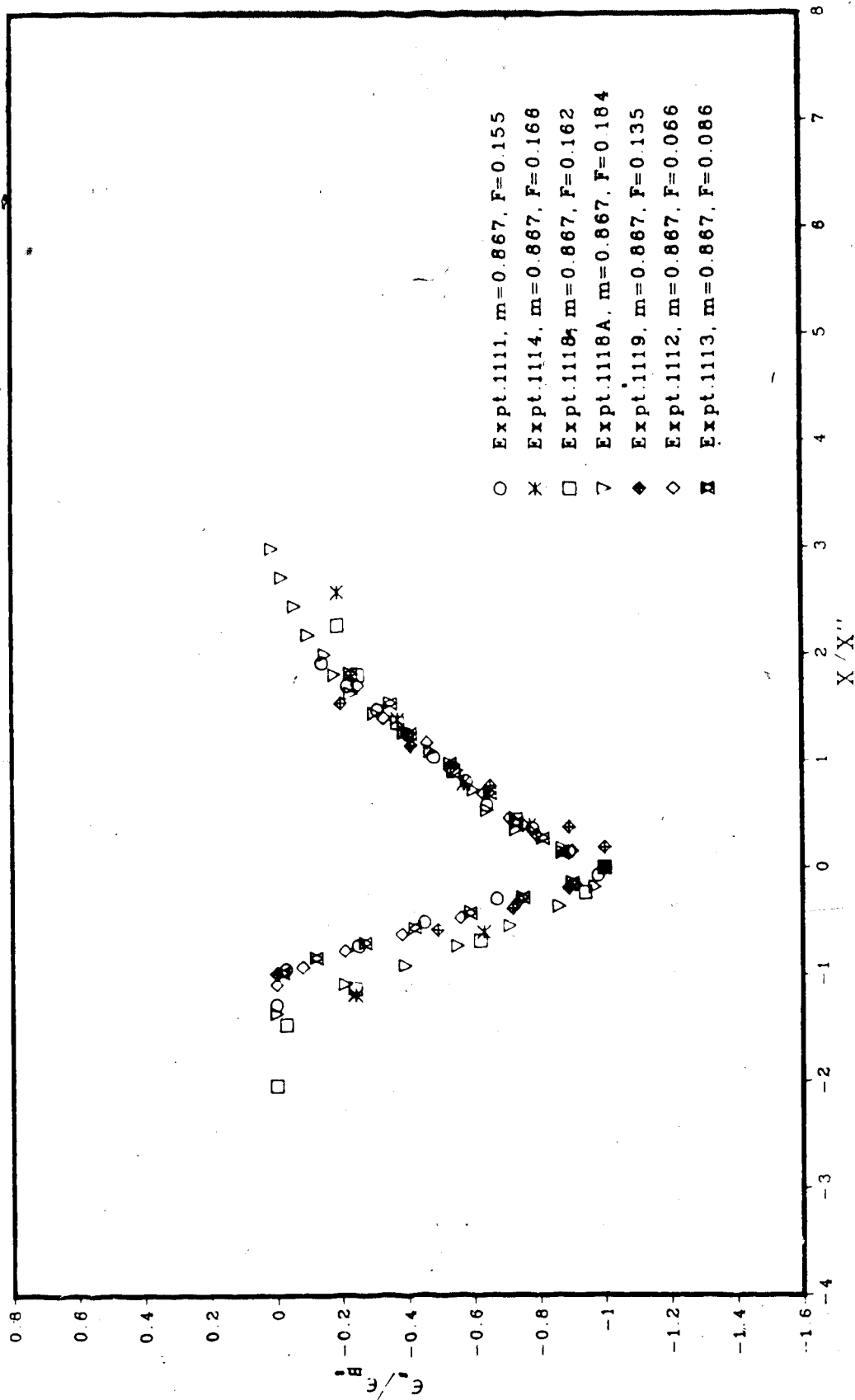FIGURE 51 — NON—DIMENSIONAL SCOUR PROFILES ALONG CHANNEL CENTRE

FIGURE 52 — NON–DIMENSIONAL SCOUR PROFILES ALONG THE LINE
PASSING THROUGH THE NOSE OF CONSTRICTION
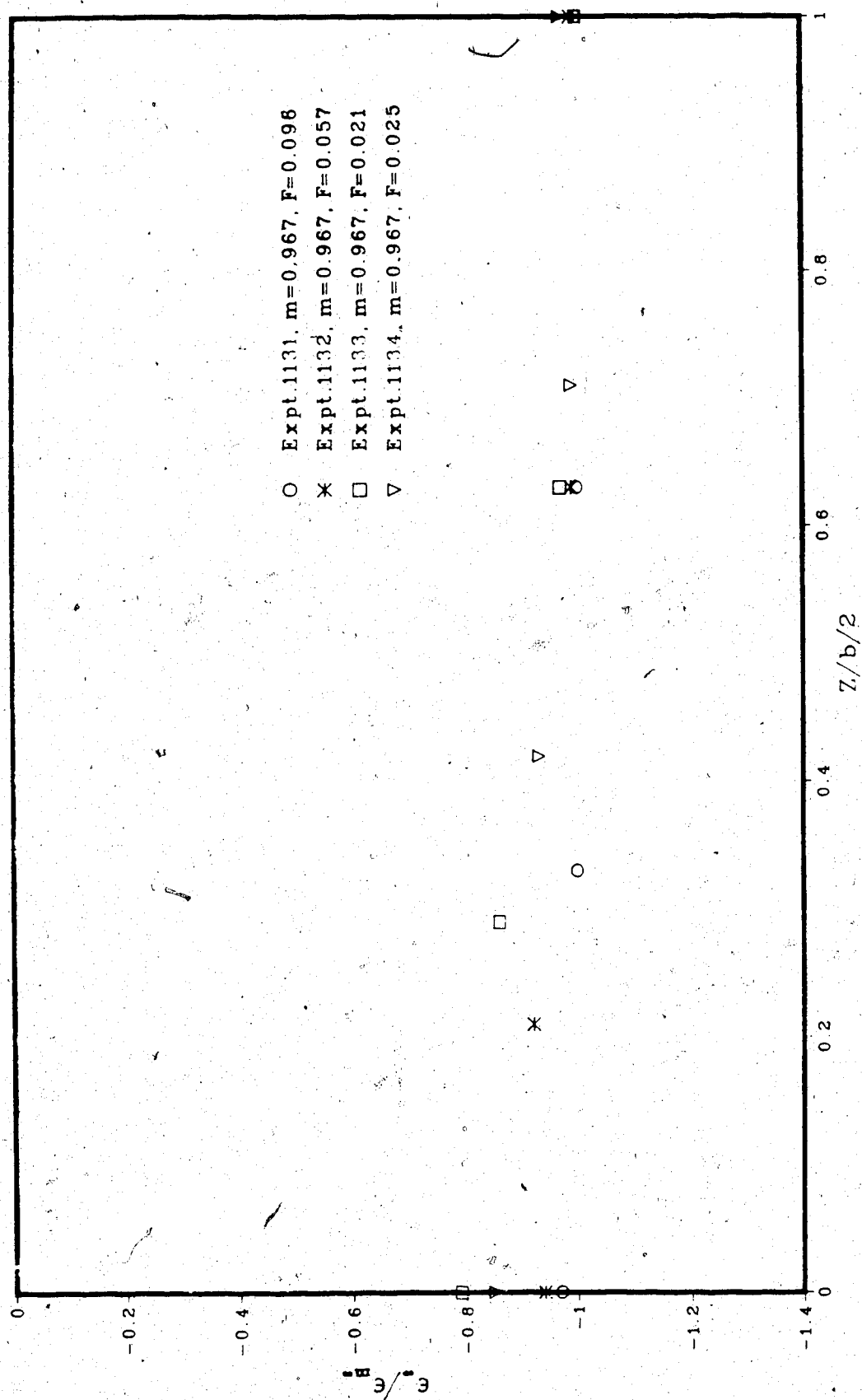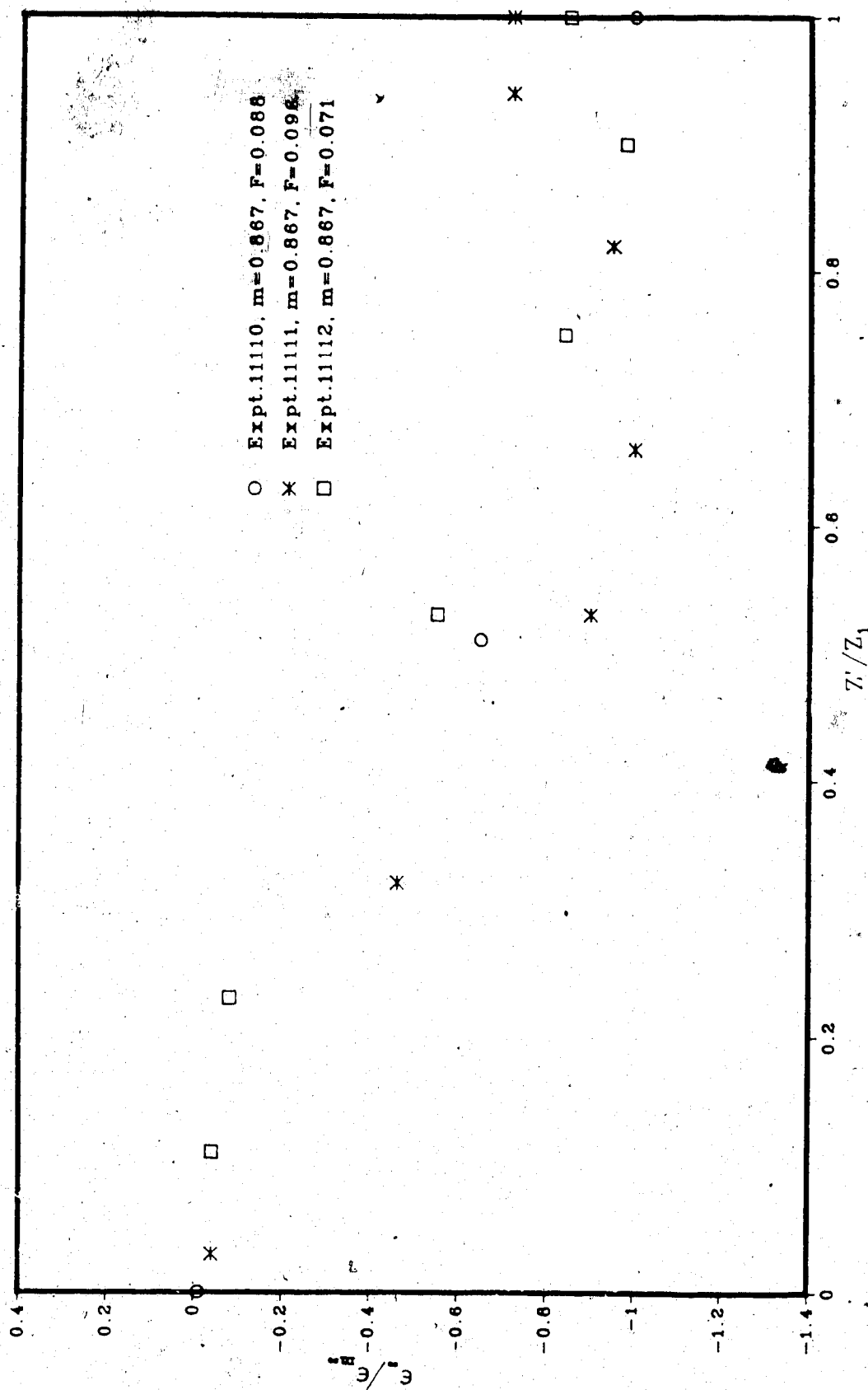
O Expt.1111, m=0.867, F=0.155
✳ Expt.1114, m=0.867, F=0.168
□ Expt.1118, m=0.867, F=0.162
▽ Expt.1118A, m=0.867, F=0.184
◆ Expt.1119, m=0.867, F=0.135
◇ Expt.1112, m=0.867, F=0.066
▣ Expt.1113, m=0.867, F=0.086
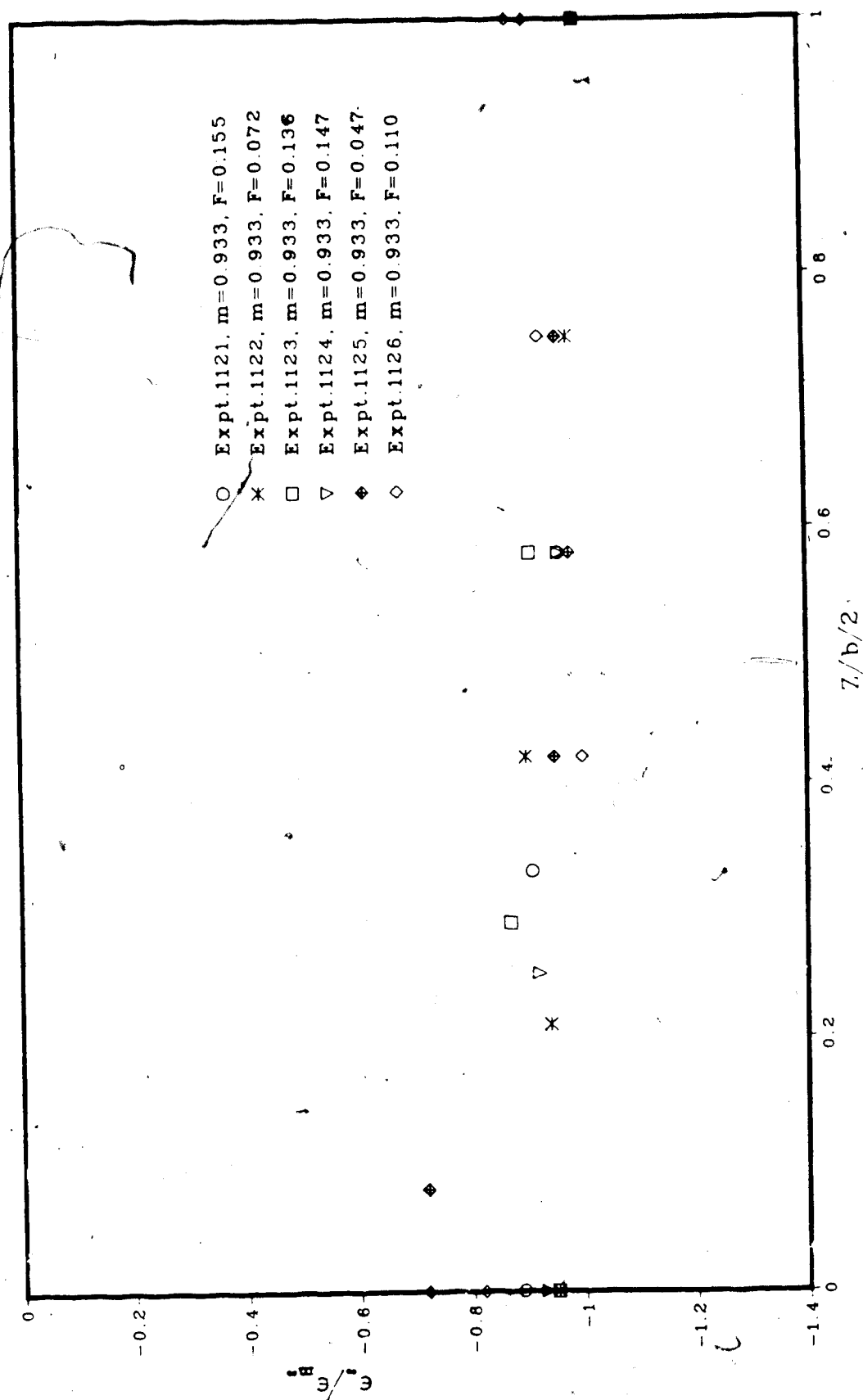
FIGURE 53 – NON–DIMENSIONAL SCOUR PROFILES ACROSS CONSTRICTION; X = 0

Legend:

○ Expt.1121, m=0.933, F=0.155
✳ Expt.1122, m=0.933, F=0.072
□ Expt.1123, m=0.933, F=0.136
▽ Expt.1124, m=0.933, F=0.147
◈ Expt.1125, m=0.933, F=0.047
◇ Expt.1126, m=0.933, F=0.110

X-axis: $z/b/2$

Y-axis: $\varepsilon_s/\varepsilon_B$

FIGURE 54 — NON-DIMENTIONAL SCOUR PROFILES ACROSS CONSTRICTION; X = 0

Legend:
- O Expt.1131, m=0.967, F=0.098
- ✳ Expt.1132, m=0.967, F=0.057
- □ Expt.1133, m=0.967, F=0.021
- ▽ Expt.1134, m=0.967, F=0.025

Axis labels: $\varepsilon_{so}/\varepsilon_m$ (vertical), $z/b/2$ (horizontal)

○ Expt.11110, m=0.867, F=0.088
✳ Expt.11111, m=0.867, F=0.094
□ Expt.11112, m=0.867, F=0.071

Z'/Z_1

ϵ_s/ϵ_{ms}

0.4
0.2
0
-0.2
-0.4
-0.6
-0.8
-1
-1.2
-1.4

0   0.2   0.4   0.6   0.8   1

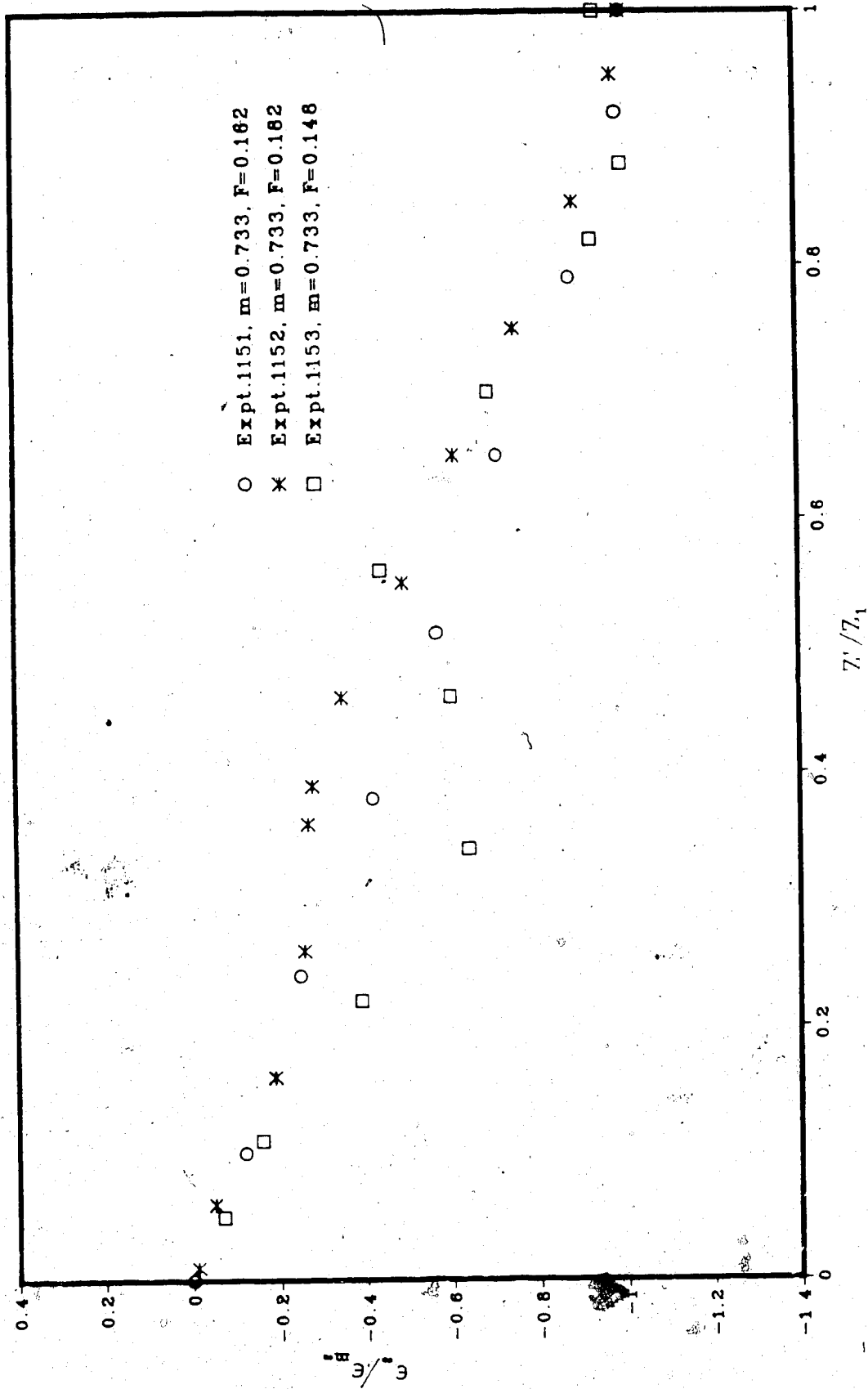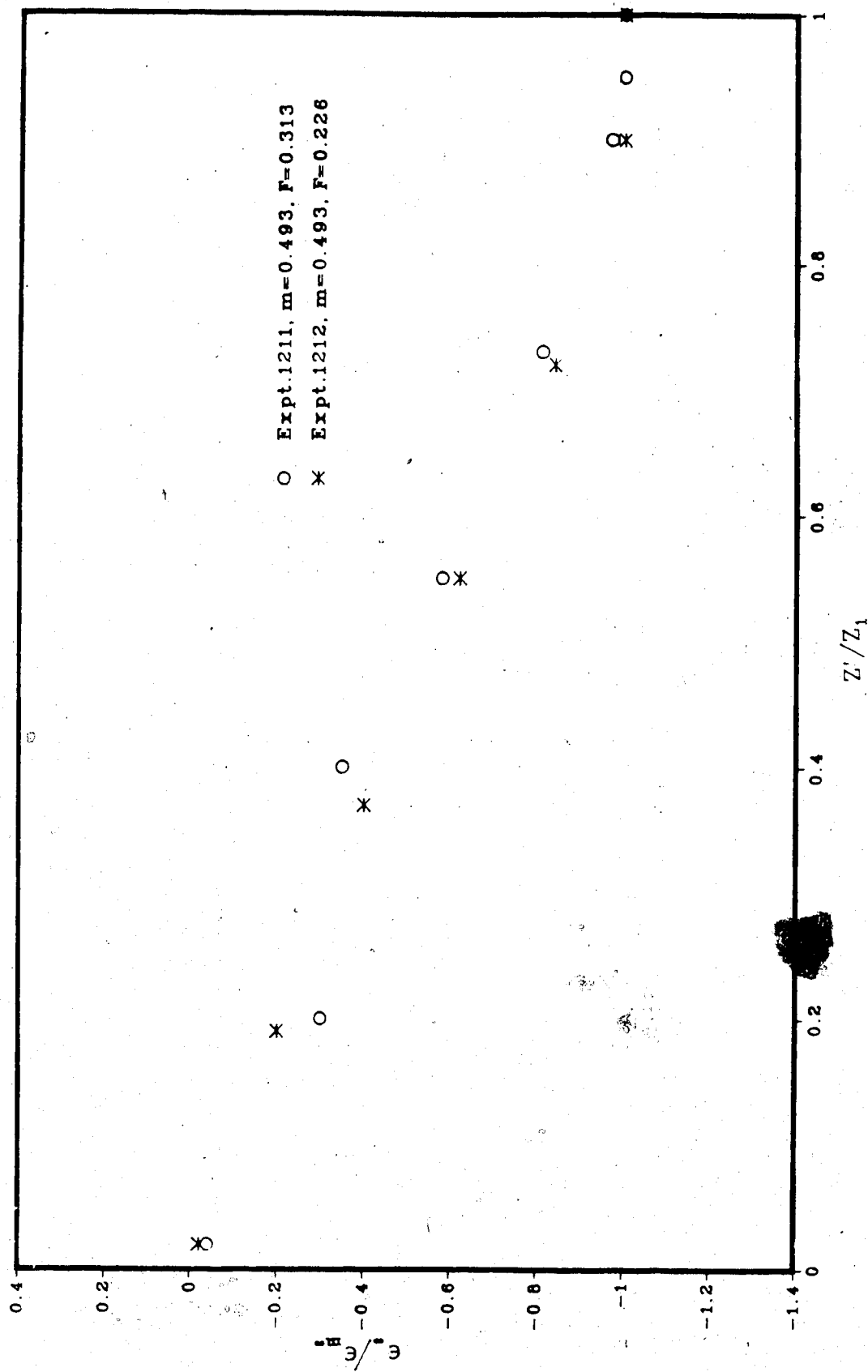FIGURE 55 – NON–DIMENSIONAL SCOUR PROFILES ACROSS CONSTRICTION; X = 0

FIGURE 56 – NON–DIMENSIONAL SCOUR PROFILES ACROSS CONSTRICTION; X = 0

FIGURE 57 — NON–DIMENSIONAL SCOUR PROFILES ACROSS CONSTRICTION; X = 0